Ariane Pessentheiner, Bakk. rer. nat. MSc.

Elucidation of genes influencing adipogenic development and energy metabolism

---

DISSERTATION

to obtain the academic degree
Doktorin der technischen Wissenschaften
submitted at

Graz University of Technology

supervised by
Assoc. Prof. Mag. rer. nat. Dr. rer. nat. Juliane Bogner-Strauss
Institute of Biochemistry

Graz, August 2014

EIDESSTATTLICHE ERKLÄRUNG
AFFIDAVIT

Ich erkläre an Eides statt, dass ich die vorliegende Arbeit selbstständig verfasst, andere als die angegebenen Quellen/Hilfsmittel nicht benutzt, und die den benutzten Quellen wörtliche und inhaltlich entnommene Stellen als solche kenntlich gemacht habe. Das in TUGRAZonline hochgeladene Textdokument ist mit der vorliegenden Dissertation identisch.

I declare that I have authored this thesis independently, that I have not used other than the declared sources/resources, and that I have explicitly indicated all material which has been quoted either literally or by content from the sources used. The text document uploaded to TUGRAZonline is identical to the present doctoral dissertation.

…… ……..

Datum / date Unterschrift / signature

Acknowledgements

"You have power over your mind - not outside events. Realize this, and you will find strength."

-- Marcus Aurelius

First of all, I want to thank my supervisor Juliane Bogner-Strauss, who has guided and supported me throughout my time as a PhD student. She was not only a scientific mentor, but also personally gave me all the advice and motivation that made me enjoy the positive moments and endure the hard times.
"What is a teacher? I'll tell you: it isn't someone who teaches something, but someone who inspires the student to give of her best in order to discover what she already knows." -- Paul Coelho

Here is also the place to mention our great team in the lab. These people are not only my colleagues, but are also dear friends. Thanks for all the support, the advice, and the fun during my years as a PhD student!
"Coming together is a beginning. Keeping together is progress. Working together is success." -- Henry Ford

I also want to thank my mentor Franz Radner and my thesis committee members Günter Hämmerle and Achim Lass who gave me new directions and shared ideas in great discussions.
I'm thankful for all the collaborators that helped me along the way in this study. They shared equipment, techniques and more importantly knowledge with me, what greatly influenced the positive outcome of this work.
Thanks to all the people of the DK-MCD. You enriched my scientific and personal life.
Also thanks to Jerrold Olefsky who gave me the opportunity to join his lab in San Diego and Dayoung Oh for her great supervision. This stay allowed me to grow scientifically and also personally.

Last, but not least, I want to express my gratitude to my family who was always been there for me, above all my husband Hannes. He was the one closest to me to share bad and good moments. I cannot express how much his support helped me.
„Gesucht und gefunden, in der Einsicht verbunden: Du gibst was du brauchst, ich glaub was ich seh', endlich mal etwas das ich fast versteh'." -- Kettcar, Balu

Abstract

The prevalence of obesity, together with associated diseases like type II diabetes and the metabolic syndrome, is constantly increasing. This is on the one hand due to overnutrition and a sedentary lifestyle, but also connected to genetic factors. Two major types of adipose tissue can be distinguished. White adipose tissue is the main lipid storage organ, which provides fatty acids in times of energy-demand. In contrast, brown adipose tissue (BAT) dissipates energy in form of heat. Our lab concentrates on the investigation of genes involved in the development and metabolism of adipocytes. In this thesis two genes have been intensively studied, focusing on adipogenesis and adipocyte energy metabolism.

Previous results from our lab showed that adipocyte plasma membrane associated protein (*Apmap*) is a crucial factor for adipogenesis of 3T3-L1 cells and a target of the adipogenic master-regulator PPARγ. To investigate the consequences of *Apmap*-loss *in vivo*, we generated *Apmap* deficient mice and characterized them in regard to fat cell development and energy metabolism. The preliminary results of this study show that *Apmap* knockout (ko) mice have decreased weight which is also maintained during high fat diet feeding. Furthermore, insulin sensitivity is increased in these mice. Although, the biochemical function of APMAP is still unknown, a role of APMAP in regulating glucose homeostasis is conceivable. This hypothesis was also addressed in adipocytes *in vitro*. The results of these experiments showed that APMAP possibly influences the translocation process of the glucose transporter GLUT4 to the plasma membrane.

Another gene which caught our attention was N-acetyltransferase 8-like (*Nat8l*), which we found deregulated in adipose tissue of mice with a metabolic phenotype, such as *ob/ob* mice and adipose triglyceride lipase (*Atgl*)-ko mice. The function of NAT8L in brain is well described as the N-acetylaspartate (NAA) producing enzyme. NAA serves as a transport form of acetyl-CoA and is essential for myelin synthesis. Until now, no role of NAT8L in other tissues has been shown. Based on the observations that *Nat8l* is highly expressed in adipose tissues, especially BAT, and that overexpression of *Nat8l* influences the metabolism of immortalized brown adipogenic cells (iBACs), this thesis aims to deeper investigate the role of this gene in brown adipocyte metabolism. We could show that the NAT8L protein is localized in mitochondria of adipocytes and that overexpression of this gene in iBACs leads to elevated lipid turnover and increased mitochondrial mass which is accompanied by an increased oxygen consumption rate. The latter may be due to the elevated protein expression of uncoupling protein 1 (UCP1), which is responsible for uncoupling oxidative phosphorylation from ATP production. Together with that, also brown adipogenic genes and genes involved in β-oxidation are upregulated, indicating that *Nat8l* overexpression boosts the brown adipogenic phenotype. Furthermore, we show that *Nat8l* is a PPARγ target.

In summary, this work provides an important contribution to deeper understand the metabolism of adipocytes and is the basis for further investigations.

Kurzfassung

Die westliche Welt wird zunehmend mit dem Problem konfrontiert, dass Fettleibigkeit und Folgeerkrankungen wie Typ 2 Diabetes und das metabolische Syndrom stark im Steigen begriffen sind. Das kann teils auf die ständige, hohe Energiezufuhr und auf einen vermehrt sitzenden Lebensstil zurückgeführt werden, aber auch genetische Komponenten spielen eine Rolle. Man unterscheidet zwei Hauptformen von Fett. Auf der einen Seite gibt es das weiße Fettgewebe, dessen Hauptaufgabe es ist, Fett in Form von Lipidtropfen zu speichern und bei Energiebedarf zu spalten. Auf der anderen Seite steht das braune Fett, dessen Rolle nicht die Speicherung, sondern die Verbrennung von Fett, um Wärme zu erzeugen, ist. Unser Labor konzentriert sich einerseits auf die Untersuchung der Funktionen von Genen, die die Fettzellentwicklung, auch Adipogenese genannt, beeinflussen und andererseits legen wir einen besonderen Fokus auf den Metabolismus von braunen Fettzellen. In der vorliegenden Arbeit werden zwei Proteine intensiv untersucht.

In der Vergangenheit konnten wir bereits zeigen, dass das Adipozyten Plasmamembran assoziierte Protein APMAP eine essentielle Rolle in der Entwicklung von Fettzellen in Zellkulturmodellen spielt. Deshalb generierten wir eine *Apmap* defiziente Maus, um die Auswirkungen des Fehlens von APMAP im ganzen Organismus zu untersuchen. Die vorläufigen Ergebnisse dieser Studie zeigten, dass *Apmap* knockout (ko) Mäuse ein geringeres Gewicht haben, welches auch bestehen bleibt, wenn sie eine fettreiche Labordiät zu sich nehmen. Außerdem konnten wir zeigen, dass die Insulinsensitiviät in *Apmap*-ko Mäusen gesteigert ist. Obwohl die biochemische Funktion von APMAP noch immer nicht bekannt ist, wäre auf Grund der vorliegenden Daten eine regulatorische Rolle von APMAP im Glukosestoffwechsel möglich. Diese Hypothese wurde in dieser Arbeit auch mit *in vitro* Versuchen in der Fettzelllinie 3T3-L1 behandelt. Vorläufige Ergebnisse zeigten, dass APMAP möglicherweise die Translokation des Glukosetransporters GLUT4 beeinflusst. Jedoch müssen diese Ergebnisse durch weiterführende Studien bestätigt werden.

Das zweite Gen, auf das wir uns konzentrierten ist N-Acetyltransferase 8-like (*Nat8l*). Die Funktion von NAT8L war bislang nur im Gehirn beschrieben, wo es die Entstehung von N-Acetylaspartat (NAA) katalysiert. NAA ist ein äußerst wichtiger Metabolit, der Acetyl-CoA für die Myelinisierung von Axonen bereitstellt. Wir konnten zeigen, dass *Nat8l* auch in Fettgeweben von Mäusen exprimiert wird und dass die stabile Überexpression von *Nat8l* zu einer Beeinflussung des Energiemetabolismus von braunen Adipozyten führt. Basierend darauf war das Ziel dieser Arbeit die Rolle von NAT8L in Fettzellen genauer zu charakterisieren. Die Ergebnisse zeigten, dass NAT8L ein mitochondriales Protein ist und dass durch erhöhte *Nat8l* Expression der Lipidstoffwechsel angekurbelt wird, was zu einem erhöhten Einbau von Glukose in Lipide führt. Außerdem wird die Lipolyse induziert. Des Weiteren konnten wir zeigen, dass sich durch *Nat8l* Überexpression die Zahl an Mitochondrien und der damit verbundene Sauerstoffverbrauch erhöhen. Letzteres könnte auch damit zusammenhängen, dass die Expression von Genen, die besonders wichtig für den „braunen“ Phänotyp der Fettzellen sind, hochreguliert ist. Besonders hervorheben kann man dabei die massive Hochregulierung von Uncoupling Protein 1 (UCP1), dem Protein, das die oxidative Phosphorylierung von der ATP-Synthese entkoppelt.

Zusammenfassend, stellt diese Arbeit einen wichtigen Beitrag zur Erforschung von Fettzellen dar und ist eine grundlegende Basis für weiterführende Studien.

Table of contents

1 Introduction 3

1.1 White, brown and beige adipose tissue: Fat is not simply fat 3

1.2 The role of adipose tissue in regulating glucose homeostasis 7

1.3 N-acetyltransferase 8-like (Nat8l) – a new player in brown adipogenic development and metabolism 9

1.4 Adipocyte plasma membrane associated protein (APMAP) and its function in adipogenesis and energy homeostasis 12

2 Materials and Methods 17

2.1 Animal studies 17

2.2 Cell culture, adipogenic differentiation and lipid staining 17

2.3 Cell culture and manipulation of murine HM-1 embryonic stem cells 18

2.4 RNA isolation, reverse transcription, and gene expression analysis 18

2.5 Mitochondria isolation 20

2.6 Western blot analysis 20

2.7 ^{14}C-glucose uptake and lipid extraction 21

2.8 Measurement of cellular oxygen consumption rate (OCR) 21

2.9 Electroporation of 3T3-L1 and iBACs 22

2.10 Live cell imaging and immunofluorescence 22

2.11 ^{3}H-Deoxyglucose uptake 23

2.12 Detection of mitochondrial mass by flow cytometry 23

2.13 Relative quantification of mitochondrial DNA 24

2.14 Transmission electron microscopy (TEM) 24

2.15 Measurement of mitochondrial membrane potential 24

2.16 Site-directed mutagenesis of Nat8l and subsequent stable transfection of iBACs 25

2.17 Luciferase reporter assays 25

2.18 Southern blot analysis 26

2.19 Plasma parameter measurements 26

2.20 Glucose and insulin tolerance test (GTT and ITT) 27

2.21 Fasting tolerance test (FTT) 27

2.22 Statistical analysis 27

3 Results – part NAT8L 31

3.1 Nat8l expression is downregulated in adipose tissue of ob/ob mice 31

3.2 NAT8L is located in the mitochondria of brown adipocytes 31

3.3 The influence of Nat8l overexpression on different pathways and metabolic phenotypes 32

3.3.1 Expression of genes directly or indirectly involved in the proposed *Nat8l*-pathway 32
3.3.2 The expression of white and brown adipogenic marker genes in *Nat8l* o/e iBACs 36
3.3.3 Overexpression of *Nat8l* in iBACs increases glucose uptake and lipogenesis 37
3.3.4 *Nat8l* overexpressing iBACs show increased lipolysis 40
3.3.5 Oxygen consumption and genes involved in β-oxidation and FFA utilization are increased upon *Nat8l* overexpression 42
3.3.6 *Nat8l* overexpression increases mitochondrial mass and number 44
3.4 The phenotype of Nat8l o/e iBACs is dependent on its enzymatic activity 46
3.5 Nat8l is a PPAR target 46
4 Results – part APMAP 49
4.1 The impact of Apmap deficiency in vivo 49
4.1.1 Generation of *Apmap*-deficient and loxP flanked ES cell clones and chimeric founders 49
4.1.2 Preliminary characterization of *Apmap* deficient mice 53
4.2 Elucidation of the function of Apmap in vitro 62
4.2.1 Transient o/e of *Apmap* influences *Glut4* expression in differentiated 3T3-L1 cells 62
5 Discussion 67
5.1 The role of Nat8l overexpression in brown adipocyte differentiation and metabolism 67
5.2 The role of Apmap in glucose homeostasis 75
6 References 81
7 Figure and table legends 91
7.1 Figure legends 91
7.2 Table Legends 92
8 Abbreviations 95
8.1 Nomenclature 96
9 Appendix 99
9.1 Published manuscript – N-acetyltransferase 8-like accelerates lipid turnover and increases energy expenditure in brown adipocytes 99
9.2 Additional data-files – Luciferase Assays 113

Introduction

1 Introduction

1.1 White, brown and beige adipose tissue: Fat is not simply fat

Obesity and its related disorders, like type II diabetes and cardiovascular diseases, have become a rising global health and economic burden, as the number of overweight people is constantly increasing[1]. Accordingly, strategies for potential therapies to fight obesity and to reduce life-threatening associated diseases are of growing interest.

Two classical types of adipose tissue (AT) are well described: White and brown adipose tissue. Excessive nutrients are stored in white adipose tissue (WAT) in form of fat and its adipocytes are characterized by large, unilocular lipid droplets and only few mitochondria[2]. In periods of food deprivation, the fat is hydrolyzed by lipases and the resulting free fatty acids (FFAs) are mobilized into the bloodstream to supply peripheral tissues with energy. The main lipases performing lipid breakdown are adipose triglyceride lipase (ATGL), hormone sensitive lipase (HSL) and monoglyceride lipase (MGL).[3] White adipose depots can be found throughout the body (distribution in mice see fig. 1)[4]. However, WAT is not only a storage depot, it is also important for mechanical protection, organ insulation and it has an essential endocrine role by which it influences systemic metabolism[5,6].

In contrast to WAT, brown adipose tissue (BAT) has the main function to dissipate energy from fat and glucose oxidation into heat, a process called non-shivering thermogenesis[2,7,8]. Brown adipocytes have multiple, small lipid droplets and numerous mitochondria which contain uncoupling protein 1 (UCP1)[8,9]. UCP1 localizes in the inner mitochondrial membrane where it uncouples oxidative phosphorylation from ATP production and thereby produces heat[10]. BAT was recognized to be important for mammals already over 50 years ago. Especially infants and smaller mammals, such as rodents, rely on its thermogenic potency to maintain their body temperature.[11,12] Astonishingly, Nedergaard and coworkers reported in 2007[13] and several others in 2009 that active BAT depots can also be found in adult humans[14–17]. In rodents, classical BAT is distributed in perirenal and interscapular regions and regions surrounding the kidney and heart[4] (fig. 1). In humans, brown adipocytes are mainly located in supraclavicular and spinal parts of the body, and around the neck[17]. BAT is highly vascularized and innervated by the sympathetic nervous system. Activation of brown adipocytes by β-adrenergic stimuli, such as norepinephrine, leads to the initiation of the thermogenic program via the induction of intracellular lipid breakdown and the release of free fatty acids (FFAs) from lipid droplets (reviewed in [8]). FFAs have several fates in brown adipocytes as they serve as allosteric activators of UCP1[18], furthermore they are fuelled into β-oxidation[19] or reesterifyed to form neutral lipids[20].

Several studies investigated how gain or loss of function of UCP1 influences whole-body metabolism. Forced UCP1 expression in murine AT not only promotes energy expenditure and reduces obesity, it also protects the animals from diet induced and genetically favoured

obesity[21,22]. However, ablation of UCP1 in mice, despite reducing energy expenditure, did not lead to the development of obesity under normal laboratory conditions (housing at 22-24°C)[23]. On the contrary, housing at thermoneutrality (30°C) promoted the onset of obesity in these mice[24]. Furthermore, a reduction of BAT itself drastically reduces overall energy expenditure and increases obesity[25]. This and the fact that the amount of active BAT depots in adult humans inversely correlates with the body mass index[14–17], suggest that novel mechanisms regulating BAT development and metabolism need to be investigated to yield new therapeutic approaches to fight obesity.

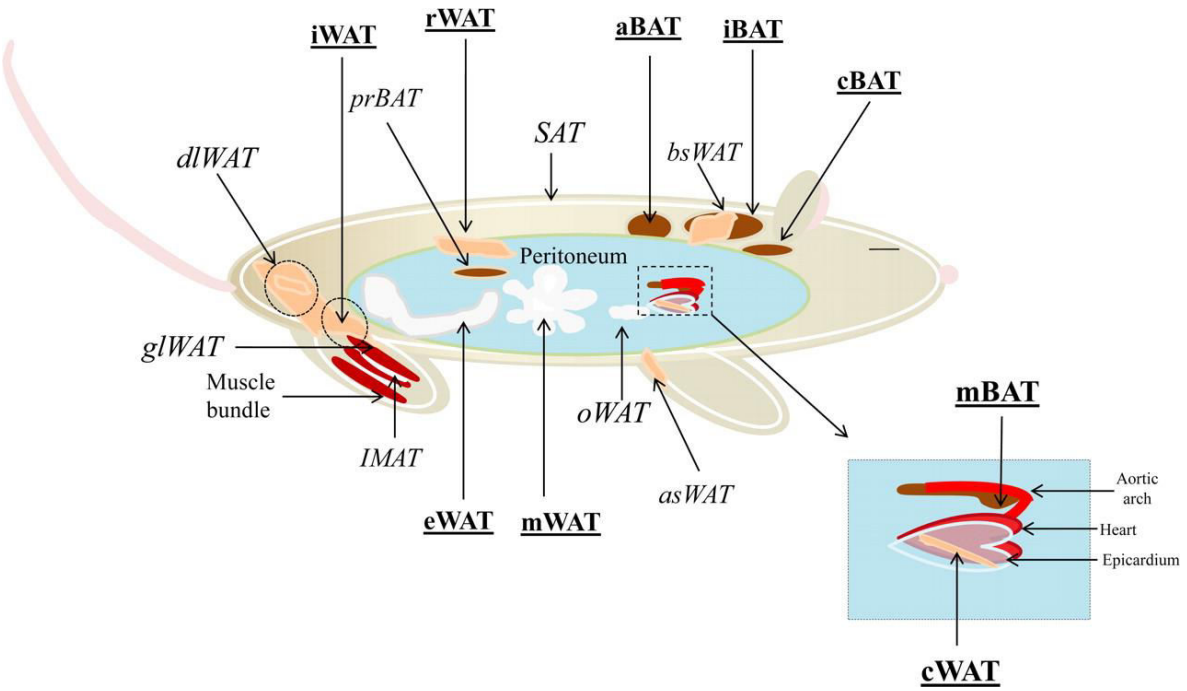

Figure 1: Distribution of white, brown and beige adipose depots in the mouse[4]. Brown adipose tissues are dark brown, beige are light brown and depots only consisting of white adipocytes are white. iBAT, interscapular BAT; cBAT, cervical BAT; aBAT, axillary BAT; mBAT, mediastinic BAT; prBAT, perirenal BAT; cWAT, cardiac WAT; dlWAT, dorsolumbar WAT; iWAT, inguinal WAT; rWAT, retroperitoneal WAT; mWAT, mesenteric WAT; eWAT, epididymal WAT; bsWAT, back subcutaneous WAT; asWAT, anterior subcutaneous WAT; glWAT, gluteal WAT; oWAT, omental WAT; IMAT, intramuscular adipose tissue; SAT, subdermal adipose tissue.

In addition to white and brown adipocytes, a third type of fat cells, namely brite ("brown in white") or beige adipocytes, is intensively investigated since a couple of years[26]. Beige adipocytes also contain UCP1 and are activated upon adrenergic stimuli, but originate from a different developmental lineage than brown adipocytes and are often found dispersed in WAT depots[6,26]. Classical brown adipocytes derive from Myf5 positive (Myf5+) progenitor cells and share a common developmental origin with muscle cells[27]. On the other hand, beige adipocytes emerge from the same stem cells like white adipocytes that are preferentially Myf5 negative[28] (fig. 2). Nevertheless, developmental origins of white and beige adipocytes are not definitely clear and may vary among different WAT depots[28,29]. In addition to the possibility that beige adipocytes differentiate from special precursor cells, a process

called “trans-differentiation” is highly investigated. This is the conversion of white adipocytes into beige adipocytes under certain stimuli such as cold or chronic, pharmaceutical β-adrenergic stimulation[2,30,31]. Recent studies suggest that human BAT more likely resembles beige adipocytes because it expresses markers predominately present in beige precursor cells[26,32]. One therapeutic approach may therefore be the activation of beige cell development and/or the induction of a white to brown shift to increase energy expenditure accompanied by a beneficial weight loss in obese patients[33].

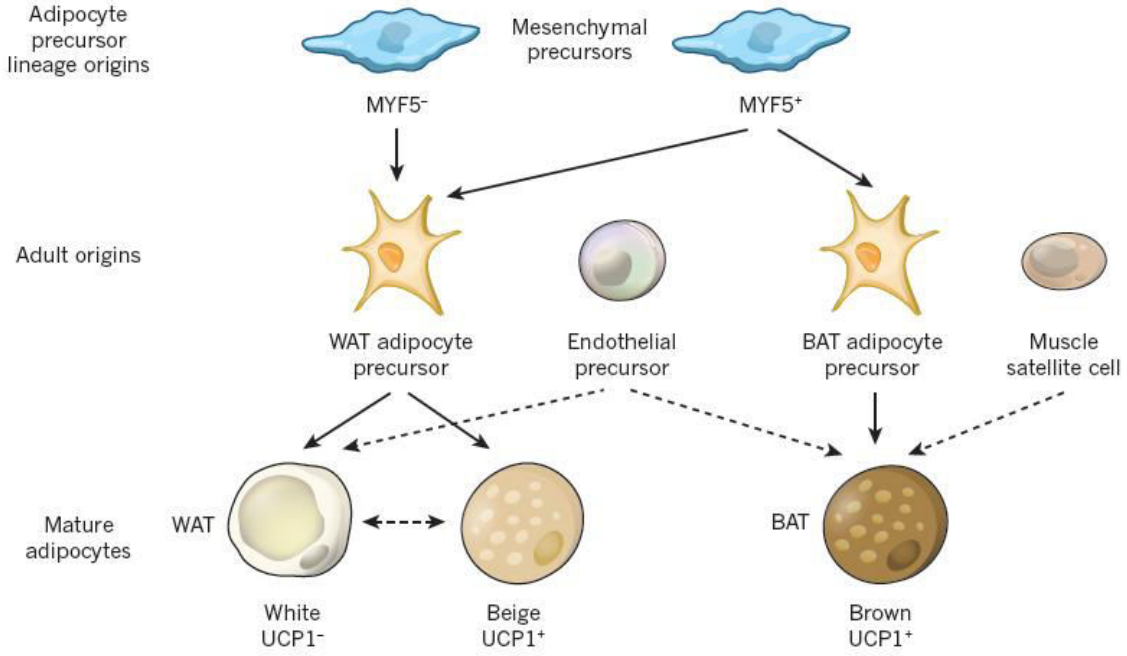

Figure 2: Different types of adipocytes derive from different progenitor cells[29].

Besides their differences, white and brown adipocytes share common features and pathways. During adipogenesis, the development of fat cells, peroxisome proliferator activated receptor-gamma (PPARγ) plays a central role in both cell types, as the “master regulator” of adipogenesis. Preadipocytes lacking PPARγ fail to differentiate into mature adipocytes.[34] PPARγ is a member of the PPAR family, a family of nuclear hormone receptors that are activated upon ligand binding and bind to the DNA after recognition of specific PPAR response elements (PPREs). PPARγ associates with retinoid X receptors (RXR) to build a heterodimer and thereby regulates transcription.[35] Activation of PPARγ leads to the transcriptional activation of a cascade of genes that are important for the phenotypic development of adipocytes, including genes important for lipid transport and metabolism (e.g. *aP2*[36] and acetyl-CoA synthetase[37]), glucose homeostasis (e.g. *Glut4*) and adipokine production (e.g. adiponectin[38]).[39–41] PPARγ performs its action in coordination with CCAAT/enhancer (C/EBP) binding proteins. This group of transcription factors is not absolutely crucial for adipogenesis, but helps in the promotion of terminal

differentiation[39,42,43]. Although the main endogenous ligand of PPARγ has not yet been discovered, several natural (e.g. derivates of archidonic acid[44]) and synthetic agonists (e.g. thiazolidinediones, TZDs[45]) have been described to activate PPARγ. Interestingly, although PPARγ is the key factor for general adipogenesis, it has been shown that chronic pharmaceutical PPARγ activation leads to "browning" of white adipose tissue depots[46].

Needless to say, there are many differential expressed genes in WAT and BAT giving them their special phenotypic features[47]. Important for adipose depot-selective transcriptional regulation are PPAR co-regulators. These proteins do not bind DNA themselves, but associate with PPARs to enhance transcriptional activity.[48] Whereas co-activator Tif2 is involved in promoting white adipogenesis[49], peroxisome proliferator-activated receptor gamma coactivator 1-alpha (PGC-1α) and PR-domain containing 16 (PRDM16) are especially relevant for brown adipogenesis[50,51]. PPARα, another member of the PPAR family, plays a special role in BAT development. PPARα together with PGC-1α, mediate mitochondrial biogenesis and regulate thermogenesis in brown adipocytes[52]. Transcriptional co-activator PRDM16 has been implicated in regulating the commitment of Myf5+ progenitors to the brown adipocyte lineage via forming a complex with C/EBPβ[27,53]. PRDM16 also interacts with other transcription factors, including PPARγ and PGC1-α[50,54] and is crucial for the recruitment of beige adipocytes in WAT[55]. Besides specific co-activators, also epigenetic markers and micro RNAs (miRNAs) play important roles in determining the adipogenic fate of precursor cells[29].

The beneficial properties of brown and beige adipocytes cannot occur without proper recruitment and activation. Thereby, the sympathetic nervous system plays a central role in regulating the metabolic differences of white, beige and brown adipose tissue in energy homeostasis. Importantly, an interplay between nutrient release, uptake and utilization must be coordinated between WAT, BAT and other metabolic tissues such as skeletal muscle and liver to permit a successful crosstalk between those tissues[56].

Lipolysis in adipose stores is activated by increasing intracellular cAMP concentrations after stimulation of β-adrenergic receptors. This activates protein kinase A (PKA) and leads to the phosphorylation of perilipin-1 and HSL. Phosphorylated perilipin releases CGI-58 which subsequently activates ATGL. Furthermore, HSL is recruited to lipid droplets where lipolysis takes place.[3] Fasting is a potent stimulator of the sympathetic outflow to WAT. Adipocytes derived FFA are transported to peripheral organs such as liver, where the very low density lipoprotein (VLDL)-production is enhanced. VLDLs contain high amounts of triglycerides (TGs) that are cleaved into FFA by lipoprotein lipase. These FFA are in turn used for energy production in peripheral tissues, like muscle and BAT.[56] Cold stimuli induce a β-adrenergic cascade in BAT, where activated PKA not only leads to the catabolism of TGs, but also phosphorylates transcription factors that increase UCP1 expression and therefore centrally impacts on thermogenesis[8].

1.2 The role of adipose tissue in regulating glucose homeostasis

The increasing prevalence of obesity is tightly connected with the development of insulin resistance and type II diabetes[1,57]. In this context, the importance of white as well as brown adipose tissue in regulating glucose homeostasis has to be mentioned. Not only nutritional lipids contribute to increased fat accumulation in AT, postprandial insulin secretion from pancreatic β-cells also leads to glucose uptake of adipose tissues via the glucose transporter *Glut4*. In parallel, the insulin signaling cascade activates lipogenesis and inhibits lipolysis in AT. Although WAT glucose uptake only accounts for a small amount of glucose disposal (75% are taken up by skeletal muscle), it is profoundly involved in glucose homeostasis.[58] An example is the fact that fat-specific deletion of the main glucose transporter *Glut4* impairs systemic glucose uptake, especially in liver and muscle[59]. In addition to classical ways of glucose disposal, adipose tissue secretes adipokines that regulate systemic glucose homeostasis. One example is adiponectin which is an insulin sensitizing protein regulating glucose uptake by liver and skeletal muscle.[60] Furthermore, the central role of AT in the development of insulin resistance is emphasized by the observation that one of the major pathophysiologies underlying the development of type II diabetes is chronic low-grade adipose tissue inflammation. In obese states, adipocytes release cytokines that recruit immune cells to the AT. Consequently, the secretion of pro-inflammatory cytokines, such as tumor necrosis factor alpha (TNF-α), is further increased which creates a feed forward loop that leads to systemic disturbances in insulin sensitivity[61,62].

In the last several years BAT has also been recognized as an important regulator of plasma glucose levels. Bartelt and associates[63] showed that activated BAT does not only potently clear TGs from the bloodstream, but also takes up substantial amounts of glucose. In a different study, Stanford and co-workers[64] showed that BAT transplantations can ameliorate already existing insulin resistance in obese mice. Importantly, human BAT depots were first recognized because of their high tracer-labeled-glucose uptake in positron-emission tomography (PET)[13,15] and BAT could therefore be an important organ contributing to glucose homeostasis in humans, too.

Lipid and glucose homeostasis are tightly intertwined in adipocytes. Glucose is converted into glycerol which is the carbon backbone of TGs. BAT especially depends on intracellular lipid synthesis and storage because of its high metabolic activity. Besides being substrate for *de novo* lipogenesis and glycerol synthesis, glucose is also used for energy production in mitochondria which further supports the high energy need in brown adipocytes.[20] A simple scheme of the glucose and lipid pathways that are activated after β-adrenergic stimulation is presented in figure 3.

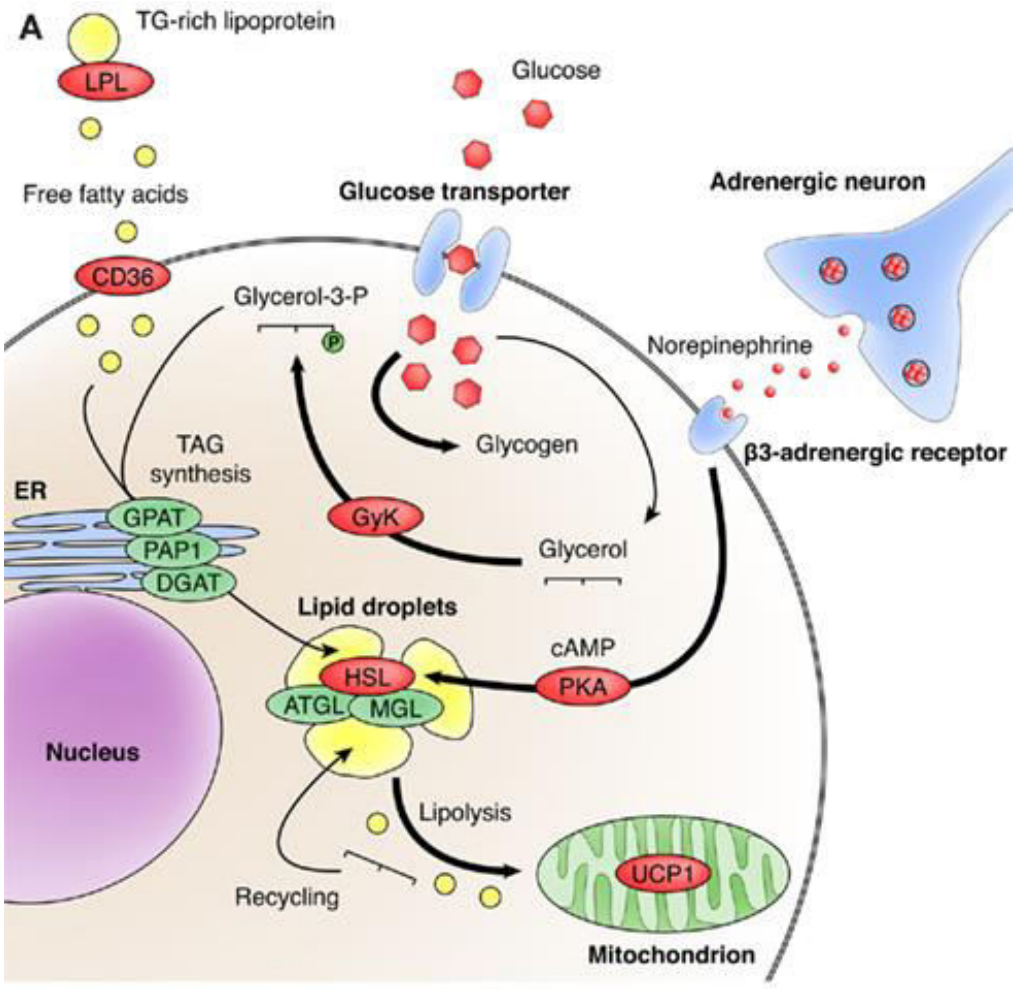

Figure 3: The glucose and lipid metabolism of brown adipocytes in response to β-adrenergic stimuli. Red marked enzymes and pathways with a thick arrow are activated after norepinephrine binding. AGPAT, acylglycerol-3-phosphate-O-acyltransferase; ATGL, adipose triglyceride lipase; CD36, fatty acid translocase; DGAT, diacylglycerol acyltransferase; GPAT, glycerol 3-phosphate acyltransferase; GyK, glycerokinase; HSL, hormone-sensitive lipase; LPL, lipoprotein lipase; MGL, monoacylglycerol lipase; PAP1, phosphatidic acid phosphatase 1; PKA, protein kinase A; UCP1, uncoupling protein 1. Adapted from ref. [20]

Strategies to counteract obesity and type II diabetes are of great importance nowadays. For developing successful therapeutic approaches, detailed understanding of adipogenesis and investigation of metabolic pathways in white and brown adipocytes is essential. For this reason, our laboratory concentrates on elucidating new candidate genes important for the development and metabolism of white and brown adipocytes.

1.3 N-acetyltransferase 8-like (Nat8l) – a new player in brown adipogenic development and metabolism

In the past, many factors influencing white and brown adipogenesis have been identified with the help of high-throughput technologies. To find new candidates that possibly control adipogenesis or influence adipocyte metabolism, we performed gene expression studies in WAT and BAT of *Atgl* and hormone sensitive lipase *Hsl* knockout mice[65]. Thereby, we focused on genes that might have a metabolic significance, but are not yet described in adipose tissue biology. Among the interesting candidates was a gene encoding for the enzyme N-acetyltransferase 8-like (*Nat8l*).

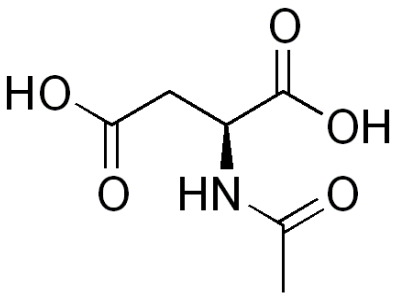

Figure 4: Molecular structure of NAA.
Source: www.wikipedia.org, July 2014

NAT8L catalyzes the formation of N-acetylaspartate (NAA, fig. 4) using acetyl-CoA and L-aspartate. In brain, NAT8L is well described as the main NAA-forming enzyme[66–68]. The *Nat8l* gene is organized in 3 exons located on mouse chromosome 5 (human chromosome 4) (accession number: NM_001001985) and encodes a 33 kilo Dalton (kDa) protein (299 amino acids) (www.ncbi.nlm.nih.gov/gene and www.ensembl.org, July 2014). The N-terminus is highly conserved among NAT8L orthologs (e.g. human, mouse and zebrafish) and contains a proline and alanine rich region of variable length[66].

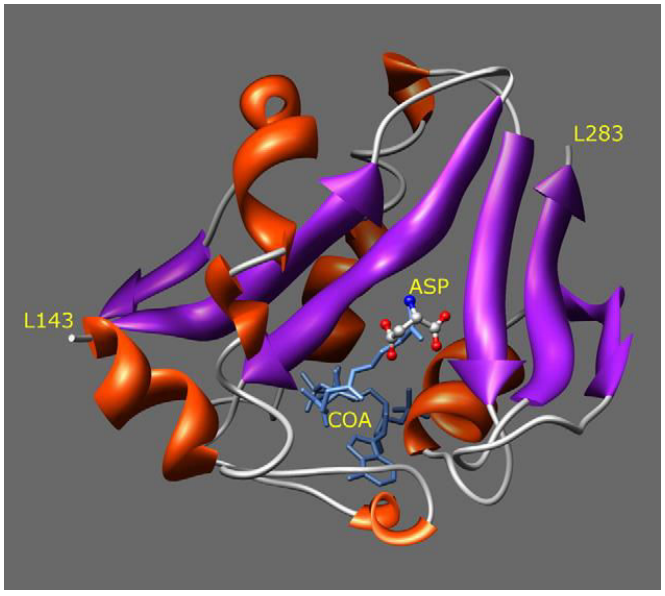

Figure 5: Structural model of NAT8L based on *in silico* homology mappings with other N-acetyltransferases[67].

Furthermore, the protein contains a highly hydrophobic stretch of about 30 amino acids (starting at amino acid 116 in the murine protein) that is suggested to be involved in membrane binding[66,69]. The consequent C-terminus is homologous within the family of N-acetyltransferases. Among them are human cysteine S-conjugate N-acetyltransferase (NAT8Hs) and polyamine N-acetyltransferase (*PaiA*) from *B. subtilis*.[66,69] Interestingly, the murine ortholog of *PaiA* spermidine/ spermine N1-acetyltransferase (SSAT) is implicated in the regulation of

adipogenesis and lipid metabolism[70,71]. Altered expression levels of SSAT in mice influence the intracellular acetyl-CoA availability and affect lipid metabolism. While SSAT transgenic mice are lean, SSAT-ko mice tend to accumulate more fat than their wt-littermates.[72]

Whereas N-terminal regions of NAT8L do not seem to contain the active site, amino acids before (R78 and E98 in mouse) and after (D165 and R217, also mouse) the membrane binding region have been shown to be involved in mediating the catalytic activity of NAT8L[69]. A structural model based on homology mapping that contains the aspartate and acetyl-CoA binding pocket is shown in figure 5 [67]. NAT8L's mammalian orthologs show a high homology on DNA and protein level (human to murine *Nat8l* >90% on nucleotide and >94% on protein level) (www.genecards.org, July 2014).

NAA, the product of NAT8L's enzymatic activity, is one of the most abundant amino acid derivatives in the brain and its concentration can reach up to 10 mM[73]. Since NAA has been discovered by Tallan and associates[74] over five decades ago, numerous functions in brain have been assigned to this molecule. NAA is involved in the osmoregulation of the brain, a precursor for the synthesis of the neuropeptide N-acetylaspartylglutamic acid (NAAG) and used in diagnostics as a marker for proton magnetic resonance spectroscopy of brain tissue because of its high abundance (for review see[75]). Most importantly, NAA is crucial for myelin-lipid synthesis, where it acts as a carrier of acetyl groups between neurons and oligodendrocytes[76–78]. Concordantly, *Nat8l* is reported to be mainly expressed in neurons[79]. The localization of NAT8L in neurons is still discussed. No signal peptide defining its localization is predicted for the protein[69]. The group of van Schaftingen localized it in the endoplasmic reticulum (ER)[69], whereas Namboodiri and co-workers found it mainly expressed in mitochondria[67].

After synthesis, NAA is transported out of neurons by a mechanism that may involve sodium-coupled high-affinity carboxylate transporter NaDC3 (SLC13A3)[80] and shuttled into oligodendrocytes. In oligodendrocytes, NAA is catabolized by the action of aspartoacylase (ASPA) into acetate and L-aspartate[78]. The resulting acetate is utilized by the enzyme acetyl-CoA synthetase for acetyl-CoA synthesis which is a building block for (myelin-) lipid synthesis[81]. A scheme of NAA production and transport between neurons and oligodendrocytes can be seen in figure 6.

The metabolic importance of NAA was shown in patients with Canavan disease. This is a severe, hereditary, neurodegenerative disorder with defective NAA catabolism that leads to reduced myelin synthesis[82,83]. Further, one human case is described with a mutation in the *Nat8l* gene that leads to the loss of NAA production. This disease is called hypoacetylaspartia and is also characterized by reduced myelin production[66,84,85]. In addition to its involvement in myelin lipid-synthesis, NAA production is proposed to be connected to energy metabolism in neurons[76,86,87]. There is a direct correlation between ATP production, oxygen consumption and NAA production. When ATP synthesis decreases, for example

through traumatic brain injury or inhibitors of the respiratory chain, NAA production also drops.[88,89]

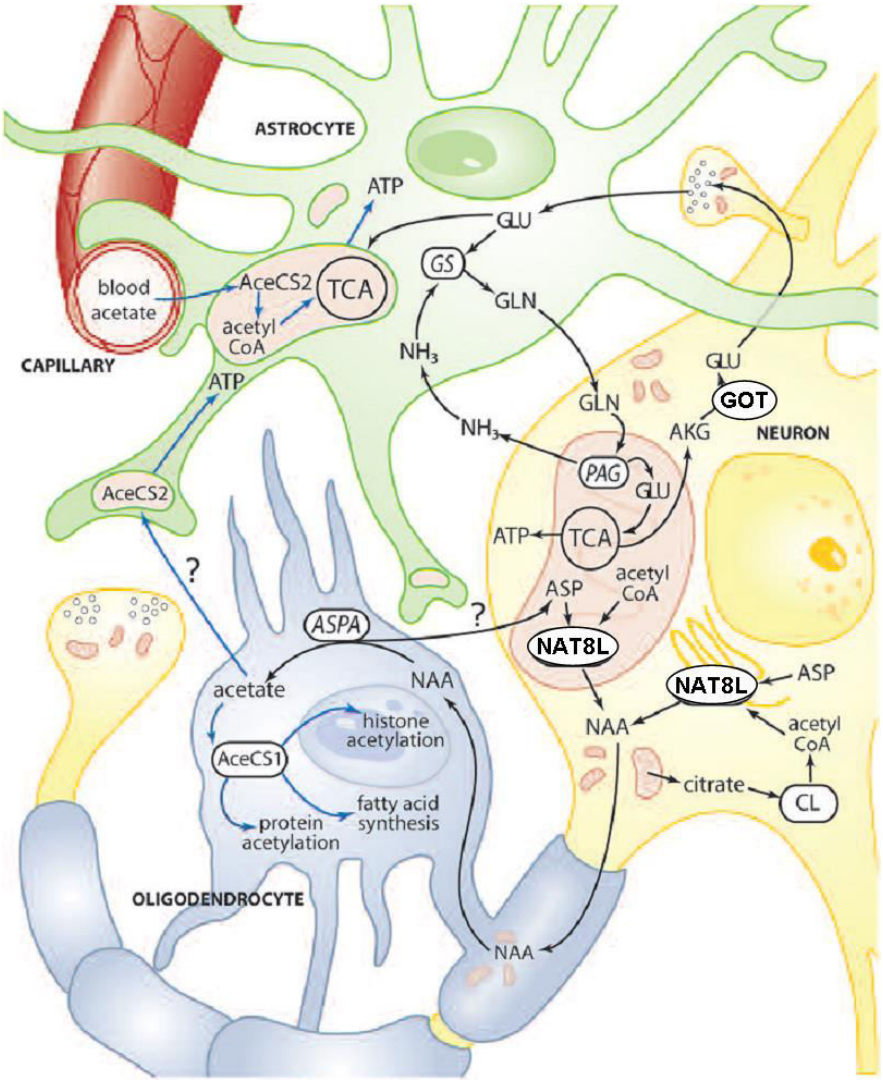

Figure 6: Scheme of NAT8L pathway and shutteling of metabolites between different cell types of the brain. AceCS1&2, acetyl CoA synthase-1&2; AKG, a-ketoglutarate; ASP, aspartate; ASPA, aspartoacylase; CL, ATP citrate lyase; GLN, glutamine; GLU, glutamate; GOT, glutamate-oxaloacetate transaminase; GS, glutamine synthase; NH3, ammonia; PAG, phosphate activated glutaminase. Adapted from reference [81]

Nat8l caught our attention because we found it deregulated in adipose tissue of mice with a metabolic phenotype, such as *ob/ob* mice and *Atgl* knockout mice[65]. Based on observations that *Nat8l* is highly expressed in ATs, especially BAT, and that its expression is induced during differentiation of various murine and human adipogenic cell lines, we established an immortalized brown adipogenic cell line (iBACs) stably overexpressing *Nat8l*[90]. The characterization of this cell line showed that overexpression of *Nat8l* leads to delayed lipid accumulation in these cells. Additionally, mRNA expression of various brown marker genes is increased in *Nat8l* overexpressing iBACs. Starting from these results, this part of this thesis aims to further investigate the role of NAT8L in brown adipocyte biology.

1.4 Adipocyte plasma membrane associated protein (APMAP) and its function in adipogenesis and energy homeostasis

Adipocyte plasma membrane-associated protein (APMAP) was first described in 2001[91]. Albrektsen and co-workers[91] searched for transcripts upregulated during the differentiation of murine 3T3-L1 cells and found *Apmap* as a novel candidate. They showed that *Apmap* is highly expressed in adipose tissue, liver, heart, kidney, and to a lower extent in brain and lung. APMAP is a glycosylated protein (amino acids 159-162) of approx. 47 kDa (415 amino acids) that contains a transmembrane region consisting of a hydrophobic stretch of 19 amino acids (amino acid 42-60). The gene is organized in 9 exons and located on murine chromosome 2 (human chromosome 20) (accession number: NM_027977) (www.ncbi.nlm.nih.gov/gene and www.ensembl.org, July 2014). Albrektsen and co-workers located APMAP in the plasma membrane of adipocytes and named it thereafter[91]. Further predictions and homology mappings indicated APMAP as a type II integral membrane protein organized in a 6-bladed β-propeller structure[92,93] (fig. 7 and 8).

The human ortholog shows a high similarity with the murine transcript and protein (87% on nucleotide level and 90% on protein level) (www.genecards.org[94]). Homology mapping of APMAP revealed that it features structural similarities to strictosidine synthase[95], serum paraoxonase PON1[96], diisopropylfluorophosphatase (DFpase)[97], and regucalcin[98]. Interestingly, these proteins share the six-bladed β-propeller structure and most of them were shown to be calcium-dependent phosphotriesterases. This group of enzymes is involved in the hydrolysis and thereby inactivation of organophosphates, which gives them detoxifying characteristics.[97,99] The plasma enzyme PON1, for example, exhibits anti-oxidant properties and has been implicated in preventing atherosclerosis[96]. Regucalcin is important for cellular calcium binding and was shown to be involved in regulating glucose and lipid metabolism[98].

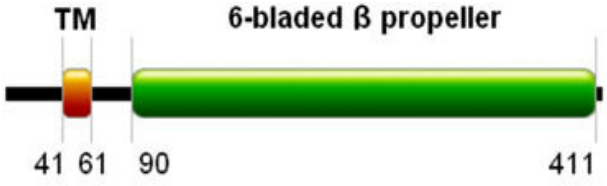

Figure 7: Protein architecture of APMAP[93].
TM... transmembrane region.

There are four conserved amino acids present in APMAP that are predicted to mediate calcium binding in the active site (E103, N201, N260 and D306/N307). Based on that information it is predicted to be a calcium dependent hydrolase.[93] Ilhan and associates[100] investigated the expression pattern of human APMAP and showed a high mRNA expression in liver and kidney. Furthermore, this research group brought APMAP in context with a detoxifying role in plasma. They found APMAP expressed on arterial walls and in endothelial cells surrounding pancreatic islets and kidney and showed a detoxifying arylesterase activity[100]. Recent studies revealed a homology of *Apmap* with the Drosophila gene

hemomucin which is involved in hemolymph clotting[101]. Thiessen and co-workers[102] performed proteomic analysis of the coagulation reaction in human plasma and also found the APMAP protein involved in this process, which renders APMAP to have a role in plasma.

We performed a novel method to prioritize gene expression data from candidate genes involved in adipogenesis[103] and found *Apmap* in the same transcriptional cluster as PPARγ.[93] Further, our working group showed that *Apmap* is upregulated during the differentiation of murine adipogenic cells (3T3-L1, OP9 and mouse embryonic fibroblasts, MEFs) and human SGBS cells (Simpson-Golabi-Behmel syndrome). When *Apmap* is stably silenced, 3T3-L1 cells lose their potential to differentiate into mature adipocytes, implicating that APMAP is required for adipogenesis. Moreover, we identified that *Apmap* is a direct and functional PPARγ target gene and we also showed that the protein translocates from the ER to the plasma membrane during adipogenesis.

To further investigate the role of *Apmap* in adipogenic development in a systemic context and to assess its functional role in metabolism, this thesis aims to generate a mouse model lacking *Apmap* and study the consequences of loss of this protein *in vivo*. Furthermore, we also included *in vitro* assays in this study to unravel the role of APMAP in the regulation of lipid and glucose homeostasis in adipocytes.

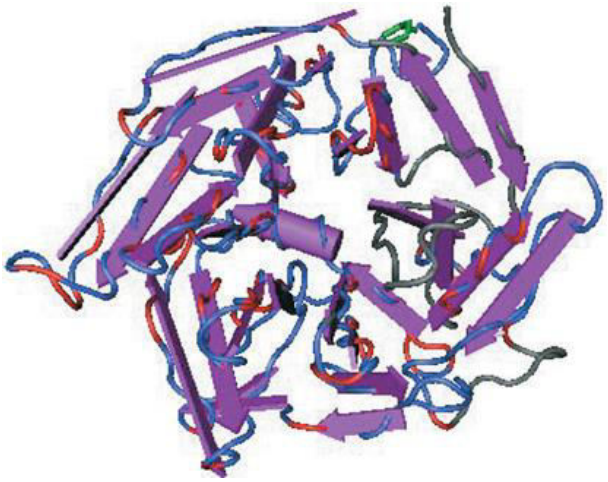

Figure 8: Three dimensional structure of APMAP[100]. B-sheets are represented as arrows. The six-bladed β-propeller is depicted in this scheme.

Materials & Methods

2 Materials and Methods

2.1 Animal studies

Male C57BL/6 (age mentioned in figures and text) and 4 months old male *ob/ob* mice were used. Male or female *Apmap* knockout mice and the respective littermates at the ages indicated in the text and figures were used for this study. Animals were kept on a 12/12 hours light/dark cycle and were fed either chow diet (4.5% calories in fat) or put on high fat diet with the indicated age (HFD; as mentioned either 40% or 60% calories in fat, Sniff Spezialdiäten GmbH). C57BL/6 mice were fed a rosiglitazone containing chow diet (0.01% w/w) for 7 weeks. Tissues were harvested from mice in *fed ad libitum* state or after overnight (o/n) fasting. Refed mice were fasted for 12 hours o/n prior to one hour access to food.
For tail-tip PCRs, Taq-polymerase and an annealing temperature of 65°C was used. Primers for *Apmap*-tailtip-PCRs are the following:

Primer 1 (LoxP_check_fw): 5'GCCATTCAGGTCTCCAGGTAG3';
Primer 2 (LoxP_check_rv): 5'CGGTGAAGGAATGTGGGGGTA3';
Primer 3 (Apmap_check_fromSA_neu_rv): 5'AAAGCAGCCATTTCACCGGGC3'.

Body composition was assessed with the miniSpec NMR Analyzer (Bruker Optics).
Mouse experiments were approved by the Austrian Federal Ministry of Science and Research, Division of Genetic Engineering and Animal Experiments.

2.2 Cell culture, adipogenic differentiation and lipid staining

Immortalized brown adipogenic cells (iBACs) were grown in DMEM (4.5 g/L glucose) supplemented with 10% FBS, 2 mM L-glutamine (L-glut), 50 µg/mL streptomycin, 50 units/mL penicillin (P/S), and 20mM Hepes at 37°C, 5% CO_2. iBACs were induced to differentiate at the day of confluence with 0.5 mM 3-isobutyl-1-methylxanthine (IBMX), 0.5 µM dexamethasone (Dex), 20 nM insulin, 1 nM T3 (triiodthyronine), and 125 µM indomethacin. Two days after induction, medium was changed to maintenance medium containing 20 nM insulin and 1 nM T3 and cells were kept in this medium until harvest. iBACs stably overexpressing *Nat8l* were already generated during the diploma thesis of H. Pelzmann[90] and the method is also described in ref. [104]. To stimulate β3-adrenergic receptors, cells were incubated with 1 µM isoproterenol for 4 hours. iBACs were treated with 10 µM PPARα antagonist GW6471 (Tocris Bioscience) from day 4 until harvest. Supernatants and cells (scraped from the culture dish with PBS) were harvested at the indicated time points. Cellular triglyceride content was determined from cells and

supernatants using Infinity Triglyceride Reagent (Thermo). Free fatty acid content was measured using the NEFA C test kit (WAKO). Values were corrected by protein content, measured in the cell lysate using the BCA reagent (Pierce Biotechnology).

Cos7 and 3T3-L1 cells were grown in DMEM (4.5 g/L glucose) containing 10% FBS L-glut and P/S at 37°C, 5% CO_2. 3T3-L1 were induced to differentiate 2 days after 100% confluence using 0.5mM IBMX, 1 µM Dex and 2 µg/mL insulin. On day 3 of differentiation, medium was changed to DMEM containing 2 µg/mL insulin and from day 5 of differentiation cells were kept in normal growth medium until harvest.

2.3 Cell culture and manipulation of murine HM-1 embryonic stem cells

HM-1 embryonic stem cells (ES cells, from mouse strain 129, agouti coat color) were a kind gift of Franz Radner and Günter Hämmerle (University of Graz). ES cells were maintained in complete medium: Knockout DMEM (Life Technologies) supplemented with 15% FCS, L-glutamine, sodium pyruvate, non-essential amino acids, β-mercaptoethanol and leukemia inhibitory factor (LIF). Cells were seeded on gelatin (0.1% in PBS) coated dishes and maintained in 10% CO_2 at 37°C.

To induce homologous recombination, the linearized targeting vector (around 250 µg, described in the result section) was electroporated into ~10^7 ES cells and positive clones were selected with G418 (400 µg/mL) for 7 days. Colonies were picked under the microscope, expanded and tested for homologous recombination with PCR and Southern blot. 2 positive clones were further manipulated with electroporation of a Cre-recombinase containing plasmid (pCrePac, kind gift of F. Radner and G. Hämmerle), selected with puromycin (1.5 µg/mL) for 36 hours, and verified with Southern blot. 2 verified knockout or floxed clones were injected into blastocysts (University of Veterinary Medicine, Vienna; Dr. Thomas Rülicke) and transplanted into pseudo-pregnant mice. A detailed description of the procedures can be found in the results section.

2.4 RNA isolation, reverse transcription, and gene expression analysis

Total RNA from cells was isolated using the Total RNA isolation kit (Sigma) and tissue RNA was isolated with TRIzol® reagent (Invitrogen, Carlsbad, USA) according to the manufacturer's protocols. cDNA was generated using Superscipt II reverse transcriptase (Invitrogen). mRNA expression was assessed using real-time PCR as described in [93] using an ABI Prism 7700 Sequence Detector system and SYBR Green PCR master mix (Applied Biosystems, Darmstadt, Germany). Gene expression was normalized to *TfIIß* in murine tissues and cells and to *ß-ACTIN* in human cells.

Relative mRNA expression levels were calculated using averaged 2^{-ddCt} values for each biological replicate as implemented before[105]. Primers are listed in table 1.

Table 1: Primer pairs used for qRT-PCR. All primers were used with murine cDNA, except the indicated human primers. -mt, mitochondrial localization; -ct, cytosolic localization.

Target gene	Forward primer 5'→ 3'	Reverse primer 5'→ 3'
Acc1-ct	TGGTGCAGAGGTACCGAAGTG	CGTAGTGGCCGTTCTGAAACT
Acc2-mt	CACAAGAAACTGGACCTGCAC	ATACACTTGACCGCAGCGATG
Acly	AGGAAGTGCCACCTCCAACAGT	CGCTCATCACAGATGCTGGTCA
Acsl1	TCCTACAAAGAGGTGGCAGAACT	GGCTTGAACCCCTTCTGGAT
Acss1-mt	GATGAAGCTGTGAAGAGCTGC	TTGGCCATCTCCTGTTCAAGG
Acss2-ct	CTGAGTGGATGAAAGGAGCAAC	CAGGAGTTCACGGTATGTGATC
Adipoq	TGTTCCTCTTAATCCTGCCCA	CCAACCTGCACAAGTTCCCTT
Agpat2	CCAGAACTGCCATGTCTGTGA	GTAGATCCACACTTTGAGATTCTCCTT
Apmap (E3/4)	CCTTGCAAAACCCGAGATGA	AACAGTCCCTTGTACGCATCAAC
Apmap 5'UTR/E1	GAGTGTCAAGGCGCTGTTGG	GGCCATCGTCCGTGACGAC
Aralar (Slc25a12)	GGCCTGTACAACGATCCAAAC	CTGGAGCACATAGAACAGATTC
Aspa	CCATATGAAGTGAGAAGGGCTC	CCTCAAGAATAAGAGTGCAACC
Atgl	GTCCTTCACCATCCGCTTGTT	CTCTTGGCCCTCATCACCAG
CD36	GGCCAAGCTATTGCGACAT	CAGATCCGAACACAGCGTAGA
C/ebpβ	GGACTTGATGCAATCCGGA	AACCCCGCAGGAACATCTTTA
Cidea	TGACATTCATGGGATTGCAGAC	GGCCAGTTGTGATGACTAAGAC
Cs	CATCTGGAGCAGAGCCCTAG	TCAGTTTCCCCCCAGTCTCC
Cox1-mt	TGAGCCCACCACATATTCACAG	AGGGTTGCAAGTCAGCTAAATAC
Cox8b	GCGAAGTTCACAGTGGTTCC	AACCATGAAGCCAACGACTATG
Cpt1b	TGTATCGCCGCAAACTGGACCG	TCTGGTAGGAGCACATGGGCAC
Dgat1	GACGGCTACTGGGATCTGA	TCACCACACACCAATTCAGG
Dgat2	CACAGACTGCTGGCTGATAGCT	CGATCTCCTGCCACCTTTCTT
Dio2	AACAGCTTCCTCCTAGATGCC	CATCAGCGGTCTTCTCCGAG
Fabp3	CCTTTGTCGGTACCTGGAAGCT	AAAGCCCACACCGAGTGACTT
Fabp4 / aP2	CGACAGGAAGGTGAAGAGCATC	ACCACCAGCTTGTCACCATCTC
Fads3	GTGATCCACACGAACCAGTG	TCCCGCTTTTTCTTGTCCTAC
Fas	GCTGTAGCACACATCCTAGGCA	TCGTGTTCTCGTTCCAGGATC
Fatp1	TCACTGGCGCTGCTTTGGTT	TAGCCGAACACGAATCAGAA
Fatp4	GAAGAGGGTCCAGATGCTCT	GTGAGATGGCCTCAGCTATC
Glut1	GGGCATGTGCTTCCAGTATGT	ACGAGGAGCACCGTGAAGAT
Glut4	CCATTCCCTGGTTCATTGTGG	TAAGGACCCATAGCATCCGCA
Got1 (AAT1)-ct	GAGTTCCGGAGCTGTGCTTC	CAATCCGAAGAGCGCCTGTC
Got2 (AAT2)-mt	TATGCCAAGAACATGGGCCTG	GAGAGGTGGGTTGGAATACAG
Gpat	GCGGAAAAACTACGGCTACGT	TCTGACTCTGGCCTTCTAAATATTCCT
Hsl	CCATCTCACCTCCCTTGG	TCCTTCCCGTAGGTCATAGG
human APMAP	CACAGCCTCTCAGCTTCAAA	ATGTGCTATGGACTCCGGTC
human NAT8L	TGTGCATCCGCGAGTTCCGT	CGGAAGGCCGTGTTAGGGAT
human β-ACTIN	CGCCGCATCCTCCTCTTC	GACACCGGAACCGCTCATT
Lpin1	GTCGTCGAGCAAGACAGATTCC	ACCAGGATCCCCATTCTTGG
Mdh1	CTTCCCCTTCTGCAGGATGTC	GGCATGGAGCCCACTAGGA
Mdh2	AGACCAGAGCAAATGTGAAAGG	TCCCGTGTCATTCCTGGTTTC
Me1	CATGCCAGCAGTACAGTTTGG	TAGCCTTGACGACATCCTCTG
Me2	CGATTGTGTACACGCCAACAG	GATCTAACATGACCTCTGTCTG
Nat8l	TGTGCATCCGCGAGTTCCGC	GCGGAAAGCCGTGTTGGGGA
Pcx	TTTGGACACAGAGGTACCCCTG	GTTGCCAGACTTCATGGTAGCC
Pdk4	TTTCTCGTCTCTACGCCAAG	GATACACCAGTCATCAGCTTCG
Pgc1α	TCTCTGGAACTGCAGGCCTAAC	TCAGCTTTGGCGAAGCCTT
Pparα	CCTGAACATCGAGTGTCGAATATG	GCGAATTGCATTGTGTGACATC
Pparγ2	TGCCTATGAGCACTTCACAAGAAAT	CGAAGTTGGTGGGCCAGAA

Target gene	Forward primer 5'→ 3'	Reverse primer 5'→ 3'
Prdm16	TCCACAGCACGGTGAAGCCA	ATCTGCGTCCTGCAGTCGGC
Psat1	AGTGGAGCGCCAGAATAGAA	TACCGCCTTGTCAAGAAACC
Retn	AAGAAGGAGCTGTGGGACAGG	CAGCAGTTCAGGGACAAGGAA
TfIIβ	GTCACATGTCCGAATCATCCA	TCAATAACTCGGTCCCCTACAA
Ucp1	ACACCTGCCTCTCTCGGAAA	TAGGCTGCCCAATGAACACT

2.5 Mitochondria isolation

Mitochondria were isolated from cell pellets of differentiated iBACs with a commercial available kit (Thermo Scientific) using a Dounce homogenizer and 3000 x g to pellet the mitochondria. BAT mitochondria were isolated as described in ref. [106]. Modifications to the protocols were the following (the method is also described in ref. [104]): Brown adipose tissues were excised from male mice fed *ad libitium*, washed with ice-cold PBS and cut into small pieces with a razorblade. Subsequently, they were homogenized with ~60 strokes of a Dounce homogenizer with 1 ml IB_c (10 mM Tris/MOPS pH 7.4, 1 mM EGTA/Tris pH 7.4, 200 mM sucrose including proteinase and phosphatase inhibitors). All centrifugation steps were carried out at 4°C. The resulting cell or tissue lysate was pre-cleared with 300 x g for 5 min to reduce cell debris, and then the nuclei were pelleted at 700 x g for 10 min. The centrifugation step to pellet the mitochondria was carried out at 3000 x g for 15 min to reduce peroxisomal contamination. Nuclear fraction and mitochondrial fraction were lysed in SDS-lysis buffer (50mM Tris/HCl pH 6.8, 10% glycerol, 2.5% SDS, 1x protease inhibitor cocktail, 1 mM PMSF) and used for western blot analysis after benzonase digestion (Merck, Vienna, Austria). The post-mitochondrial supernatant containing cytosolic/ER proteins was precipitated using the TCA (trichloroacetic acid) method. Briefly, cytosolic protein lysate was mixed with 50% ice-cold TCA to obtain a concentration of 10% TCA and incubated 1.5 h on ice. Then it was centrifuged for 10 min at 13000 rpm (~18000 x g), and 4°C. The pellet was washed twice with ice-cold acetone, air-dried, and dissolved in SDS-lysis buffer. Protein measurement of all fractions was performed using the BCA protein assay kit.

2.6 Western blot analysis

After washing cells with PBS, iBACs proteins were harvested by scraping the cells with SDS-lysis buffer and thereafter benzonase digested. Protein concentrations were determined with the BCA protein assay kit. The samples were loaded onto an SDS-polyacrylamide gel (NuPAGE, Invitrogen, 10% or 4-12% depending on the protein size) and separated with MOPS buffer (Invitrogen) according to their size (175 V, approx. 1 h). Thereafter, proteins were transferred onto nitrocellulose membranes (500 mA, 1.5 h). Blots were incubated with primary antibodies at 4°C overnight and secondary antibodies at room temperature for 2 hours. Secondary antibody signals were visualized by enhanced chemiluminescence

detection (ECL SuperSignal West PICO Chemiluminescence substrate from Pierce and Amersham ECL prime substrate from GE Healthcare) using Lucent Blue films (Biozym).
All used antibodies are listed in table 2 and 3.

Table 2: Primary antibodies used for western blot analysis, including used concentration, origin and company.

Primary antibody	used concentration	origin	company
APMAP (NBP1-59984)	1:1000	rabbit	Novusbio
NAT8L (NBP1-06599)	1:1000	rabbit	Novusbio
β-ACTIN	1:250000	mouse	Sigma Aldrich
Hexokinase 1	1:1000	rabbit	Cell signaling technology
Histone H3	1:2000	rabbit	Cell signaling technology
GLUT4 (07-1404)	1:1000	rabbit	Millipore
PDI	1:1000	rabbit	Cell signaling technology
UCP1	1:750 or 1:1000	rabbit	Calbiochem

Table 3: Secondary antibodies used for detection of primary antibodies.

Secondary antibody	used concentration	origin	company
HRP-conjugated anti-mouse	1:3000	goat	DAKO
HRP-conjugated anti-rabbit	1:5000	swine	DAKO

2.7 ^{14}C-glucose uptake and lipid extraction

^{14}C-glucose uptake was performed as described in ref. [104]. Briefly, iBACs were incubated overnight with DMEM supplemented with 1 nM T3, 20 nM insulin, 0.5 g/L glucose, and 0.1 µCi D[^{14}C(U)]- glucose/mL (ARC). Thereafter, the cells were washed four times with ice-cold PBS and neutral lipids were extracted with hexane/isopropanol (3:2, vol). Thin layer chromatography was performed with hexane:diethylether:acetic acid (70:29:1, vol) as mobile phase, lipids were visualized with iodine vapour and cut out. The excised lipids were transferred into scintillation cocktail and shaken overnight. The incorporated radioactivity was measured by liquid scintillation counting in the Tri-Carb 2300TR (Packard HP) or the LS6500 (Beckman) scintillation-counter. Total glucose incorporation into each lipid class was calculated and values were normalized to protein content.

2.8 Measurement of cellular oxygen consumption rate (OCR)

Oxygen consumption rate measurement was performed as described in ref. [104]. Briefly, iBACs o/e *Nat8l* and controls were used on day 6 of differentiation, counted and plated in XF96 polystyrene cell culture microplates (Seahorse Bioscience) at a density of 40000 cells

per well. The next day, cells were washed and preincubated for 30 min in unbuffered XF assay medium (Seahorse Bioscience) supplemented with 5.5 mM D-glucose and 1 mM sodium pyruvate at 37°C in a CO_2-free environment. OCR was subsequently obtained in a time interval of 7 min using an XF96 extracellular flux analyzer (Seahorse Bioscience). Prior to the experiments, optimal concentrations of specific inhibitors/accelerators of the electron transport chain were determined by titration. The following working concentrations were used: 1 µM oligomycin, 2 µM FCCP (carbonyl cyanide-p-trifluoromethoxyphenylhydrazone), 2.5 µM antimycin A, and 10 µM norepinephrine (NE). The inhibitors/accelerators were added at the time points indicated in the figure legend. Preincubation with NE was performed for 1 hour at 37°C.

2.9 Electroporation of 3T3-L1 and iBACs

Differentiated 3T3-L1 cells were used for electroporation at the indicated time points. Either overexpression-vectors (pMSCV_Apmap and pMSCV_puro as control) or siRNA particles (non-targeting control, ntc or siRNA against *Apmap*: NM_027977, Sigma) have been used for electroporation (EP) with the Neon® Transfection System (Life Technologies) following the general protocol guidelines. Optimizations to the protocol were the following: 3T3-L1 were trypsinized with 2.5% trypsin/0.5 M collagenase for 3.5 min and then resuspended in pre-warmed growth medium. Cells were pelleted at 300 x g for 3 min and washed with PBS. Cells were counted and 70000 cells per 10 µL EP-tip or 450000 cells per 100 µL EP-tip were used. 0.5 µg plasmid DNA/10 µL tip or 2 µg plasmid DNA/100 µL tip were used and 200 nM/10 µL EP tip of siRNA particles. The EP was performed with the following program: 1400 V, 20 ms, 1 pulse and the cells were seeded at 300000 – 450000 cells per 12-well in DMEM supplemented with FBS, but without antibiotics. The medium was changed to growth medium 24 h after EP and the cells were harvested for RNA analysis or used for glucose uptake assays 48 h after EP.

2.10 Live cell imaging and immunofluorescence

3T3-L1 cells were differentiated for 5 days. Then they were prepared for electroporation as described in 2.9 and plasmids containing CFP-tagged-APMAP and YFP-tagged-GLUT4 were used for electroporation (pECFP-N1-Apmap and pEYFP-C1-Glut4, respectively). The cells were seeded on either gelatine coated coverslips (thickness #1) or on glass bottom dishes. Cells were left to recover for 2 days and then microscoped with a Leica SP5 confocal microscope.

For immunofluorescence, cells were differentiated directly on coverslips or glass bottom dishes to the indicated time points. The cells were washed and several fixation and

permeabilization methods were tested. The standard method that was used was the following: 2% paraformaldehyde (stock: 4% in PBS, pH 7.4, frozen at -20°C) and 0.2% glutaraldehyde in PBS, pH 7.4 and was incubated for 15 min at RT. After that, cells were washed thoroughly and permeabilized with 0.1% Triton X-100 for 5 min, followed by quenching and blocking with 20 mM glycine and 5% goat serum for 5 min. Alternatively, cells were permeabilized and quenched with 0.1% saponine/5% goat serum/20 mM glycine in PBS for 1 hour. Thereafter, cells were incubated with primary antibody in a dilution of 1:100 in 0.1% Tween-20 and 5% goat serum in PBS o/n at 4°C in a humid chamber. The next day, slides were washed three times for 5 min and then incubated with secondary antibodies (anti-rabbit Dylight488 and anti-rabbit Dylight594, Vector labs) for 1 hour in a humid chamber in the dark (RT). The slides were washed, counterstained with 0.025 µg/mL 4′,6-Diamidin-2-phenylindol (DAPI) and microscoped with a Leica SP3 or SP5 confocal microscope.

2.11 ^{3}H-Deoxyglucose uptake

For these experiments we used electroporated 3T3-L1 cells or iBACs o/e *Nat8l* and according controls were grown in 12-well plates and differentiated to the indicated time points in the text. On the day of the assay cells were starved in Krebs-Ringer-buffer (KRB) (140 mM NaCl, 4.7 mM KCl, 1.2 mM MgSO4*7 H_2O, 2.5 mM CaCl*2 H_2O, 20 mM Hepes, 1.2 mM KH_2PO_4*H_2O, pH 7.4) supplemented with 2% BSA (p/v) for 1.5 hours. After starving, cells were incubated in absence (basal) or presence of insulin (100 ng/mL) in KRB for 15 min. Glucose uptake was determined in duplicates with a substrate consisting of 5 mM D-glucose and 2-[^{3}H]deoxyglucose (0.1 µCi/well) in KRB for 5 min. The assay was stopped with three subsequent washing steps with ice-cold PBS. Cells were lysed with 0.5 M NaOH/0.1% SDS (p/v) and shaken for at least 30 min. Incorporated radioactivity was counted using liquid scintillation counting. Counts were normalized to protein concentrations measured with the BCA method.

2.12 Detection of mitochondrial mass by flow cytometry

The method described in ref. [104] was used. More specifically, iBACs were grown in 6 well-plates until day 7 of differentiation, trypsinized, and incubated for 20 min in suspension in DMEM supplemented with 200 nM MitoTracker™ Green (Invitrogen) at 37°C, washed with PBS and resuspended in 500 µL PBS and subjected directly to a flow cytometer (BD FACSCalibur, BD Biosciences). The forward scatter (FCS) detector was used as a measure for cell size, sideward scatter (SSC) for granulosity. The incorporated fluorescence was exited with 488 nm and detected in detector FL-1 (530 nm emission). 90% of all cells were found in Sector II and IV. We assumed that most viable cells were present in sector II.

Therefore, Sector II was chosen to compare fluorescence intensities between control and *Nat8l* o/e cells.

2.13 Relative quantification of mitochondrial DNA

iBACs o/e *Nat8l* or respective controls were harvested on day 3 or day 7 of differentiation in PBS and scraped from 6-well plates. Genomic DNA (gDNA) was isolated from the pelleted cells using the DNeasy Blood and Tissue Kit (Qiagen) following the manufactorer's instructions. The obtained gDNA was diluted to a concentration of 10 ng/µL. Relative mitochondrial DNA content was measured using the following primer:
mActb_I4_3'UTR_F: 5'TAAAACGCAGCTCAGTAACAGTCC3', and
mActb_I4_3'UTR_R: 5'CCATGAAGATCAAGGTAAGCTAAG3',
mND1_F: 5'ATTCTCCTTCTGTCAGGTCGAA3', and
mND1_R: 5'CAGCCTGACCCATAGCCATA3'.
A region located in intron 4 and 3'UTR of beta Actin (Actb_I4_3'UTR) (part of nuclear genomic DNA) was used for normalization of the mitochondrial gDNA content (NADH dehydrogenase, subunit 1, ND1 as a mitochondrial coded gene).

2.14 Transmission electron microscopy (TEM)

TEM was performed as described in ref. [107]. Briefly, iBACs were grown on an Aclar film (Gröpl, Tulln, Austria) fixed on day 7 in 2.5% (wt/vol) glutaraldehyde and 2% (wt/vol) paraformaldehyde in 0.1 M phosphate buffer, pH 7.4, for 1 h and then postfixed in 2% (wt/vol) osmium tetroxide for 1h at room temperature. The samples were dehydrated in graded series of ethanol and embedded in a TAAB epoxy resin (Gröpl). Ultrathin sections (75 nm) were cut with a Leica UC 6 Ultramicrotome and stained with lead citrate for 5 min and with uranyl acetate for 15 min. Images were taken using a FEI Tecnai G2 20 transmission electron microscope (FEI Eindhoven) with a Gatan ultrascan 1000 ccd camera. Acceleration voltage was 120 kV.

2.15 Measurement of mitochondrial membrane potential

The method is also described in ref. [104]. Fully differentiated iBACs (day 7) were seeded on 30 mm coverslips and allowed to recover overnight. Cells were incubated with the ratiometric indicator JC-1 (500 nM, Invitrogen) in full medium at 37°C for 30 min. After washing, fluorescence intensities were detected over mitochondrial regions using an array confocal laser scanning microscope built on an inverse, automatic microscope (Axio Observer.Z1, Zeiss, Germany) equipped with a 100x/1.45 NA oil immersion objective (Plan-Fluor, Zeiss,

Germany), an AOTF-based laser merge system (Visitron Systems, Germany) and a CCD camera (CoolSNAP-HQ, Photometrics, USA). Excitation/emission wavelengths were 488/529 and 535/590 nm for green fluorescent monomers and red fluorescent J-aggregates, respectively. During experiments, cells were maintained in a buffer containing (in mM): 145 NaCl, 5 KCl, 2 $CaCl_2$, 1 $MgCl_2$, 10 D-glucose and 10 HEPES; pH 7.4. Basal fluorescence intensity ratios were normalized to corresponding ratios after dissipation of mitochondrial membrane potential using 2 µM FCCP.

2.16 Site-directed mutagenesis of Nat8l and subsequent stable transfection of iBACs

Site directed mutagenesis was performed as described in [104]. *Nat8l* coding sequence was transferred into a pMSCV-hygro vector for better selectivity (kind gift from E.D. Rosen). Site-directed mutagenesis was performed by PCR amplification with *Phusion* polymerase using pMSCV-*Nat8l* as template with the following primers (the base substitution is marked as a small letter in a grey box):

*Nat8l*_D165A_fw: 5'TGCACACGGCcATGGCTGACATTGAGCAGTACTACATGAAGC3';

*Nat8l*_D165A_rv: 5'AGCCATgGCCGTGTGCAGCGCACACTCCAGGTAGGC3'

This base substitution changed aspartic acid to alanine. The purified PCR product was digested for 1 h at 37°C with 20 units of *Dpn*I in order to eliminate the template and the mutated vector was transformed into *E. coli*. After verification of the mutation in the *Nat8l* coding region through sequencing, supernatants containing retroviral particles were made by transfecting packaging cells (PhoenixEco, Biontex Laboratories GmbH) with pMSCV_*Nat8l*_D165A and pMSCV-hygro and collecting the supernatants 48 h after transfection. iBACs overexpressing *Nat8l*_D165A were generated by incubating the cells (30 000 cells/6-well, resulting in ~30% confluence) with viral supernatant including 8 µg/mL polybrene for 16-24 hours. Selection of positive clones was performed with 500 µg/ml hygromycin for at least 7 days.

2.17 Luciferase reporter assays

Genome organization around the *Nat8l* transcription start site was visualized using the University of California at Santa Cruz (UCSC) genome browser (http://genome.ucsc.edu/). Custom tracks include data from chromatin immunoprecipitation (ChIP) followed by sequencing or microarray analysis, respectively, for PPARγ at day 6 [108] of 3T3-L1 adipocyte differentiation and in epididymal, inguinal and brown adipose tissue[109].

One region within intron 2 of *Nat8l* (2610-3081 downstream from TSS) was identified as a potential PPAR binding site and was cloned into a luciferase reporter vector pTK-Luc

(Addgene), and was cotransfected with *Pparγ2* and *Rxrα* containing pCMX expression vectors. Used primers were:

fw: cgtaagcttCTCTACTGGACAATGAGCCTGAC

rv: ccaggatccCTCCTCCCTACACTTCTTACCTC

As described before[93], renilla reporter vector pGL4.75 (Promega, Madison, USA) was cotransfected in all experiments in a ratio of 1:100 (2 ng/well) to firefly luciferase reporter vectors as a control for varying transfection efficiencies. Transfection into Cos7 cells was performed in 24-well plates using MetafectenePro (Biontex, Martinsired, Austria) according to the manufacturer's instructions in a ratio of MetafectenePro to DNA 3:1 (µL:µg). 200 ng of luciferase reporter vector and either 100 ng of *Pparγ2* and *Rxrα* or 200 ng of the empty pCMX as a control were used. PPRE X3-TK-luc[110] (Addgene, Cambridge, MA, kind gift of Dayoung Oh) was used as a positive control. Twenty-four hours after transfection, cells were treated with 10 µM rosiglitazone (Sigma Aldrich, St. Louis, MO) for 24 hours. Thereafter, cells were harvested with 100 µL passive lysis buffer, and luciferase activities in the cell extracts were measured with the Dual-luciferase assay system (Promega, Madison, USA) according to the manufactorer's instructions. Luminescence was detected with a Berthold Orion II luminometer. Firefly luciferase values were normalized to *Renilla* luciferase readout and values of the empty vector control were subtracted from PPARγ/RXRa co-transfections.

2.18 Southern blot analysis

Genomic DNA of ES cell clones was isolated with the DNeasy Blood and Tissue Kit (Qiagen) and afterwards digested with restriction enzymes indicated in text and figures o/n (Fermentas). The resulting DNA fragments were separated by gel electrophoresis and the DNA in the gel was depurinated with 0.2 N HCl. Afterwards, the DNA was denaturated (1.5 M NaCl in 0.5 M NaOH), neutralized (1.5 M NaCl, 1 M TrisHCl, pH7.5) and blotted onto a nylon membrane (N+ Hybond, Amersham) with capillary transfer overnight. The DNA was cross linked with the membrane with UV light (1600*100 µJ/cm^2) and dried. Probes complementary to the DNA fragments were labeled with radioactive 25 µCi ^{32}P-dATP (American Radiolabeled Chemicals) and cleared with a sephadex column. The denaturated probe was pipetted into prewarmed QuikHyb hybridization solution (Stratagene) and incubated with the membrane in the presence of salmon sperm DNA as a blocking agent at 68°C for 4 hours. After washing, the labeled DNA was visualized on a STORM 860 molecular imager (GMI).

2.19 Plasma parameter measurements

Plasma glucose levels were measured from fresh blood with a glucose meter (Accu Chek Performa, Roche). Blood was drawn from isoflurane anesthetized mice from the retrobulbar

sinus vein and mixed with some µL of 0.5 M EDTA. Blood samples were centrifuged at 3600 rpm (~1800 x g), 4°C for 10 min and 2 µL plasma were used for measuring FFAs using the NEFA-HR (2) kit (Wako), and TGs using the triglyceride reagent (Thermo Scientific). Plasma insulin levels were determined from plasma drained from the tail vein during glucose tolerance test (at time point 0, 20 min and 90 min after glucose bolus) using the Mouse Ultrasensitive Insulin ELISA (ALPCO Diagnostics) according to the manufacturer's guidelines. The proposed 5 µL format was used. Plasma samples 20 min and 90 min after the glucose bolus were diluted 1:2 in Zero Standard solution.

2.20 Glucose and insulin tolerance test (GTT and ITT)

Mice were fasted prior to GTT and ITT for 6 or 4 hours, respectively. In case of GTT, 1.5 g/kg glucose (stock: 0.2g/ml D-glucose in 0.9% NaCl solution) were injected intraperitonally (i.p.). Plasma glucose levels were monitored before glucose injection and 15, 30, 60 and 90 (and if indicated 120) min from the tail vein after injection using glucose meter (Accu Chek Performa, Roche). For ITT, 0.5U/kg insulin (or dose indicated in the figure legend) (stock: 0.1U/mL in 0.9% NaCl solution supplemented with 0.8% BSA) was injected i.p. and plasma glucose levels were monitored as described for GTT.

2.21 Fasting tolerance test (FTT)

Fasting tolerance was assessed with mice fed *ad libitum*. In the morning basal glucose was measured and thereafter the mice were fasted. Fasting glucose was monitored every hour for the first 6 hours and after 8, 10, 12 and 24 hours of fasting. After 1 hour *ad libitum* re-feeding period, another blood glucose measurement was performed.

2.22 Statistical analysis

If not otherwise stated, results are mean values (± standard deviation) of at least three independent experiments, or results show one representative experiment out of at least three. Statistical analysis was done on all available data. Statistical significance was determined using the two-tailed Student's *t*-test. * $p \leq 0.05$, ** $p \leq 0.01$, *** $p \leq 0.001$

Results

3 Results – part NAT8L

3.1 Nat8l expression is downregulated in adipose tissue of ob/ob mice

Data generated in our lab showed that *Nat8l* is not only strongly expressed in brain, but also in brown and white adipose tissues. To investigate whether *Nat8l* might play a role in the development of the metabolic syndrome, we assessed its mRNA expression in genetically obese mice that suffer from diabetes[111,112]. Interestingly, *Nat8l* expression significantly decreased in BAT and is nearly blunted in WAT of *ob/ob* mice (fig. 9, A). In contrast to that, *Nat8l* mRNA expression did not change in BAT of mice fed a HFD. Furthermore, we observed a small decrease of *Nat8l* mRNA expression in the brain, and a small, but significant, increase in WAT of HFD fed animals (fig. 9, B).

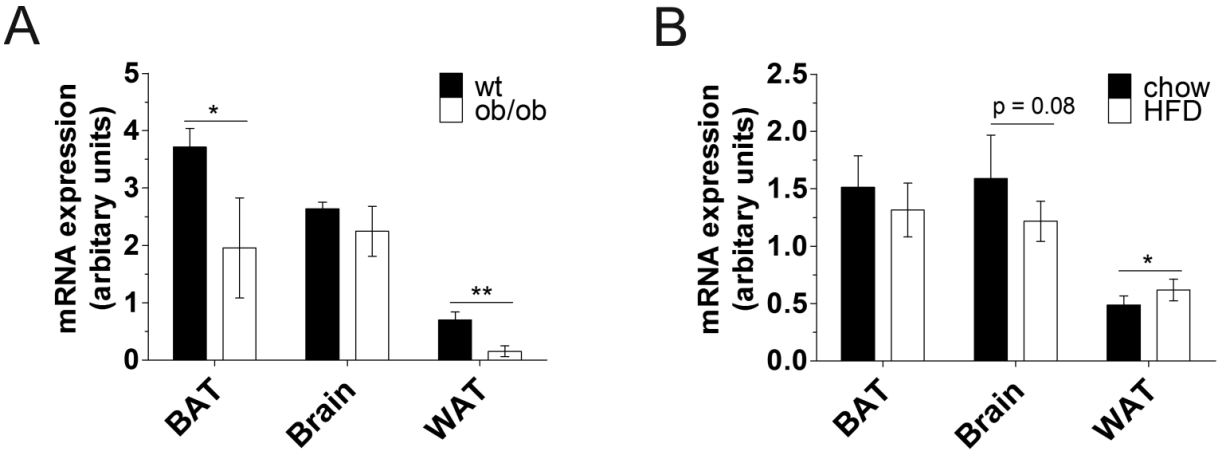

Figure 9: Tissue expression of *Nat8l* in mice with an obese phenotype. (A) Wild type (wt) n = 3, ob/ob n = 4. (B) C57BL/6 mice fed either chow or HFD for 16 weeks (starting at 8 weeks of age). n = 5 each. * ≤ 0.05; ** ≤ 0.01

3.2 NAT8L is located in the mitochondria of brown adipocytes

It is under debate whether NAT8L localizes in the ER or mitochondria of neurons[67,69]. However, to investigate the function of NAT8L in brown adipocytes, it is crucial to determine its localization in these cells. As immunofluorescence approaches failed, we fractionated differentiated iBACs and BAT samples of male C57BL/6 wild type (wt) mice into one fraction enriched in nuclei, one that contains mitochondria and the cytosolic fraction in which also the endoplasmic reticulum (ER) can be found. Figure 10 clearly shows that NAT8L is expressed in mitochondria *in vitro* and *in vivo* without any expression in the ER-containing cytosolic fraction. Hexokinase-1 (HK1) and UCP1 serve as controls for the mitochondrial fraction, Histone H3 (HH3) for the nuclear fraction and protein disulfide isomerase (PDI) and β-Actin (Actb) were used as controls for the cytosolic/ER fraction. Furthermore, we also tested whether the overexpressed NAT8L protein localizes in mitochondria, as an overexpression

often leads to a shift towards ER-localization. Figure 12C (right panel) shows that also overexpressed NAT8L exclusively localizes in the mitochondria of iBACs.

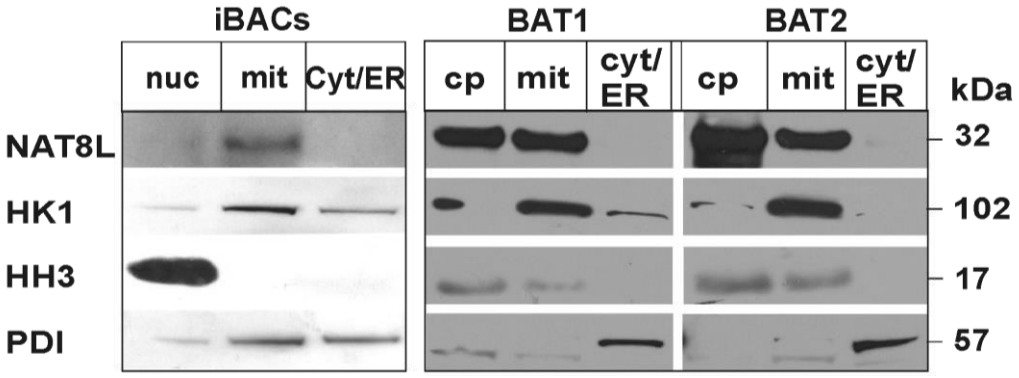

Figure 10: Localization of NAT8L in fractionates of iBACs and BAT. iBACs were harvested on day 3 of differentiation. Western blot represents one out of three independent experiments. BAT 1 and 2 represent two male C57BL/6 mice fed *ad libitum* on chow diet. Nuc, nucleus; mit, mitochondria; cyt/ER, cytosol/endoplasmic reticulum.

3.3 The influence of Nat8l overexpression on different pathways and metabolic phenotypes

To test the influence of forced *Nat8l* expression on adipocyte development and metabolism we previously generated immortalized brown adipocytes (iBACs) that stably overexpress *Nat8l*. These cells showed interesting phenotypes as they accumulate less lipid droplets during differentiation (most pronounced on day 3 of differentiation), but show increased expression of brown adipogenic marker genes such as peroxisome proliferator-activated receptor gamma coactivator-1 alpha (*Pgc-1α*) and peroxisome proliferator activated receptor-alpha (*Pparα*), and most remarkably uncoupling protein 1 (*Ucp1*). Based on these results, we aimed to further investigate these cells and the impact of *Nat8l* overexpression (o/e) on brown adipocyte differentiation and metabolism.

3.3.1 Expression of genes directly or indirectly involved in the proposed *Nat8l*-pathway

NAT8L catalyzes the formation of NAA from acetyl-CoA and L-aspartate. We assume that pathways upstream or downstream of NAT8L might be influenced upon *Nat8l* o/e. According to the scheme presented in fig. 11A, *Nat8l* o/e could impact on the expression of genes further down in the pathway, or pathways that supply the acetyl-CoA or aspartate need for the NAA-producing reaction.

The aspartate-malate shuttle (MAS) plays a central role in moving intermediates from glycolysis and citric acid cycle (TCA cycle) between cytosol and mitochondrial matrix and may thereby play an important role in the replenishment of substrates for the NAA-producing reaction[75]. A scheme of this pathway can be seen in figure 11C. Malate-dehydrogenases (MDH), glutamate-oxaloacetate transaminases (GOT), and antiporters such as aspartate-glutamate carriers (important here is ARALAR) and α-ketoglutarate-aspartate shuttles are key components of this shuttle system[113,114]. We measured the expression of several genes involved in aspartate/glutamate and malate/oxaloacetate (OAA) utilization. *Mdh1* and *2*, key enzymes in the reversible conversion of malate to OAA[115], are upregulated upon *Nat8l* o/e on day 3 of differentiation (fig. 11, E). The mitochondrial *Got1* and the cytosolic *Got2* are both upregulated in *Nat8l* o/e iBACs (fig. 11, D). These enzymes catalyze the conversion of OAA and glutamate to aspartate and α-ketoglutarate and play therefore an important role in providing substrates for shuttles (e.g. ARALAR) and downstream pathways (e.g. the NAT8L pathway)[75,116,117]. Furthermore, the expression of the mitochondrial aspartate-glutamate carrier *Aralar* (Slc25a12) is increased upon *Nat8l* o/e (Ct-values of *Aralar* ~26 on day 7) (fig. 11, D). ARALAR is involved in maintaining intracellular aspartate levels and thereby connects aspartate transport to NAA production[118]. Additionally, we measured mRNA expression of malic enzymes 1 and 2 (*Me*) which produce pyruvate (NADP dependent) out of malate and are important for the maintenance of energy production and FA synthesis[119]. Whereas mitochondrial *Me2* expression is increased, cytosolic *Me1* expression is decreased in *Nat8l* o/e iBACs (fig. 11, E). No changes could be observed in phosphoenolpyruvate-carboxy-kinase 1 or 2 (*Pepck*) (fig. 11, E).

It has been shown that NAA, the product of NAT8L's catalysis, is cleaved in the cytosol by aspartoacylase (ASPA) into aspartate and acetate[78]. The resulting acetate is used by acetyl-coA synthetases (ACSS) for acetyl-CoA synthesis, the building block of liponeogenesis[77,78]. Figure 11B shows that *Aspa* is highly expressed in BAT and upregulated in mice fed a high fat diet (HFD). Furthermore, it is expressed in iBACs (Ct-values of Aspa ~26 on day 7) and upregulated upon *Nat8l* o/e (fig. 11, C). There are two isoforms of *Acss*, a soluble (cytosolic) and a mitochondrial one. Both are involved in the biosynthesis of acetyl-CoA from acetate and coenzyme A[120,121]. The mitochondrial isoform *Acss1* is highly upregulated in *Nat8l* o/e cells throughout differentiation, while the cytosolic *Acss2* only shows a slight increase on day 7 of differentiation (fig. 11, D).

In addition to the catabolism of NAA, we wanted to test whether carriers involved in neuronal NAA transport are expressed in adipose tissue and influenced by *Nat8l* o/e. Little is known about transport mechanisms of NAA through mitochondrial membranes, but Arun *et al.*[122] suggested that the dicarboxylate-carrier DIC (also Slc25A10) is implicated in shuffling NAA from mitochondria to the cytosol. *Dic* has a well detectable expression level in brown adipocytes (mean Ct values reach an average of 22 on day 7), but there is no increase of *Dic*

mRNA expression upon *Nat8l* o/e. iBACs on day 7 of differentiation even show decreased *Dic* expression (fig. 11, D). NAA has been found in human urine[123]; therefore a transport out of brown adipocytes is conceivable. Previously, it has been shown that the sodium-coupled high-affinity carboxylate transporter NaDC3 (Slc13A3) transports NAA across the cell membrane in brain[80]. *NaDC3* has a very high Ct-value of >30 on day 7 of differentiated iBACs and its expression did not change upon *Nat8l* o/e (fig. 11, D). This indicates that if transport of NAA out of brown fat cell occurs, NaDC3 might not be the responsible transporter in these cells.

These data show that the NAA pathway exists in brown adipocytes. Furthermore, in contrast to brain, where biosynthesis and catabolism of NAA are separated between neurons and oligodendrocytes, the whole process occurs within one cell type. Moreover, the whole pathway seems to be boosted by *Nat8l* o/e and its overexpression also affects pathways upstream and downstream of NAA production.

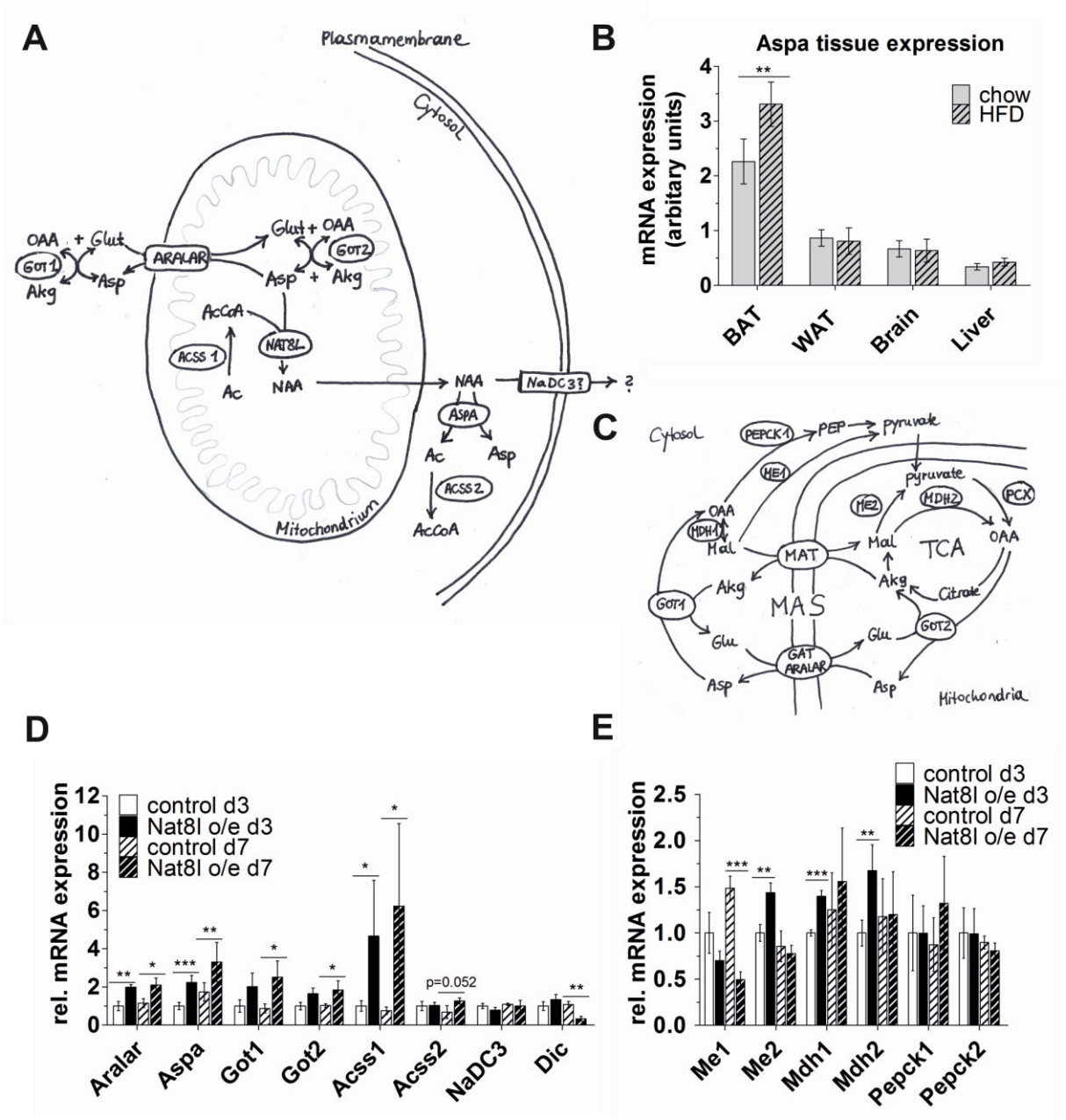

Figure 11: mRNA expression of genes directly and indirectly connected to the NAT8L pathway in *Nat8l* overexpressing iBACs. (A) Scheme of the NAT8L pathway and upstream or downstream located pathways. ACSS, acetyl-CoA synthetase; Ac, acetate; AcCoA, acetyl-coenzyme A; Akg, α-ketoglutarate; Asp, aspartate; ASPA, aspartoacylase; GOT, glutamate oxaloacetate transaminase; Glut, glutamate; NAT8L, N-acetyltransferase 8-like; NaDC3, sodium-coupled high-affinity carboxylate transporter. Adapted from ref. [81] (B) Tissue distribution of Aspa in male C57BL/6 mice on chow or high fat diet (HFD) (n=4-5). (C) Scheme of the malate-aspartate shuttle (MAS) and connected pathways. MAT, malate-alpha-ketoglutarate-transporter; Mal, malate; MDH, malate dehydrogenase; ME, malic enzyme; PEP, phosphoenolpyruvate; PCX, pyruvate carboxylase. Adapted from ref. [124] (D) mRNA expression of genes involved in upstream or downstream pathways of NAT8L. (Got1&2 d3, n =2, all others n ≥ 3). (E) mRNA expression of genes depicted in (C).
* ≤ 0.05; ** ≤ 0.01; *** ≤ 0.001

3.3.2 The expression of white and brown adipogenic marker genes in *Nat8l* o/e iBACs

Our previous observations show that *Nat8l* o/e highly increases the expression of *Ucp1*, *Pparα*, *Pgc-1α* and PR-domain containing 16 (*Prdm16*). This prompted us to investigate additional brown marker genes as well as general and white-specific adipogenic markers. Furthermore, we wanted to confirm that UCP1 expression is also affected on protein level.
General adipogenic markers, except *Pparγ* which is increased on day 3 of differentiation, are not influenced (adipocyte protein 2, aP2; adiponectin, *AdipoQ*), but some white specific markers are decreased (resistin, *Retn*; and phosphoserine aminotransferase 1, *Psat1*) upon *Nat8l* o/e (fig. 12, A). A slight, but not significant, decrease could also be observed in fatty acid desaturase 3 (*Fads3*) expression. Remarkably, in addition to the brown marker genes mentioned above, also other brown phenotypic genes, such as cytochrome c oxidase subunit 8b (*Cox8b*), cell death-inducing DFFA-like effector A (*Cidea*) and type 2 iodothyronine deiodinase (*Dio2*) are highly increased in *Nat8l* o/e cells (fig. 12, B). Moreover, we found a massive increase of basal and isoproterenol stimulated UCP1 protein levels. The left panel of figure 12C displays one representative western blot with cell lysates of *Nat8l* o/e and control iBACs and the right panel of figure 12C shows fractionated cells, where the exclusive mitochondrial localization of NAT8L, together with the increased UCP1 expression is displayed. iBACs protein lysates for these experiments were harvested on day 7 of differentiation.
Together these results indicate that *Nat8l* o/e boosts the brown adipogenic phenotype.

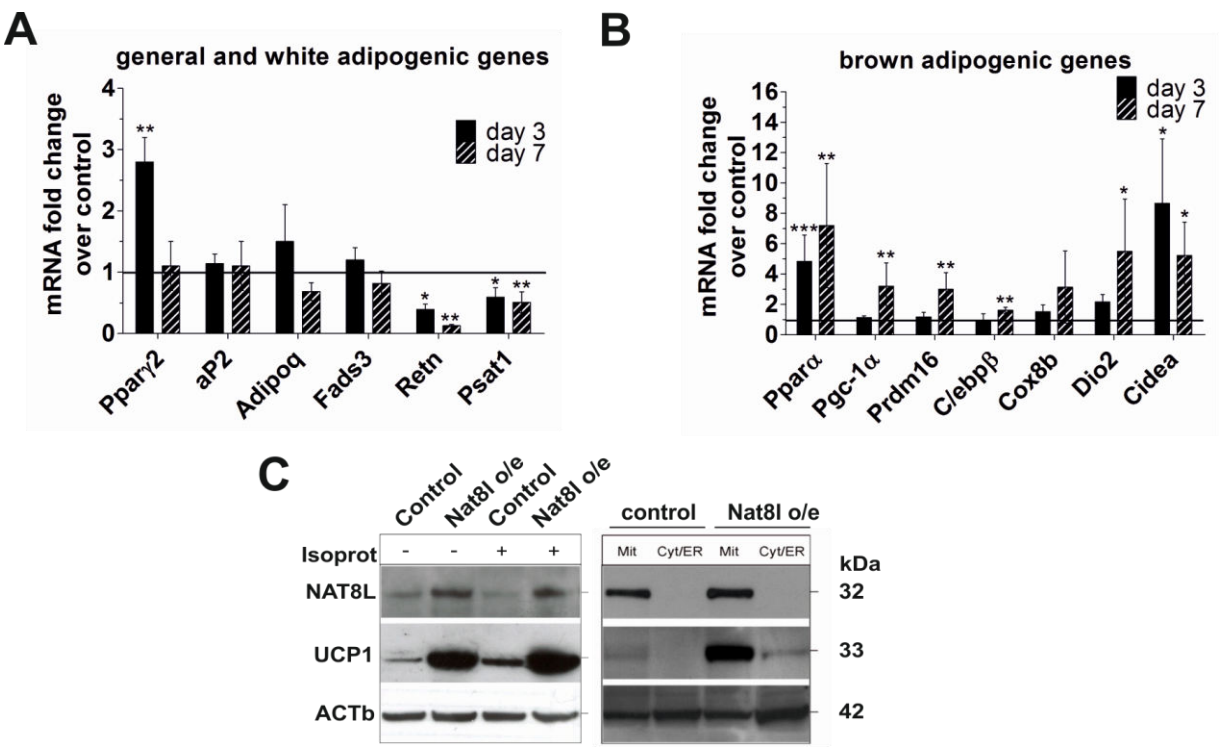

Figure 12: The expression of white and brown adipogenic marker genes in *Nat8l* o/e iBACs. (A) and (B) Relative mRNA expression of white, general and brown adipogenic genes in *Nat8l* o/e and control iBACs on day 3 and 7 of differentiation. Data shown in A and B resemble relative mRNA fold changes over control. All abbreviations are in listed in the text. (C) Western blot analysis of *Nat8l* o/e iBACs cell lysate (left panel) with and without isoproterenol stimulation and fractionated *Nat8l* o/e iBACs (right panel). iBACs on day 7 of differentiation were used. Mit, mitochondria; cyt/ER, cytosol/ER.

3.3.3 Overexpression of *Nat8l* in iBACs increases glucose uptake and lipogenesis

As already mentioned in the introduction, *Nat8l* overexpressing iBACs show delayed lipid accumulation during adipogenesis, which was most evident on day 3 of differentiation. That prompted us to investigate lipid metabolism of *Nat8l* o/e iBACs in more detail.

First, we wanted to investigate whether lipid-synthesis from glucose is altered upon *Nat8l* o/e. Therefore, we incubated the cells with radioactive-labeled glucose (^{14}C-glucose) and measured the incorporation of the provided glucose into several lipid classes. Glucose-incorporation into TG, diglycerides (DG) and FFA was significantly increased in *Nat8l* o/e iBACs on day 3 and day 7 of differentiation (fig. 13, B and C). Additionally, there was also more glucose metabolized to cholesterol esters (CE) on day 7 (fig. 13, C). A representative radiograph of a thin layer chromatogram (TLC) with radiolabeled neutral lipids can be seen in figure 13D. Because of the higher glucose incorporation, we wondered whether glucose uptake *per se* is altered in *Nat8l* o/e iBACs. To test this, we performed glucose uptake assays with radiolabeled ^{3}H-deoxyglucose. Insulin stimulated glucose uptake was slightly

increased in *Nat8l* o/e iBACs on day 3, but basal glucose uptake was strongly reduced on day 3 and day 7 in these cells (fig. 13, E). This indicates that the increased incorporation of glucose into various lipids in *Nat8l* o/e brown adipocytes is insulin dependent. However, qRT-PCR analysis of the glucose transporters *Glut4* and *Glut1* did not reveal significant changes in mRNA expression (fig. 13, F).

Furthermore, lipogenic genes have been measured on day 3 and day 7 of differentiation (a scheme of lipogenesis is provided in fig. 13, A). Figure 13F shows that mRNA expression of fatty acid synthase (*Fas*) and long-chain fatty acid-CoA ligase 1 (*Acsl1*), the enzyme that is important for the activation of fatty acids with coenzyme A, is not changed. No significant differences could be observed in ATP-dependent citrate lyase (*Acly*) expression. *Acly* is part of the classical pathway to supply acetyl-CoA for cytosolic reactions. *Acly* action leads to the ATP-dependent cleavage of citrate into acetyl-CoA and OAA in the cytosol and has been shown to be very important for fatty acid biosynthesis.[125] Interestingly, mRNA expression of acetyl-CoA carboxylase 1 (*Acc1*) on day 3 and *Acc2* on day 3 and 7 is increased in *Nat8l* o/e iBACs (fig. 13, F). Cytosolic *Acc1* catalyzes the carboxylation of acetyl-CoA to form malonyl-CoA which is important as a building block of FA-biosynthesis[126]. Mitochondrial generated malonyl-CoA (through *Acc2*) acts a regulator of β-oxidation[127].

Together, these results indicate increased insulin stimulated glucose utilization and enhanced lipogenesis from glucose in *Nat8l* o/e iBACs.

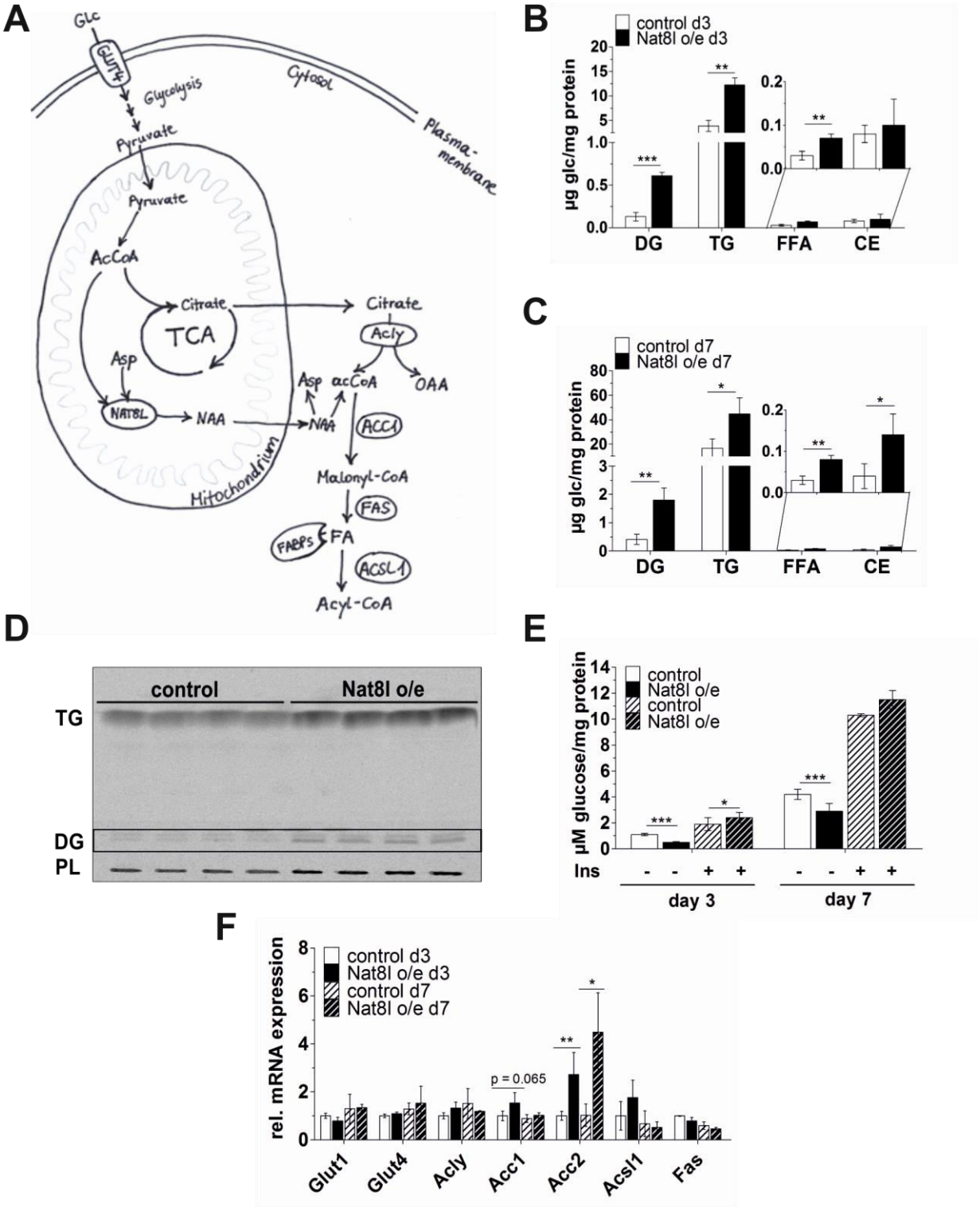

Figure 13: The impact of *Nat8l* o/e on glucose uptake and lipogenesis in iBACs. (A) Working model of NAT8L impact on glucose uptake and fatty acid (FA)-biosynthesis. Adapted from ref. [124] (B) & (C) ^{14}C-glucose incorporation in neutral lipids of *Nat8l* o/e iBACs and control cells on day 3 and 7 of differentiation. (D) Representative TLC radiograph from ^{14}C-labeled neutral lipids. DG, diglycerides; TG, triglycerides; FFA, free fatty acids; CE, cholesterol esters; PL, phospholipids. (E) Basal and insulin (Ins) stimulated (100 nM for 15 min) glucose uptake in *Nat8l* o/e and control iBACs. (F) mRNA expression of genes involved in glucose transport and lipogenesis (genes indicated in A).

3.3.4 *Nat8l* overexpressing iBACs show increased lipolysis

As a next step, we wanted to investigate whether TG synthesis and lipid catabolism is altered in *Nat8l* o/e iBACs. Therefore, we measured cellular and extracellular glycerol and FFA content. We already showed before that intracellular glycerol/TG content was significantly decreased on day 3 of differentiation in *Nat8l* o/e iBACs. In contrast to that, intracellular glycerol/TG on day 7 was equal between controls and *Nat8l* o/e iBACs under basal and isoproterenol stimulated conditions (10 µM for 4 hours) (fig. 14, B). Interestingly, FFA release was in increased up to 3-fold under basal and doubled under isoproterenol stimulated conditions (fig. 14, C). This argues for increased lipolysis in these cells, although gene expression of *Atgl* and *Hsl* did not change on mRNA level (fig. 14, D). Furthermore, the expression levels of genes that mediate TG-synthesis (shown in scheme fig. 14, A) have been obtained. Some of these genes showed differential expression in *Nat8l* o/e iBACs. Glycerol-3-phosphate acyltransferase (*Gpat*) is downregulated and 1-acylglycerol-3-phosphate-O-acyltransferase (*Agpat*) is upregulated, but no significant changes in mRNA expression could be observed in other TG-synthesis genes (fig. 14, D).
Taken together, these results indicate that *Nat8l* o/e in iBACs increases lipolysis.

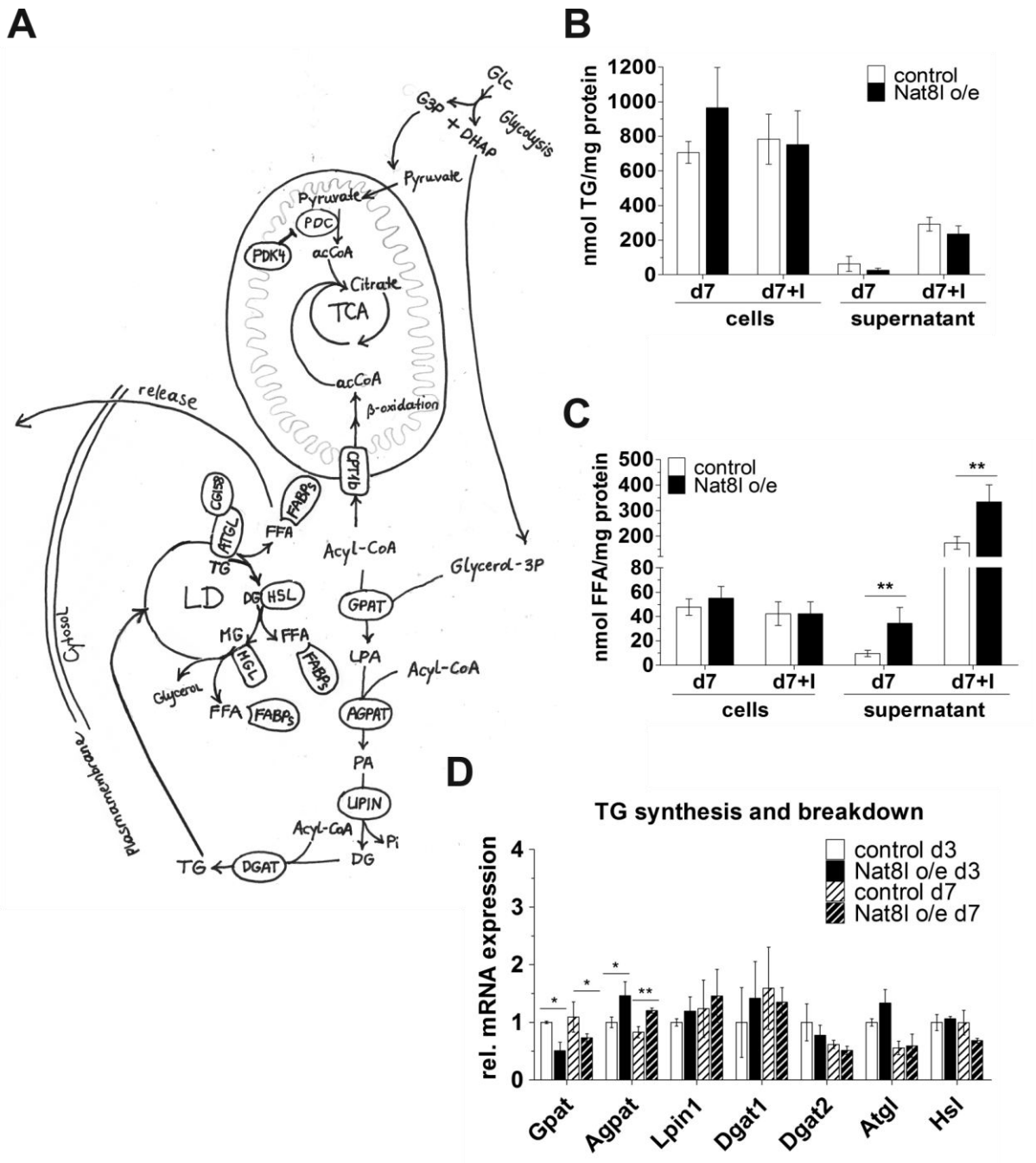

Figure 14: The impact of *Nat8l* o/e on TG synthesis and breakdown. (A) Scheme of the fate of acyl-CoA towards TG synthesis and β-oxidation. Adapted from ref. [124] (B) TG content in cell lysates and supernatants of *Nat8l* o/e and control iBACs on day 7. (C) FFA content in cell lysates and supernatants of *Nat8l* o/e and control iBACs on day 7. (D) mRNA expression of genes involved in TG synthesis and breakdown (indicated in A).

3.3.5 Oxygen consumption and genes involved in β-oxidation and FFA utilization are increased upon *Nat8l* overexpression

We could show that lipid biosynthesis and degradation are enhanced in *Nat8l* o/e iBACs, but in addition to re-esterification, acyl-CoAs have the fate to undergo β-oxidation in mitochondria. This pathway has a special importance for brown adipocytes because a lot of energy is needed to maintain the function of these cells. This prompted us to study whether the catabolism of fatty acids is altered in *Nat8l* o/e iBACs. For this reason, we measured the expression of genes directly or indirectly involved in β-oxidation (fig. 15, A). We observed increased expression of cytochrome c oxidase subunit 1 (*Cox1*), a mitochondrial encoded gene that is part of the electron transport chain (fig. 16, B). Carnitoyl palmitoyl transferase 1b (*Cpt1b*), pyruvate dehydrogenase kinase 4 (*Pdk4*) and fatty acid binding protein 3 (*Fabp3*) are important regulators of β-oxidation and showed elevated mRNA expression in *Nat8l* o/e in comparison to control cells (fig. 15, B and C). While mRNA expression of genes that code for fatty acid transporters *Fatp1* and *Fatp4* did not change upon *Nat8l* o/e, *CD36* showed a significant upregulation on day 3 (fig. 15, C).
In summary, the results of the previous chapters (3.3.3 and 3.3.4) and these data indicate that lipid turnover *per se* is increased in *Nat8l* o/e cells.

The observation of the massive upregulation of UCP1 expression suggested that also oxygen consumption rate (OCR) might be influenced by *Nat8l* o/e. In cooperation with Wolfgang Graier and Lukas Groschner at the Medical University of Graz, we performed oxygen consumption measurements using the Seahorse extracellular flux analyzer. With this method we could clearly show that basal, as well as maximal respiration after administration of carbonyl cyanide-p-trifluoromethoxyphenylhydrazone (FCCP, www.pubchem.ncbi.nlm.nih.gov, July 2014) are elevated in *Nat8l* o/e cells (fig. 15, D). However, the relative increase in respiration did not change between the different cells after administration of FCCP, which acts as an uncoupling reagent by mechanical disseminating the mitochondrial proton gradient (fig. 15, D). Oligomycin, a compound which inhibits ATP-synthase and therefore coupled respiration (OM, www.pubchem.ncbi.nlm.nih.gov, July 2014), showed very little effect on *Nat8l* o/e iBACs. This might indicate a high uncoupled status in these cells. To test, whether the increased respiration is due to the elevated UCP1 expression, we incubated the cells with norepinephrine (10 µM) for one hour prior to the OCR-measurement. Under these conditions an additional 15% increased relative OCR in *Nat8l* o/e compared to control iBACs could be observed (fold-change basal to NE-stimulated in control cells 3.3-fold vs. 3.8-fold in *Nat8l* o/e cells, respectively) (fig. 15, E).

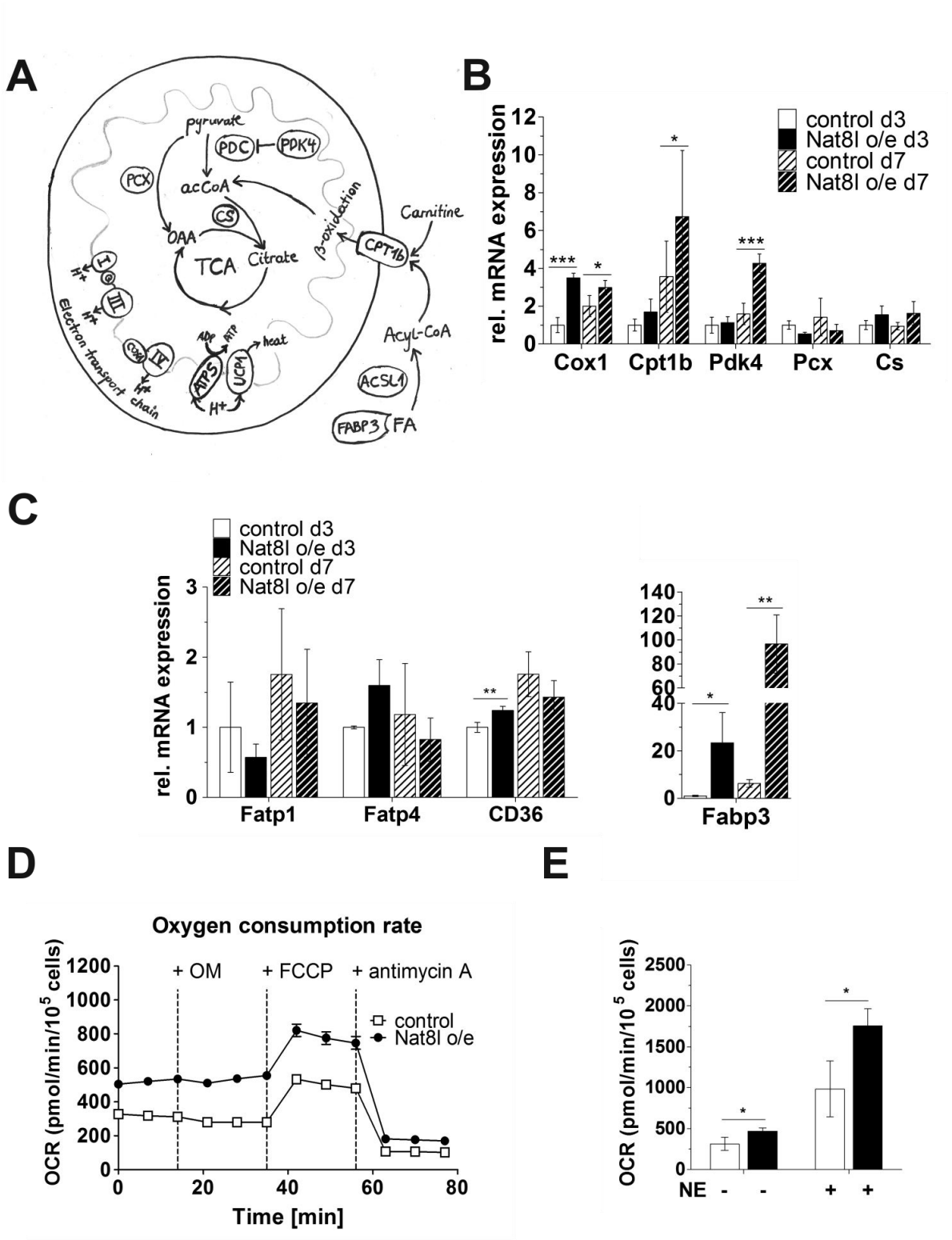

Figure 15: *Nat8l* o/e influences expression of genes directly or indirectly involved in β-oxidation and FFA utilization and increases oxygen consumption rate (OCR). (A) Simplified scheme of the intertwined pathways citric acid cycle (TCA), β-oxidation and oxidative phosphorylation. Adapted from ref. [124] (B) mRNA expression of genes involved in TCA-cycle, β-oxidation and oxidative phosphorylation. (C) mRNA expression of genes involved in fatty acid transport. (D) OCR of *Nat8l* o/e and control cells on day 7 of differentiation. The broken lines indicate the time points of oligomycin (OM, 1 µM), FCCP (2 µM) and antimycin A (2.5 µM) administration. Data in (D) are presented as mean ± SEM. (E) OCR after pre-incubation with norepinephrine (NE, 10 µM for 1 hour).

3.3.6 *Nat8l* overexpression increases mitochondrial mass and number

We showed that *Nat8l* o/e led to an increase in brown marker gene expression. Among them *Pparα* and *Pgc-1α* were highly upregulated. Both positively impact mitochondrial biogenesis[52,128]. Additionally, the increased OCR is an indicator of a higher mitochondrial number or performance. Thus, we wanted to assess mitochondrial mass and number of *Nat8l* o/e iBACs. For this purpose we used cells on day 7 of differentiation, where changes in brown adipogenic marker gene expression and increased lipid turnover were most significant. We used different approaches, to investigate mitochondrial number. First, we incubated trypsinized control and *Nat8l* o/e cells with a fluorescent labeled mitochondrial dye (MitoTracker Green) and subjected the cells to flow cytometry (fluorescence-activated cell sorting, FACS). *Nat8l* o/e cells showed increased fluorescence intensity which indicates a higher incorporation of MitoTracker and thus, a higher mitochondrial mass or number (fig. 16, A). The quantification of the fluorescence intensity in sector II of the FACS scatter blot can be seen in figure 16B. We used this sector to compare the fluorescence intensity, because we assumed from the cell size that most viable adipocytes can be found in this sector. Although MitoTracker Green is described to stain mitochondria in a membrane potential independent manner[129], there are studies that state the opposite[130,131]. Therefore, we measured the mitochondrial membrane potential in *Nat8l* o/e iBACs compared to control cells by incubating the cells with the mitochondrial dye JC-1. JC-1 changes its fluorescence properties regarding to the membrane potential from green (529 nm) to red (590 nm). The ratio between the red and the green signal is normalized to the maximal depolarization after FCCP administration. A representative fluorescent picture of *Nat8l* o/e and control cells is shown in figure 16D. The white arrows indicate regions that show red JC-1. Figure 16E displays that there are no significant changes in mitochondrial membrane potential of *Nat8l* o/e cells, although a slight decrease could be observed.

In addition to flow cytometry, we isolated genomic DNA from iBACs and measured the content of mitochondrial DNA with primers recognizing the mitochondrial coded gene NADH dehydrogenase 1 (ND1) normalized to the qRT-PCR signal of primers within a nuclear coded intron region of β-Actin. With this approach we could show that there was significantly more mitochondrial DNA in iBACs o/e *Nat8l* on day 3 of differentiation (fig. 16, C). To verify increased mitochondrial mass or number, we performed transmission electron microscopy (TEM) in corporation with Dagmar Kolb at the Medical University of Graz. As depicted in fig. 16F, mitochondria of *Nat8l* o/e cells show a denser morphology, indicating higher metabolic activity of these mitochondria. Furthermore, we counted the mitochondria of 14 individual control and *Nat8l* o/e cells and found a doubling of mitochondrial number in the latter (fig. 16, G). Thus, we conclude that *Nat8l* o/e in iBACs increases mitochondrial mass and number.

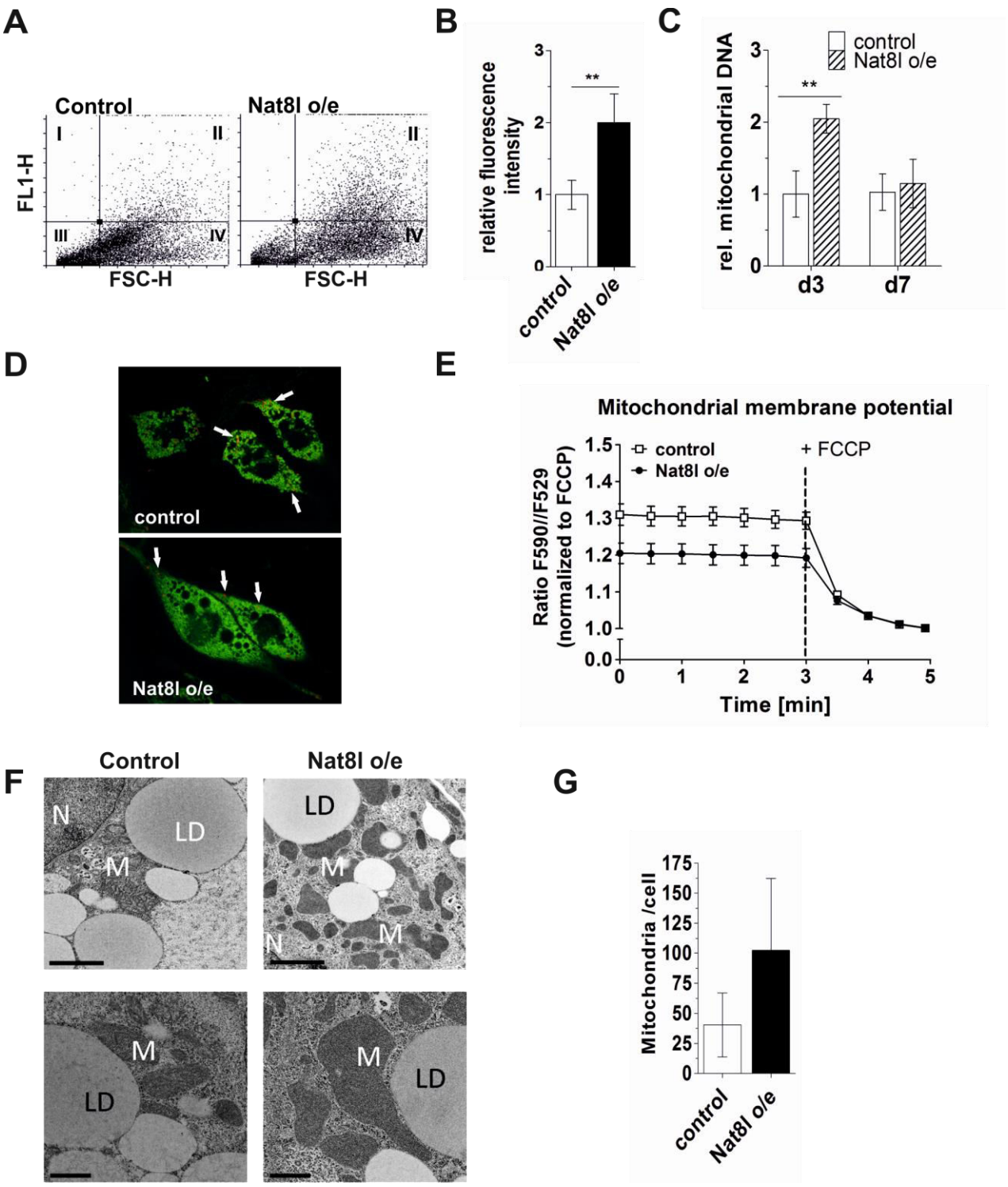

Figure 16: *Nat8l* o/e increases the number of mitochondria in iBACs. (A) and (B) FACS analysis of control and *Nat8l* o/e iBACs incubated with MitoTracker Green (200 nM for 20 min at 37°C). (A) shows a representative scatterblot of MitoTracker signal (FL1-H) against forward scatter (FSC-H) as a measure for cell size. In (B) the fluorescence intensity in sector II has been quantified. (C) Relative mitochondrial DNA content of *Nat8l* o/e vs. control cells. (D) Fluorescent microscopy picture of *Nat8l* o/e and control iBACs incubated with mitochondrial stain JC-1. The white arrows indicate the green to red shift of the dye. (E) The mitochondrial potential of *Nat8l* o/e cells relative to control cells is displayed as ratio 590/529 nm before and after FCCP administration. (F) Transmission electron micrograph of *Nat8l* o/e and control cells. Scale bars upper panels = 2 µm, scale bars lower panels = 1 µm. (G) Mitochondria of 14 individual control and *Nat8l* o/e cells have been counted and the mean of the mitochondrial number per cell is displayed.

3.4 The phenotype of Nat8l o/e iBACs is dependent on its enzymatic activity

Tahay and associates[69] published that the enzymatic activity of *Nat8l* is crucial for its function in neurons. They also elucidated the regions important for its catalytic activity by introducing point mutations into the human *Nat8l* gene. Based on this study, we generated a mutant murine *Nat8l* gene in which we exchanged aspartate on position 165 to alanine (*Nat8l* D165A). It is described that this mutant has no N-acetyltransferase activity[69]. Subsequently, we stably overexpressed *Nat8l* D165A in iBACs and characterized these cells compared to controls. As depicted in figure 17A, we achieved a 7-fold overexpression of the *Nat8l* D165A mutant, but the mutated *Nat8l* did not influence adipogenic marker gene expression (fig. 17, A). Furthermore, whether cellular lipid content, nor basal and isoproterenol stimulated glycerol/FFA release were changed in iBACs overexpressing the mutated *Nat8l* in comparison to control cells (fig. 17, B and C). Thus, we conclude that NAT8L activity is required for its impact on brown adipogenic development and metabolism.

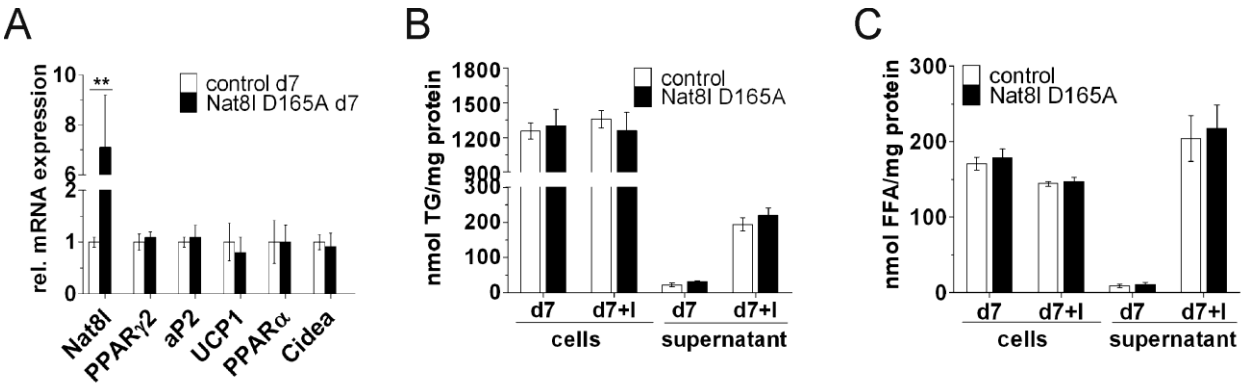

Figure 17: Overexpression of the enzymatic defective *Nat8l* mutant D165A in iBACs has no influence on marker gene expression, TG accumulation and FFA release. (A) Relative mRNA expression of white and brown adipogenic marker gene expression in *Nat8l* D165A o/e and control cells on day 7 of differentiation. (B) TG content in cell lysates and supernatants of *Nat8l* o/e D165A and control cells. (C) FFA content in cell lysates and supernatants of *Nat8l* D165A o/e and control cells.

3.5 Nat8l is a PPAR target

Nothing is known about the regulation of *Nat8l* expression during fat cell development. Our lab is highly interested in the behavior and the regulation of genes during adipogenesis. In both white and brown adipogenesis, PPARγ is a known to be the master-regulator[34]. Many genes are described as PPARγ targets, among them adipocyte plasma membrane associated protein (*Apmap*)[93] and abhydrolase domain containing 15 (*Abhd15*)[132]. PPARα has a great impact on brown adipocyte development, as it regulates lipid catabolism and mitochondrial biogenesis[47,52,133]. As *Nat8l* expression increases during adipogenesis of

several white and brown adipogenic cell lines, we wanted to reveal a possible impact of PPARs on its transcription. For this reason, we first determined whether *Nat8l* expression is influenced by thiazolidinediones (TZDs) *in vivo*. Figure 18A shows that *Nat8l* mRNA expression was increased up to 3-fold in WAT of mice fed a chow diet supplemented with PPARγ agonist rosiglitazone (Rosi). Interestingly, *Nat8l* expression was 30% decreased in BAT of Rosi treated mice, indicating a different transcriptional regulation in those tissues. Furthermore, *Nat8l* mRNA expression was blunted in iBACs treated with a synthetic PPARα antagonist (GW6471, 10 µM from day 4 until day 7; fig. 18, B). These results indicated a transcriptional regulation of the *Nat8l* gene through PPARs. Therefore, we analyzed the *Nat8l*-promotor and -genomic region using already published ChIP datasets[108,109] and identified a putative PPAR binding site within intron 2 (2610-3081 downstream from TSS) of the *Nat8l* gene (fig. 18, C). To assess a functional PPAR binding, we cloned this construct into a luciferase reporter vector and assayed for enhanced reporter activity in Cos7 cells. Luciferase counts were normalized to empty vector controls (pCMX). Figure 18D shows that the relative luciferase activity after co-transfection of the *Nat8l*-luciferase-reporter vector with PPARγ and RXRα containing vectors is increased and could further be elevated after stimulation with Rosi (10 µM for 24 hours). The figure represents one individual experiment. Due to the different luciferase counts, data could not be averaged, but showed similar trends. The graphs of the other two experiments can be found in the appendix (chapter 9.2). PPARγ response elements (PPRE) in the luciferase reporter vector[110] served as a positive control in this assay. From this data, we conclude that *Nat8l* is a PPARγ target, at least in WAT.

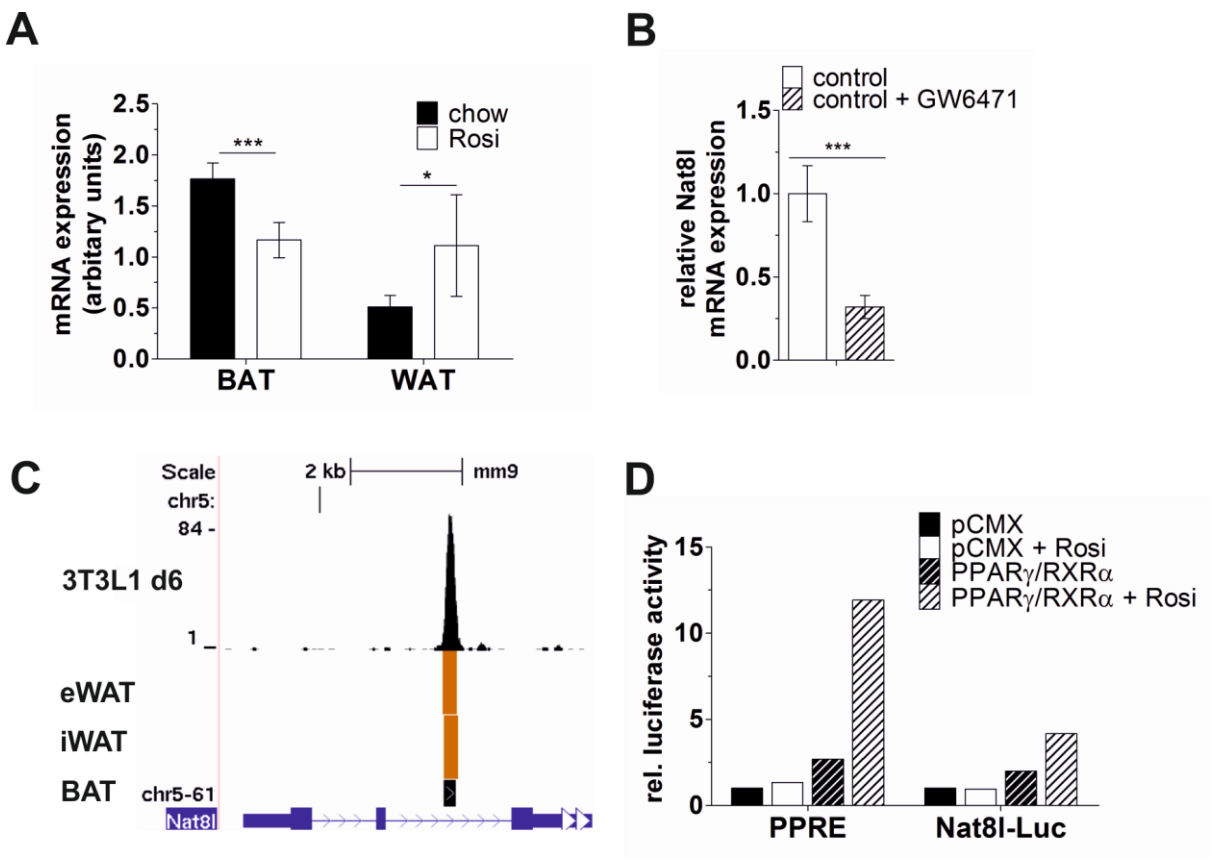

Figure 18: *Nat8l* is a PPAR target. (A) *Nat8l* mRNA expression in C57BL/6 mice on rosiglitazone supplemented chow diet (0.01% w/w for 7 weeks). (B) *Nat8l* mRNA expression in iBACs treated with 10 µM PPARα antagonist GW6471 from day 4 until day 7 of differentiation. (C) Custom tracks from ref. [108,109] displayed in the USCS genome browser (D) Relative luciferase activity of *Nat8l* 2610-3081TSS (*Nat8l*-Luc) normalized to empty vector control, basal and after 24 hours Rosi treatment (10 µM for 24 h). PPRE X3-TK-luc (PPRE) serves as a positive control.

4 Results – part APMAP

4.1 The impact of Apmap deficiency in vivo

4.1.1 Generation of *Apmap*-deficient and loxP flanked ES cell clones and chimeric founders

A replacement vector for the manipulation of exon 1 of the murine *Apmap* gene has been generated. Exon 1 harbours the transcription start site and therefore the transcription of a functional protein should be prevented. The targeting sequence was designed with a "short" and a "long" homologous region (short and long arm) of the *Apmap* gene. The vector contains a single loxP site (marked with black arrows in fig. 19) within intron 1 of the genomic sequence and a neomycin resistant cassette flanked by loxP sites[134]. A single diphtheria toxin A cassette (DtA) for enrichment of correctly targeted ES cells was introduced at the 5' end of the long arm of homologous recombination[135]. *Sal*I was used for linearization of the vector. Sites for homologous recombination are marked with crosses (fig. 19).
129 HM-1 embryonic stem (ES) cells[136] were used for homologous recombination and were electroporated with the linearized targeting vector. After selection of G418 resistant HM-1 ES clones, two PCRs confirming homologous recombination were performed (primer 1, 2, 3, and neo, fig. 20, B). If homologous recombination of the short arm occurred, a PCR with primers located in the genomic region and in the neo-cassette resulted in a 1700 bp band (Fig. 20, upper panel). The existence of loxP sites was indicated with a band at 450 bp. The wild type allele gave a band of 390 bp (Fig. 20, lower panel). Genomic DNA from wt ES cells, which was used to optimize the PCR, served as a positive control. Two clones (#11 and #129) out of 6 positive targeted clones were selected due to optimal phenotypic appearance under the microscope. After Cre-mediated manipulation of the targeted clones, *Eco*RV generated fragments were used to verify site specific recombination by Southern blot analysis (probe I). The wt allele is detected with a band of 9.5 kb, the knockout allele had 7.5 kb and the floxed one 3.5 kb. Figure 21 shows that Cre-mediated recombination resulted in 3 knockout (ko) clones and 4 floxed clones. Two of the floxed clones were used for blastocyst injection and transferred into pseudo-pregnant mice. This was performed by Thomas Rülicke at the Institute of Laboratory Animal Science at the University of Veterinary Medicine in Vienna.
First, 18 chimeric male mice were born; whereof 13 showed a coat color chimerism over 50% and were used for breeding. The higher the percentage of agouti coat color, the better the chance that the manipulated gene is present in germ cells. In this approach, none of the founders showed germline transmission of the manipulated *Apmap* gene. Therefore, the blastocyst injection had to be repeated. The second attempt resulted in 10 male chimeras over 50% agouti coat color. 5 over 70% were used for breeding and only one male showed

germline transmission of the manipulated *Apmap* gene and its offspring was 100% agouti. Male agouti litters were mated with CMV-Cre and wild type C57BL/6 females to generate total ko and floxed mice on an inbred C57Bl/6 background (backcrosses ≥10). The transgenic expression of the Cre-recombinase under the CMV-promoter leads to a deletion of the floxed gene in the early development of the embryo and therefore leads to a ko mouse[137].

The primers for performing tailtip PCRs of *Apmap*-ko or floxed mice are marked in figure 19B. Primers 1+2 generate a wt-fragment with 390 bp and a floxed fragment with 450 bp. A knockout mouse generates a fragment of 610 bp with primers 1+3.

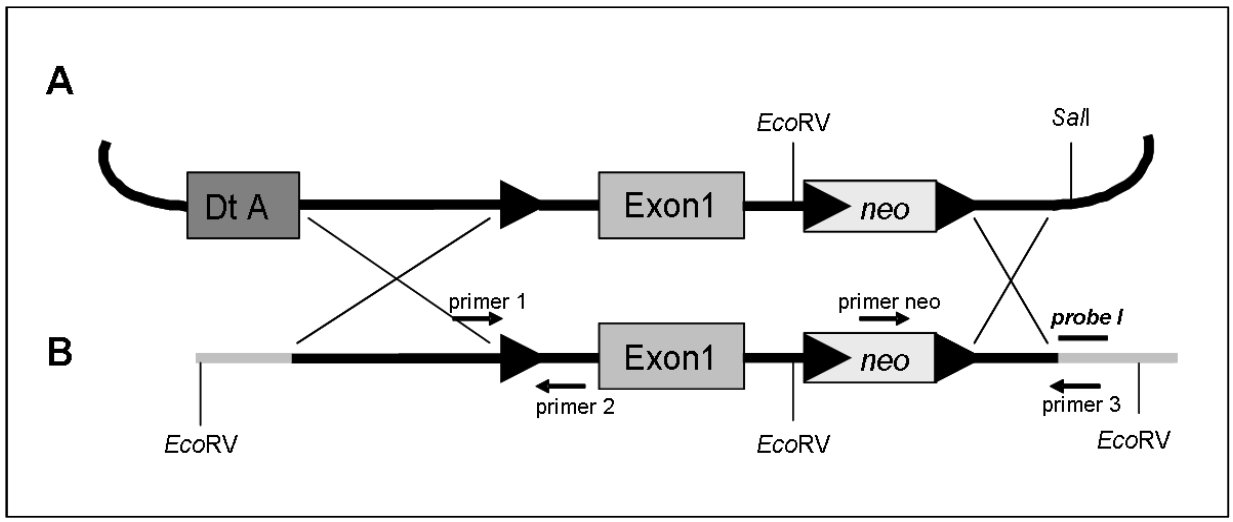

Figure 19: Scheme for generation of the *Apmap*-ko mouse. (A) *Apmap* gene targeting vector. (B) Homologous recombinant allele. Grey parts represent genomic parts of the DNA. The black arrows represent loxP targeting sites. Used restriction enzymes are depicted in italics. Neo, neomycin cassette; DtA, diphtheria toxin A cassette.

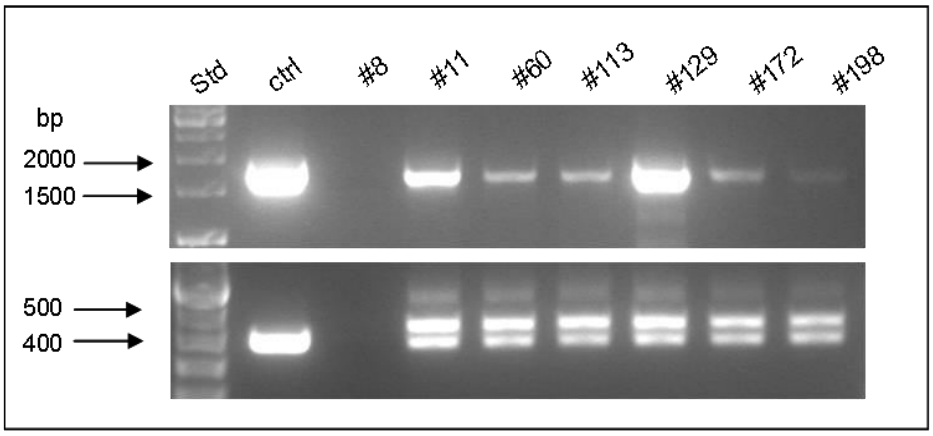

Figure 20: PCR of ES cell clones after homologous recombination. Upper panel: verification of the homologous recombination of the short arm and the neo-cassette with primer 3 and neo of fig. 19, B. Lower panel: verification of the insertion of a loxP site (primer 1+2 of fig. 19, B).

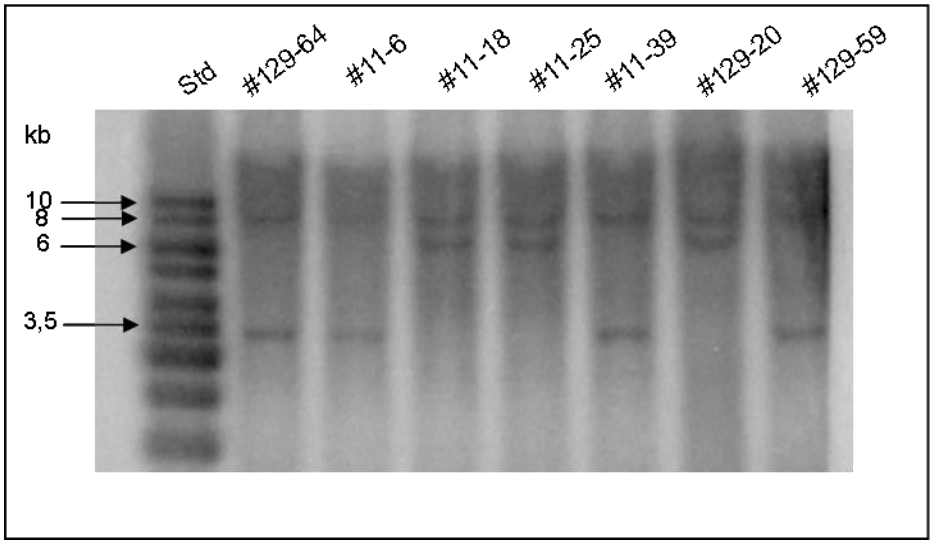

Figure 21: Southern blot of ES cell clones after homologous and Cre- mediated recombination. Genomic DNA from ES cell clones after homologous and Cre-mediated recombination has been digested with *EcoR*V (indicated in fig. 19, B) and subjected to Southern blot analysis. wt-allele at 9.5 kb, ko-allele at 7.5 kb and floxed-allele at 3.4 kb.

Heterozygous ko-mice were used for breeding. The birth of *Apmap*-ko, heterozygous and wt littermates followed Mendelian's rules, meaning that around 25% of all pups were knockout. No differences in viability, size and bodyweight could be observe in the initial cohort of *Apmap*-ko mice.

After backcrossing the mice for 2 generations, *Apmap*-ko mice and control littermates were used to verify the knockout. Various tissues were harvested and RNA was isolated. With primers located in the 5' untranslated region (5'UTR) and exon 1 (Apmap 5'UTR/E1) the knockout of the intended region could be verified in all tested tissues using qRT-PCR (BAT; eWAT; sWAT; skeletal muscle, SM; cardiac muscle, CM; liver; lung; spleen; brain; genitals – testis or ovaries; and kidney (fig. 22, A; n = 1; error bars represent technical replicates). To test whether the whole transcript was missing, a second pair of primers was used that recognizes a fragment at the exon 3-exon 4 junction (Apmap E3/4). Figure 23B shows that expression of an *Apmap* transcript in *Apmap*-ko mice could still be detected in BAT, eWAT and sWAT. A decreased amount of the *Apmap* transcript was seen in all other tissues, except liver, where hardly any *Apmap* mRNA could be measured (fig. 22, B). This argues for an alternative transcription start site (TSS) downstream from exon 1 and a differential splicing in different tissues of the mouse.

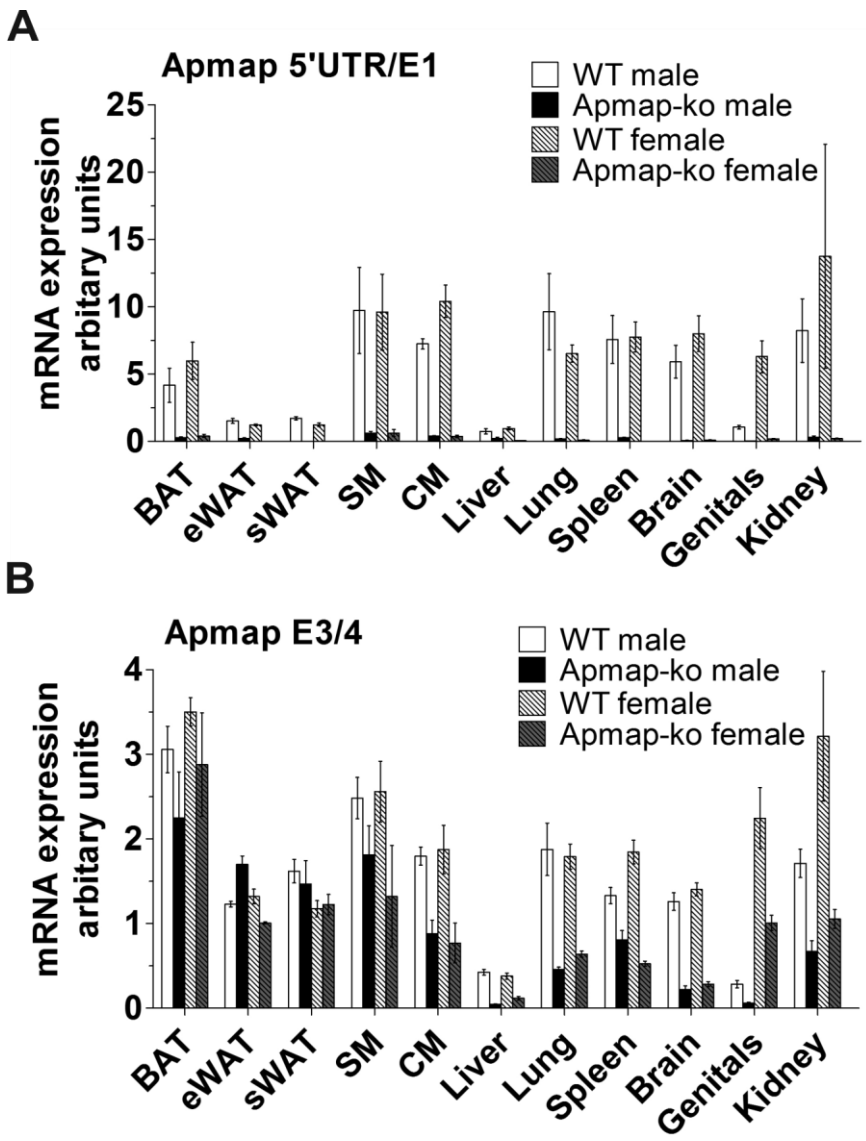

Figure 22: qRT-PCR from *Apmap*-wt and -ko tissues from a male and a female mouse. (A) qRT-PCR with primers located in the 5'UTR and exon 1. (B) qRT-PCR with primers located in exon 3 and 4 of the *Apmap* transcript. eWAT, epididymal WAT; sWAT, subcutanous WAT; SM, skeletal muscle; CM, cardiac muscle. n = 1, error bars represent technical variance.

To evaluate APMAP protein levels in various tissues of *Apmap*-ko mice and wt littermates, we performed western blot analyses. Figure 23 shows that APMAP protein was not detectable in BAT, sWAT and lung of *Apmap*-ko mice, whereas protein expression could be seen in eWAT and liver. No APMAP protein could be detected kidney (fig. 23), SM, brain and genitals (data not shown).

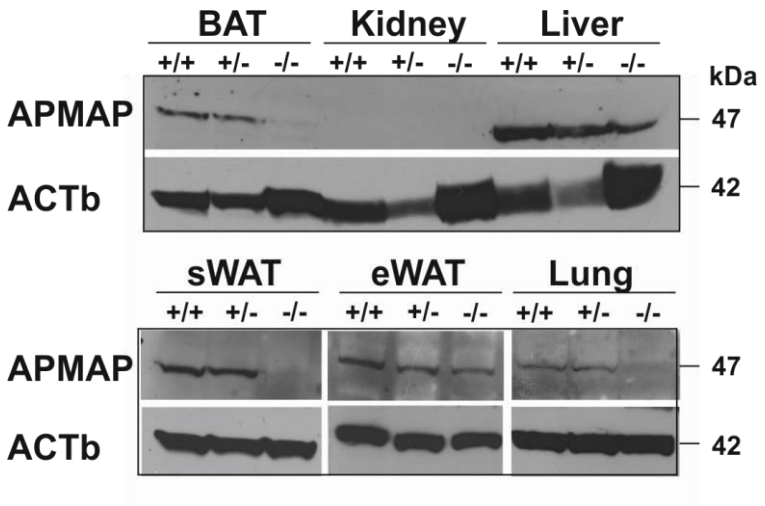

Figure 23: Western blot of mouse tissues of *Apmap*-ko mice and wt littermates. sWAT and liver: one representative out of 3 blots is shown. BAT: 1 out of n=2 is shown. n=1 for kidney, eWAT, and lung. 100 µg protein lysate of BAT, sWAT, eWAT, and lung were analyzed; 300 µg protein lysate of kidney and liver were used for western blot analysis.

4.1.2 Preliminary characterization of *Apmap* deficient mice

Different cohorts of *Apmap*-ko mice and wt littermates have been tested for phenotypical alterations. Since they were used after different generations of backcrossing, individual results are shown.

4.1.2.1 First cohort of *Apmap*-ko mice

The first cohort was comprised of 6 male *Apmap*-ko mice and 8 male wt littermates. These mice were offspring from heterozygous breedings from the F2 generation (accordingly after 2 backcrosses on a C57BL/6 background). After weaning, mice were kept chow diet (4.5% calories in fat). At 16 weeks of age, plasma parameters were measured in the fed and fasted state. *Apmap*-ko mice showed an increase in plasma glucose levels in the fed *ad libitum* state (table 4, highlighted with a grey box). No other phenotypic alterations could be observed on chow diet. To assess how high fat-feeding influences body weight and plasma parameters, these mice were put on high fat diet (HFD, 40% calories in fat) at 16 weeks of age. Body weight changes were monitored after 1, 3, 5, 9, 11, and 13 weeks on HFD. Figure 24 shows that *Apmap*-ko mice had a slightly decreased starting weight, but gained the same amount of bodyweight during the 13-week time course as their wt littermates. Plasma parameters did not show any significant changes after 9 weeks on HFD in the fed *ad libitum* state or after 11 weeks on HFD in the fasted state (12 hours overnight) (table 5). Mice were sacrificed after 13 weeks on HFD at the age of 7 months. Organ appearance seemed normal between *Apmap*-ko mice and wt littermates at this age.

In the first cohort, a small group of female *Apmap*-ko (n = 5), *Apmap*-heterozygous (n = 2) and wt (n = 2) littermates were weighed and blood samples were taken in the fed *ad libitum* and fasted state. These mice were littermates of the tested male animals and 16 weeks old at the time of the experiments. There were no changes in body weight, but a trend towards increased plasma glucose in the fed state could be seen (table 6).

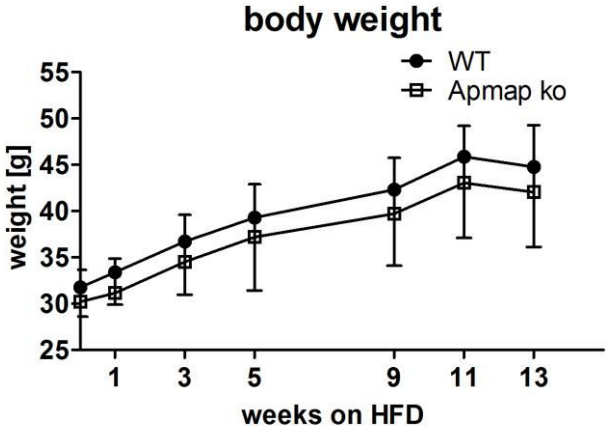

Figure 24: Body weight of male *Apmap*-ko and wt littermates on HFD. HFD diet was initiated at the age of 16 weeks. wt, n = 8; *Apmap*-ko, n = 6.

Table 4: Body weight and blood parameters of the first cohort of male wt and *Apmap*-ko mice on chow diet at the age of 16 weeks. Significant changes are highlighted with grey boxes. wt, n = 8; *Apmap*-ko, n = 6.

	fed			fasted		
parameter	**wt**	**ko**	**p-value**	**wt**	**ko**	**p-value**
Weight [g]	31.8 ± 3.2	30.2 ± 3.4	0.398	29.3 ± 3.6	27.3 ± 3.3	0.298
Glucose [mg/dL]	136.4 ± 37.7	183.8 ± 37.7*	0.026	93.3 ± 37.6	104.8 ± 49.8	0.628
FFA [mg/dL]	9.9 ± 4.7	8.6 ± 2.7	0.550	15.2 ± 4.1	19.0 ± 7.1	0.240
TG [mM]	0.72 ± 0.29	0.76 ± 0.54	0.867	0.47 ± 0.13	0.52 ± 0.29	0.724

Table 5: Body weight and blood parameters of the first cohort of male wt and *Apmap*-ko mice on HFD. Fed plasma parameters were obtained after 9 weeks of HFD, fasted after 11 weeks. n.d.; not determined; wt, n = 8; *Apmap*-ko, n = 6.

	fed			fasted		
parameter	**wt**	**ko**	**p-value**	**wt**	**ko**	**p-value**
Weight [g]	42.3 ± 8.2	39.7 ± 6.0	0.528	n.d.	n.d.	n.d.
Glucose [mg/dL]	241.1 ± 30.4	229.0 ± 27.4	0.457	135.6 ± 68.9	114.0 ± 37.9	0.510
FFA [mg/dL]	14.9 ± 5.9	15.8 ± 6.8	0.809	14.4 ± 3.2	15.7 ± 4.4	0.535
TG [mM]	1.3 ± 0.6	1.4 ± 0.3	0.746	1.6 ± 0.4	1.6 ± 0.5	0.975

Table 6: Body weight and blood parameters of the first cohort of female wt, *Apmap*-heterozygous and *Apmap*-ko mice on chow diet at the age of 16 weeks. wt, n = 2; heterozygous (+/-), n = 2; *Apmap*-ko, n = 5.

	fed			fasted		
parameter	wt	+/-	ko	wt	+/-	ko
Weight [g]	20.6 ± 0.1	22.5 ± 0.7	21.4 ± 2.1	18.5 ± 1.3	20.1 ± 0.6	19.4 ± 1.9
Glucose [mg/dL]	183.5 ± 19.1	199.5 ± 12.0	216.6 ± 21.1	105.0 ± 14.2	96.5 ± 19.1	112.5 ± 0.7

4.1.2.2 Second cohort of *Apmap*-ko mice

Since we could not detect big phenotypical changes, we decided to wait until more generations of breeding on a C57BL/6 background have passed. The next cohort of mice we used were in generation 6 (counting started with the first breeding of heterozygous male with C57BL/6 females). In this second cohort, we used 3 male *Apmap*-ko mice and 4 according wt littermates that were kept on normal chow diet after weaning. At 8-weeks of age we measured body weight and blood parameters after 5 hours fasting. Table 7 shows that there were no significant differences in body weight at the beginning of the diet, although a trend of decreased body weight could be seen. No significant differences in plasma parameters could be measured, although 5-hour fasting blood glucose was slightly increased.

Table 7: Body weight and blood parameters of the second cohort of male wt and *Apmap*-ko mice at the age of 8 weeks fed a chow diet. Light grey marks results that show a trend. wt, n = 4; *Apmap*-ko, n = 3.

	fasted 5 hours		
parameter	wt	ko	p-value
Weight [g]	22.9 ± 2.5	19.8 ± 0.7	0.084
Glucose [mg/dL]	152.5 ± 42.1	194.3 ± 8.5	0.139
FFA [mg/dL]	28.9 ± 4.3	27.8 ± 2.1	0.666
TG [mM]	0.71 ± 0.14	0.79 ± 0.03	0.343

Next, these mice were put on HFD at the age of 8 weeks. After 16 weeks on HFD, we assessed plasma parameters in the fed *ad libitum* state and after 12 hours fasting. Interestingly, after 16 weeks of HFD, fasted blood glucose was elevated and FFAs were significantly decreased in *Apmap*-ko mice compared to control littermates (table 8). All other parameters did not differ between *Apmap*-deficient mice and wt littermates.

Table 8: Body weight and blood parameters of the second cohort of male wt and *Apmap*-ko mice after 16 weeks of HFD. Light grey marks results that show a trend. Parameters that showed a significant change are highlighted in dark grey. wt, n = 4; *Apmap*-ko, n = 3.

	fed			fasted		
parameter	**wt**	**ko**	**p-value**	**wt**	**ko**	**p-value**
Weight [g]	33.3 ± 5	31.0 ± 3.3	0.511	31.2 ± 4.5	29.2 ± 4.3	0.584
Glucose [mg/dL]	186.0 ± 29.6	183.0 ± 28.2	0.872	100.0 ± 18.0	138.7 ± 32.3	0.061
FFA [mg/dL]	5.6 ± 2.0	6.3 ± 1.2	0.633	15.5 ± 2.0	11.5 ± 3.5*	0.025
TG [mM]	1.1 ± 0.3	1.3 ± 0.3	0.277	1.2 ± 0.3	1.2 ± 0.2	0.890

After 12 on HFD, a glucose tolerance tests (GTT) and after 14 weeks on HFD an insulin tolerance test (ITT) was performed in *Apmap*-ko mice and wt-littermates. Figure 25A and C show that 4-hour and 6-hour fasting glucose levels were increased in the plasma of *Apmap*-ko mice. Furthermore, glucose tolerance was impaired in *Apmap*-ko mice compared to their wt-littermates (fig. 25, B). In contrast to that, insulin sensitivity was slightly increased in *Apmap*-ko mice (fig. 25, D). As we detected increased plasma glucose levels upon fasting, we wanted to elucidate how glucose levels change along a fasting period of 24 hours, followed by 1 hour refeeding. Figure 25E shows that glucose levels were higher in *Apmap*-ko already after 2 hours of fasting, which lasted until 5 hours of fasting, although these results did not reach statistical significance. After 24 hours of fasting, no difference between *Apmap*-ko mice and wt littermates could be observed. Plasma glucose levels were also similar after one hour of full access to food.

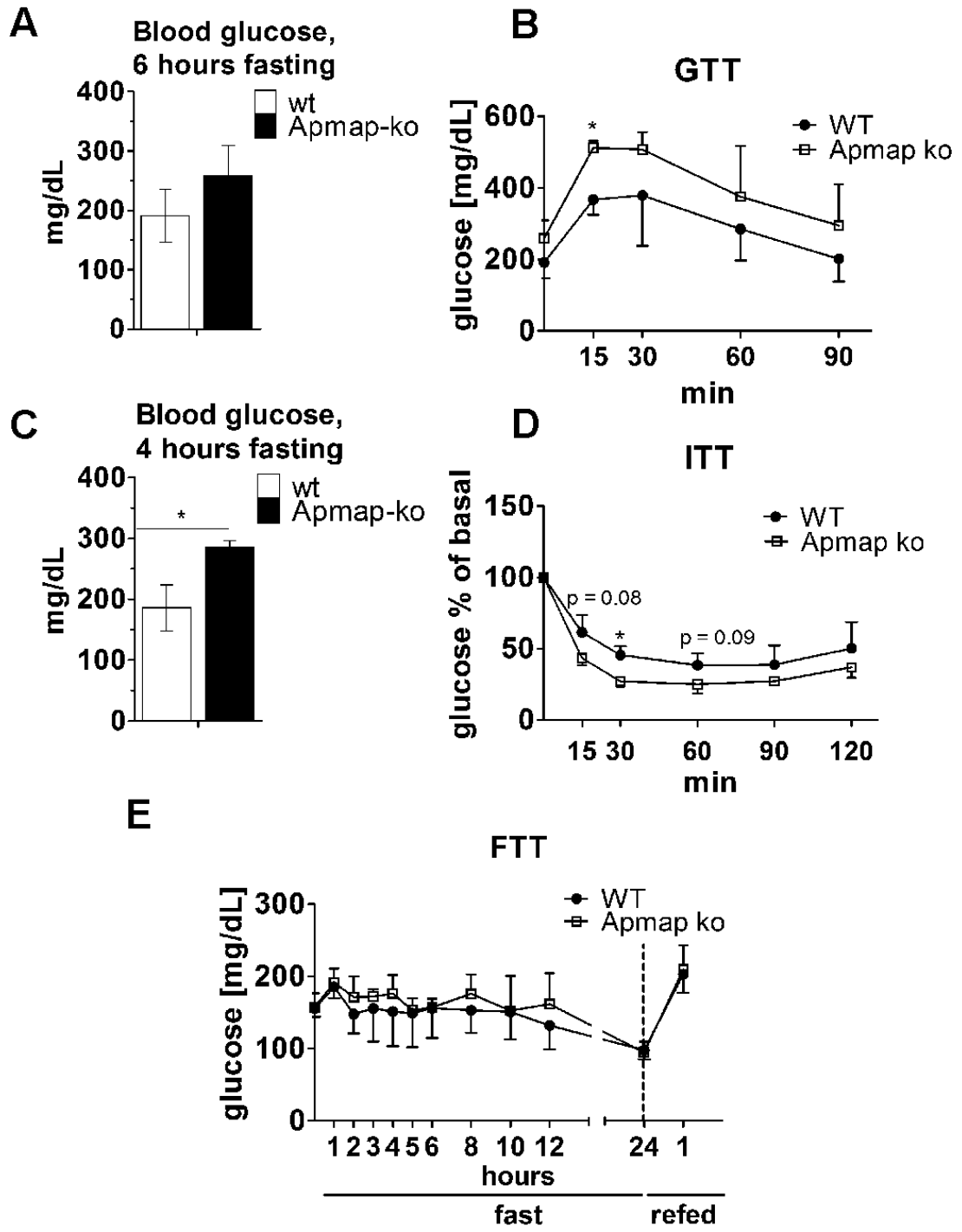

Figure 25: Glucose levels, glucose, insulin, and fasting tolerance tests of male *Apmap*-ko mice compared to wt littermates after 12-14 weeks on HFD. (A) Plasma glucose levels after 6 hours of fasting. (B) Glucose tolerance was assessed with a glucose bolus (1.5 g/kg bodyweight) after 6 hours of fasting and plasma glucose was monitored at the indicated time points. (C) Plasma glucose after 4 hours of fasting. (D) Insulin tolerance was assessed with 0.5 U insulin/kg bodyweight after 4 hours of fasting and plasma glucose was monitored at the indicated time points. (E) Fasting tolerance test started with fed *ad libitum* mice in the morning. After 24 hours of fasting, the mice had free excess to food for one hour. *Apmap*-ko n = 3; wt n = 4. Mice were fed a HFD for 12-14 weeks prior to the experiments.

Since there was always a small difference in body weight between *Apmap*-ko and wt littermates, we performed a lean and fat mass measurement with the miniSpec NMR Analyzer (Bruker Optics). Results revealed that there are no differences in body composition of *Apmap*-ko and wt mice after 24 weeks on HFD (fig. 26).

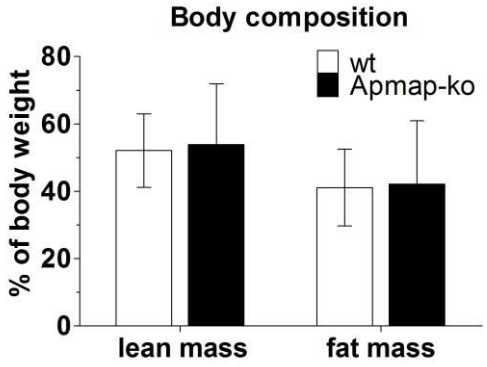

Figure 26: Body composition of male *Apmap*-ko and wt littermates after 24 weeks on HFD. *Apmap*-ko n = 3; wt n = 4.

4.1.2.3 Third cohort of *Apmap*-ko mice

After 8 generations of breeding on a C57BL/6 background, a third cohort was used. In this cohort, male and female *Apmap*-ko mice were kept on chow diet after weaning until 8 or 12 weeks of age, respectively (females n = 6 each, males, wt n = 4; *Apmap*-ko n = 5). At this age, male *Apmap*-ko were significantly lighter than their wt littermates and female *Apmap*-ko mice showed a trend towards decreased body weight (fig. 27, A and B, table 9 and 10). Furthermore, female *Apmap*-ko mice showed decreased plasma TG levels in the fasted state (table 9). Male *Apmap*-ko mice, however, showed a trend towards increased plasma glucose and FFA levels in the fed *ad libitum* state (table 10). At the above indicated ages, the mice were put on HFD. Food intake and weight gain were monitored weekly. Until now, 8 weeks of HFD have passed. Female *Apmap*-ko mice showed a slightly decreased starting weight, but gained the same amount of weight as their wt littermates after 8 weeks of HFD (fig. 27, A). Male *Apmap*-ko mice were significantly lighter from the beginning, which was preserved throughout the HFD (fig. 27, B). Food intake on HFD was not significantly changed between the groups, although male *Apmap*-ko mice showed a trend towards decreased food intake (fig. 27, C and D).

Table 9: Body weight and blood parameters of the third cohort of female wt and *Apmap*-ko mice on chow diet at the age of 12 weeks. Light grey marks results that show a trend. Parameters that showed a significant change are highlighted in dark grey. wt, n = 6; *Apmap*-ko, n = 6.

	fed			fasted		
parameter	wt	ko	p-value	wt	ko	p-value
Weight [g]	21.5 ± 1.6	20.2 ± 1.1	0.147	19.8 ± 1.2	18.4 ± 1.0	0.057
Glucose [mg/dL]	130.0 ± 39.6	125.5 ± 25.9	0.821	98.8 ± 20.2	105.7 ± 11.7	0.490
FFA [mg/dL]	6.6 ± 3.0	5.3 ± 0.3	0.291	18.7 ± 5.3	16.3 ± 3.6	0.380
TG [mM]	0.58 ± 0.11	0.57 ± 0.20	0.973	0.71 ± 0.08	0.53 ± 0.09**	0.006

Table 10: Body weight and blood parameters of the third cohort of male wt and *Apmap*-ko mice on chow diet at the age of 8 weeks. Light grey marks results that show a trend. Parameters that showed a significant change are highlighted in dark grey. wt, n = 4; *Apmap*-ko, n = 5.

	fed			fasted		
parameter	wt	ko	p-value	wt	ko	p-value
Weight [g]	26.4 ± 2.1	20.4 ± 1.7**	0.002	23.7 ± 2.2	18.2 ± 1.3**	0.002
Glucose [mg/dL]	112.5 ± 11.0	143.2 ±30.3	0.098	121.6 ± 19.7	120.0 ± 6.7	0.882
FFA [mg/dL]	6.8 ± 1.3	9.5 ± 1.9	0.053	16.5 ± 3.8	13.6 ± 2.5	0.209
TG [mM]	0.66 ± 0.17	0.71 ± 0.20	0.722	0.91 ± 0.3	0.82 ± 0.47	0.726

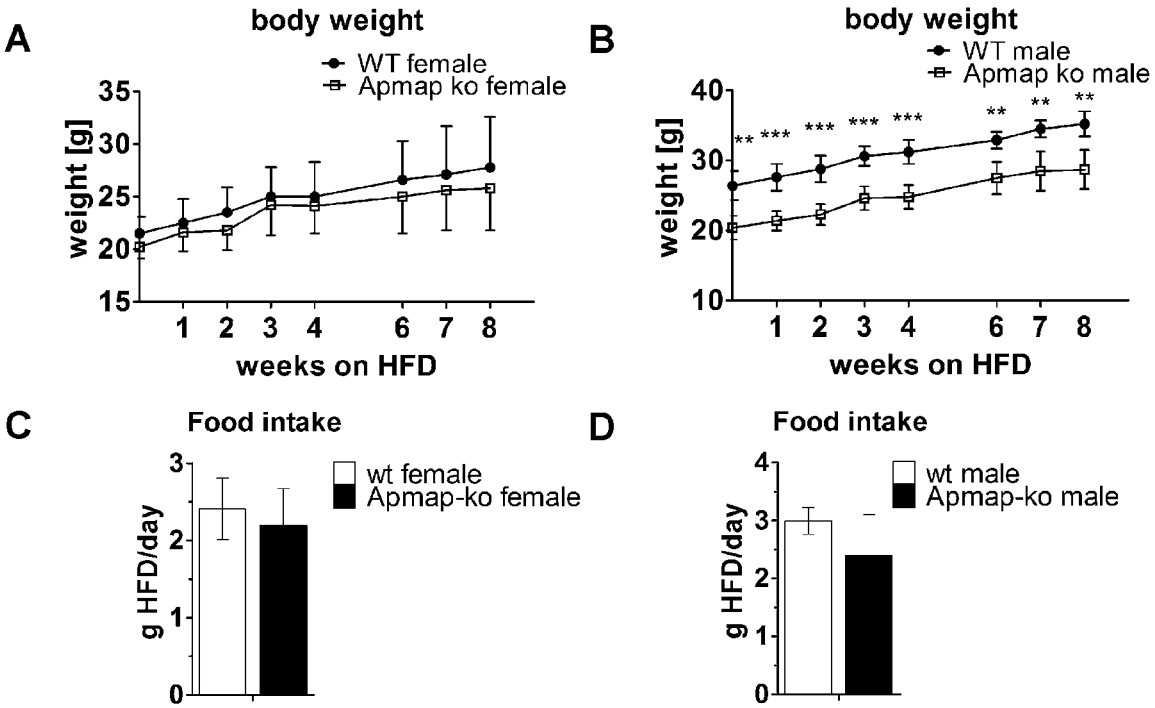

Figure 27: Body weight gain of female and male *Apmap*-ko mice and wt littermates on HFD. (A) Body weight gain on HFD of female mice. n = 6 each. (B) Body weight gain on HFD of male mice. wt, n = 4; ko, n = 5. (C) and (D) HFD food intake measured in g per mouse per day.

After 6 weeks on HFD an ITT and after 7 weeks a GTT was performed with the male cohort. Notably, the trend towards increased short-term fasting plasma glucose could be reproduced in this cohort (fig. 28, A and D). Glucose tolerance was not changed in *Apmap*-ko mice (fig. 28, B). However, figure 28E shows that insulin tolerance is increased in *Apmap*-ko mice, reproducing the result of cohort 2. Additionally, plasma insulin levels during GTT were assessed in this group of *Apmap*-ko mice and wt littermates. No differences in plasma insulin levels at the beginning of the GTT (6 hours fasted) and 20 or 90 min after the glucose bolus could be observed between *Apmap*-ko mice and wt littermates (fig. 28, C).

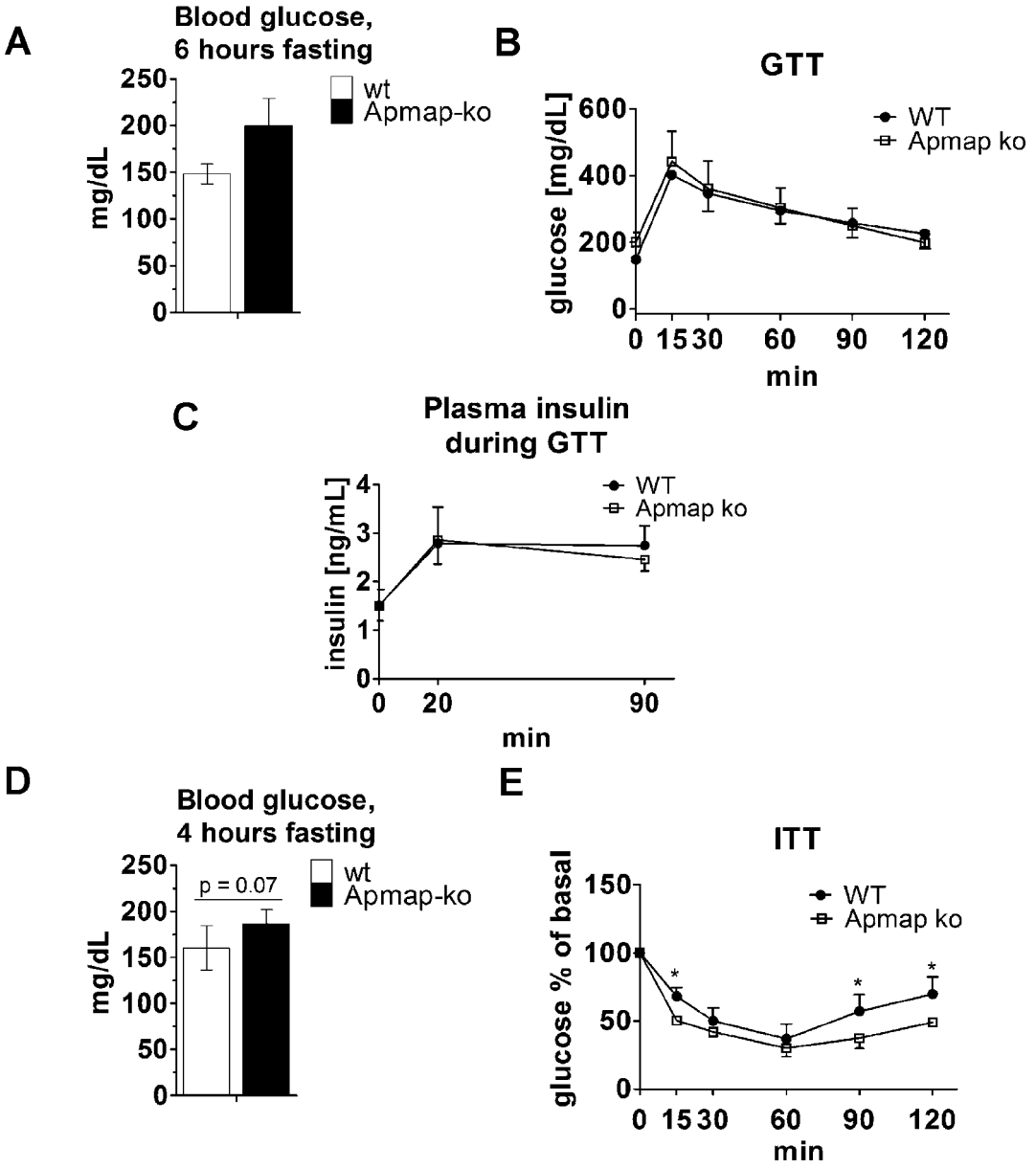

Figure 28: Glucose levels, glucose and insulin tolerance tests of male *Apmap*-ko mice compared to wt littermates after 6-7 weeks of HFD. (A) Plasma glucose after 6 hours of fasting. (B) Glucose tolerance was assessed with a glucose bolus (1.5 g/kg bodyweight) after 6 hours of fasting and plasma glucose was monitored at the indicated time points. (C) Plasma insulin levels at indicated time points during the GTT. (D) Plasma glucose after 4 hours of fasting. (E) Insulin tolerance was assessed with 0.45 U insulin/kg bodyweight after 4 hours of fasting and plasma glucose was monitored at the indicated time points. *Apmap*-ko n = 5; wt n = 4. Mice were fed a HFD for 6 or 7 weeks prior to the GTT or ITT.

Together, some of the results as the decreased body weight, increased plasma glucose upon short-time fasting, decreased fasting plasma FFAs, and increased insulin sensitivity could be shown in more than one cohort of *Apmap*-ko mice. It has to be mentioned here that cohort 3 has been on HFD for only 6-7 weeks, while cohort 2 stayed on this diet for up to 14 weeks before measuring GTT and ITT. Therefore, some inconsistent data could be explained by the different duration of the HFD.

In summary, this data indicate that the missing APMAP protein in some tissues already leads to a phenotype. Notably, glucose homeostasis seems to be mostly affected by the ablation of *Apmap*. This led us to investigate the influence of *Apmap* silencing and overexpression in our established *in vitro* adipogenic cell models in more detail.

4.2 *Elucidation of the function of Apmap in vitro*

4.2.1 Transient o/e of *Apmap* influences *Glut4* expression in differentiated 3T3-L1 cells

We wanted to unravel whether transient silencing or overexpression of *Apmap* in differentiated 3T3-L1 adipocytes influences their capacity to maintain an adipocyte phenotype. For silencing, we electroporated *Apmap*-specific siRNA and non-targeting control (ntc) siRNA particles into nearly full differentiated adipocytes (day 5). A 50% average silencing rate could be achieved with this method (one representative qPCR result is shown in fig. 29, B). The strongest downregulation of *Apmap* could be seen between 24 and 48 hours after electroporation and declined after three days (fig. 29, A). For transient overexpression of *Apmap*, we electroporated plasmids expressing *Apmap* into day 5 adipocytes (pMSCV_Apmap and pMSCV_puro as control). An overexpression from 8 to 40-fold could be achieved (one representative qPCR result is shown in fig. 29, B).
Neither transient silencing nor overexpression of *Apmap* in mature 3T3-L1 adipocytes changed the triglyceride content, indicating that both conditions do not alter the maintenance of the adipocyte phenotype (fig. 29, C, n=1 for each day and microscopic observations of n>3). Interestingly, transient *Apmap* overexpression led to a downregulation of *Glut4* mRNA expression; also *Pparγ*, *C/ebpα* and *aP2* expression was decreased (fig. 29, D). *Apmap* silencing did not alter gene expression (fig. 29, D). As *Apmap*-ko mice showed a phenotype with respect to glucose metabolism, we investigated the influence of transient *Apmap* overexpression or silencing on cellular glucose uptake. Although the assay has been repeated numerous times, no conclusive result could be obtained. When all experiments are averaged, no change in glucose uptake could be observed (fig. 29, E). To unravel whether *Apmap* influences the translocation of GLUT4, we performed life cell-imaging with differentiated 3T3-L1 that were electroporated with vectors containing C-terminal CFP-tagged APMAP (Apmap CFP-N1) or N-terminal YFP-tagged Glut4 (Glut4 YFP-C1). Microscopy was performed in collaboration with Heimo Wolinski at the University of Graz. Apmap-CFP showed a circular localization around lipid droplets (fig. 30, middle row), whereas Glut4-YFP appeared in vesicles-like structures in the cytosol (fig. 30, upper row). This localization in the basal state was already published before[138]. When both were co-expressed in one cell, no co-localization could be observed. However, a higher percentage of GLUT4 protein seemed to localize at the plasma membrane (fig. 30, lower row). This could indicate that the APMAP protein is involved in the regulation of GLUT4 translocation to the plasma membrane, but more experiments to confirm this hypothesis are needed in the future.

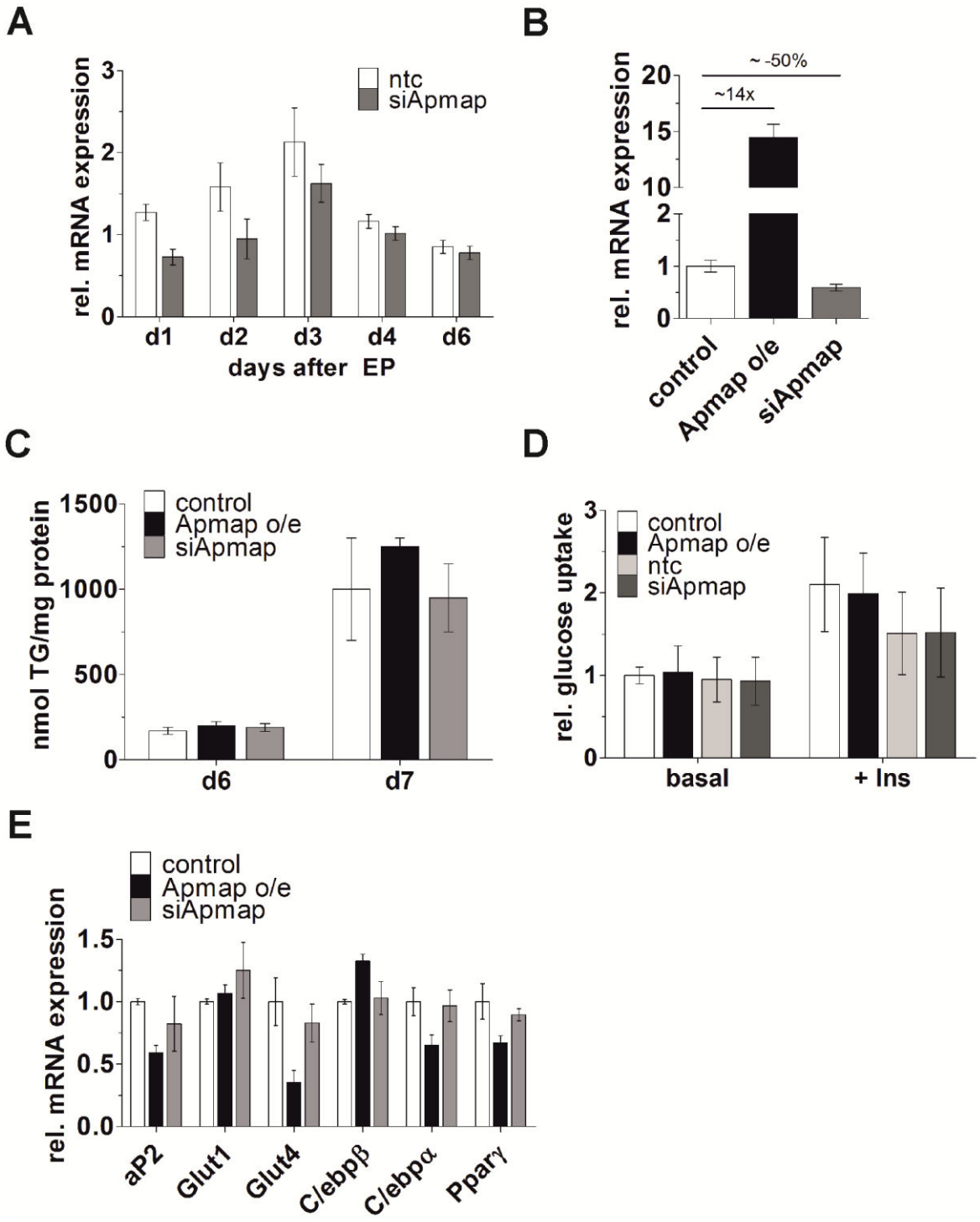

Figure 29: Effects of transient overexpression or silencing on lipid and glucose metabolism of 3T3-L1 cells. (A) Time course of *Apmap* silencing stability from day 1 until 4 and 6 days after electroporation. n = 1. (B) - (E) All experiments or measurements were performed two days after electroporation. (B) Relative mRNA expression of overexpressed or silenced *Apmap* in electroporated 3T3-L1 cells. (C) TG content electroporated 3T3-L1 cells. The indicated day represents the day of harvest. n = 1 each, standard deviations derive from technical replicates. (D) Relative glucose uptake of *Apmap* silenced, o/e and control 3T3-L1 cells. (E) mRNA expression of adipogenic genes in control 3T3-L1 and *Apmap* silenced or o/e cells. One representative qRT-PCR result including 2 biological replicates out of n>3 is shown.

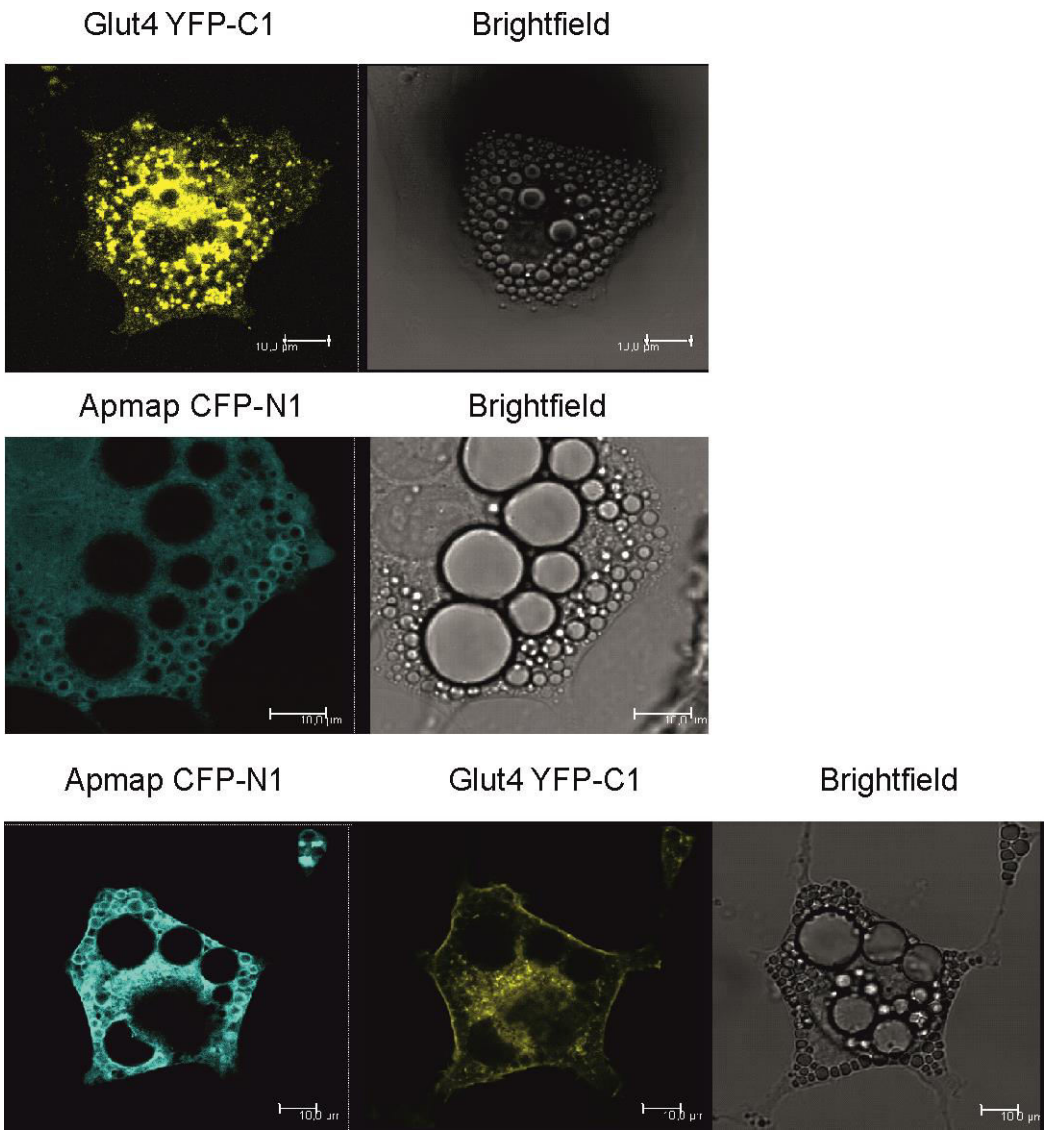

Figure 30: Life-cell imaging of electroporated 3T3-L1 expressing CFP-tagged APMAP and/or YFP-tagged GLUT4. Scale bars = 10 µm

Discussion

5 Discussion

5.1 The role of Nat8l overexpression in brown adipocyte differentiation and metabolism

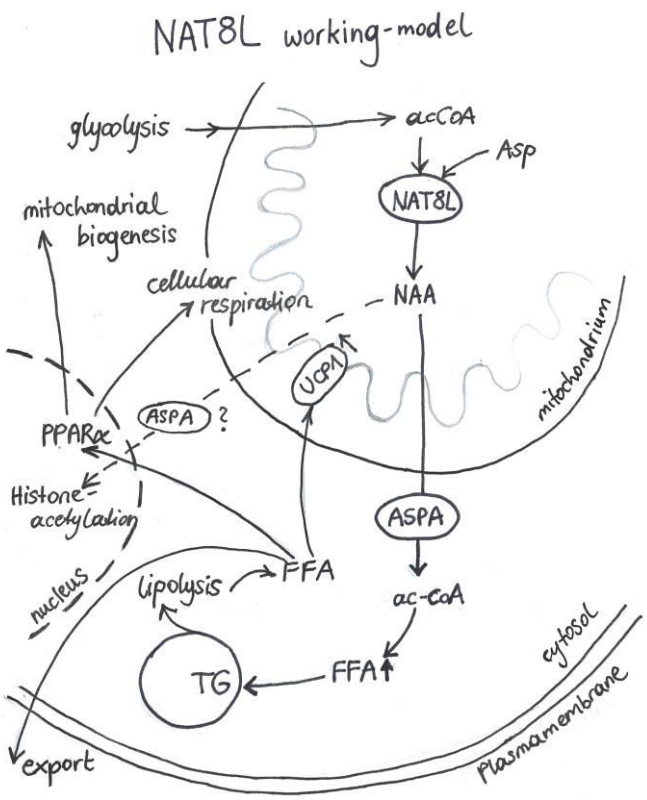

Figure 31: Working model of the proposed NAT8L action in brown adipocytes. Adapted from ref. [104]

The first part of my thesis dealt with the investigation of N-acetyltransferase 8-like (NAT8L) and its impact on brown adipogenic development and metabolism. NAT8L is the enzyme that catalyzes NAA production out of acetyl-CoA and L-aspartate. Numerous studies described its function in brain tissue, but until now nothing was known about its role in adipose tissue. During evaluation of micro-array data sets, we came across this gene, because it is decreased in BAT of Atgl knock-out mice[65]. These mice are characterized by massive accumulation of lipids in adipose tissues, especially BAT, but also other metabolic tissues such as liver and cardiac muscle[139].

Initial investigations in our lab showed that *Nat8l* is equally high expressed in BAT and brain of C57BL/6 mice and to lesser extent also in WAT. Furthermore, *Nat8l* mRNA expression increases during the differentiation of several adipogenic cell lines. Importantly, it is also upregulated during the differentiation of an immortalized brown adipogenic cell line (iBACs).[104] Here, we also show that *Nat8l* expression is downregulated in BAT and WAT of genetically obese (*ob/ob*) mice in comparison to their wt littermates, which is in line with the observation that *Nat8l* expression is decreased in obese Atgl-ko mice. Both animal model are characterized by a massive accumulation of fat in adipose tissue, especially BAT[111,139]. These data implicate a possible role of *Nat8l* in adipose tissue metabolism.

Based on the results obtained in this thesis, we developed a working model that delineates the role of NAT8L in brown adipocytes and its impact on brown adipocyte metabolism upon

overexpression (fig. 31). Important for the construction of such a model was the localization of the NAT8L protein. Although there are controversies about its expression in neuronal tissue[67,69], rendering mitochondria and ER as possible organelles for NAT8L localization, we could clearly show that NAT8L is located in mitochondria of iBACs and BAT. Also overexpressed NAT8L localized exclusively in the mitochondrial compartment. Thus, we assume that NAA, the product of NAT8L's enzymatic reaction, is generated in the mitochondria of brown adipocytes.

We generated iBACs stably overexpressing NAT8L for further investigating its role in brown adipocytes. Since NAT8L consumes acetyl-CoA, we hypothesize that the intra-mitochondrial energy metabolism is influenced by its overexpression (o/e). Initial experiments revealed that *Nat8l* o/e iBACs showed a delay in lipid accumulation during initial differentiation (most pronounced on day 3)[90]. We suppose that *Nat8l* o/e drains acetyl-CoA into the NAA producing pathway. As a consequence, less of this important metabolite would be available for example for lipid synthesis. On day 7 no more differences in lipid accumulation could be observed. This indicates that compensatory mechanisms to produce acetyl-CoA are upregulated. This hypothesis was addressed in this thesis.

Initial characterization of *Nat8l* o/e iBACs also revealed that brown marker gene expression (Pparα, Pgc-1α, and Prdm16) was elevated upon *Nat8l* o/e. In this thesis, these results were confirmed and further brown marker genes with increased expression could be added to this list, such as type 2 iodothyronine deiodinase (*Dio2*)[140], CCAAT/enhancer binding protein beta (*C/ebpβ*)[141] and cell death-inducing DFFA-like effector A (*Cidea*)[142]. These genes are especially important for the development and the maintenance of a brown phenotype. More specifically, *Dio2* catalyzes the conversion of thyroxine (T4) to 3,5,3'-triiodothyronine (T3), an important hormone that regulates intracellular cAMP concentrations. A loss of *Dio2* leads to impaired thermogenesis in BAT due to the inability of generating sufficient amounts of cAMP after sympathetic stimulation.[140] C/EBPβ and CIDEA on the other hand impact on lipid storage in brown adipocytes[141,142]. Moreover, we showed that general adipogenic markers (*aP2* and *AdipoQ*) did not change upon *Nat8l* o/e, except *Pparγ*, which is upregulated on day 3 of differentiation. This could be a compensatory mechanism to stimulate adipogenesis and overcome the delayed lipid accumulation generated through *Nat8l* o/e. In contrast to that, expression of so-called white-specific genes, such as fatty acid desaturase 3 (*Fads3*), resistin (*Retn*) and phosphoserine aminotransferase 1 (*Psat1*) (all from ref. [50]) decreased upon *Nat8l* o/e. We conclude from these data that adipogenesis *per se* is not inhibited by *Nat8l* o/e, but these results indicate a boost in the brown adipogenic phenotype of these cells. Together, this led us to investigate the pathway in more detail.

In brain, biosynthesis and catabolism of NAA are separated between neurons and oligodendrocytes, respectively. The breakdown of NAA into aspartate and acetate is performed through aspartoacylase (ASPA). In this study, we show that *Aspa* is also highly expressed in BAT and upregulated upon *Nat8l* o/e. Furthermore, ongoing studies in our laboratory show that ASPA localizes in the cytosol of brown adipocytes. This indicates that the NAA-pathway exists as a whole in brown adipocytes. Thus, we elucidated the expression of genes involved in pathways that supplement the NAA-pathway with either acetyl-CoA or aspartate and found further evidence that *Nat8l* o/e affects according metabolic pathways.

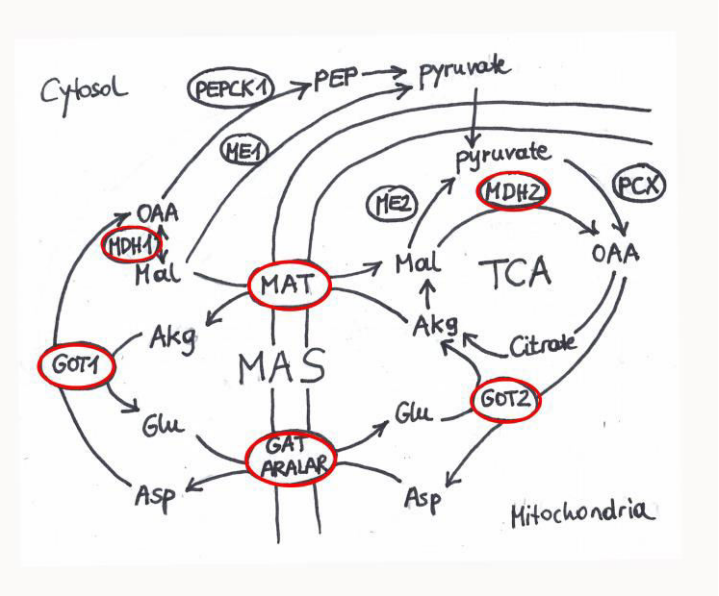

Figure 32: The malate-aspartate shuttle (MAS). Direct components of the shuttle system are marked with a red circle. Abbreviations can be found in the text. Adapted from ref. [124].

Aspartate and α-ketoglutarate (Akg) are produced by the reversible transamination of oxaloacetate (OAA) and glutamate. This reaction is performed by glutamate-oxaloacetate transaminases (GOT) that are either located in the cytosol or the mitochondria. GOTs are important components of the malate-aspartate shuttle (MAS) which consists of several transporters and enzymes (fig. 32, direct components of the MAS are marked with a red circle).[113] Both *Gots* are upregulated upon *Nat8l* o/e, indicating an enhanced flux through this pathway and thereby increased production of aspartate that is needed for NAT8L action. An important step for maintenance of mitochondrial aspartate levels is the transport of glutamate into the mitochondria. Patel and Clark[76] already showed in 1979 that neuronal NAA production is increased by glutamate addition. The glutamate-aspartate antiporter ARALAR is proposed to mediate glutamate transport into the mitochondria of neurons. Thereby, it is also part of the MAS. In brain of *Aralar*-ko mice aspartate levels are concomitantly decreased due to the impaired glutamate import which correlates with decreased neuronal NAA content.[118] Until now, ARALAR was not implicated in adipose tissue metabolism, but we show in this study that *Aralar* is expressed in iBACs and upregulated upon *Nat8l* o/e. This further supports that glutamate-aspartate flux is increased in *Nat8l* o/e cells, guaranteeing a stable aspartate supply for NAA production.

Malate is another important metabolite in the MAS system. Firstly, it is transported into the mitochondria in exchange of α-ketoglutarate and secondly it is metabolized in the

mitochondria into other components, such as OAA and pyruvate (fig. 32). It seems that there is an increased malate utilization in *Nat8l* o/e iBACs, since malate dehydrogenases 1 and 2 (*Mdh*), other components of the malate-aspartate shuttle[113], are elevated. *Mdh* converts malate to OAA and vice versa. This reaction could therefore fuel the mitochondrial OAA pool which can subsequently be used for downstream reactions, such as the GOT-mediated transamination of glutamate. Through the MDH-mediated reaction the important reducing equivalent NADH is produced that is required for the electron transport chain. Thereby, proper oxidation of glucose is garanteed.[113] Moreover, malate can also be used by malic enzymes (MEs) to produce pyruvate[119]. In *Nat8l* o/e iBACs we see a decreased expression of the cytosolic form *Me1*, but an increase of the mitochondrial *Me2* on day 3 of differentiation. This may also indicate enhanced malate utilization in the mitochondria of *Nat8l* o/e cells to support downstream substrate availability.

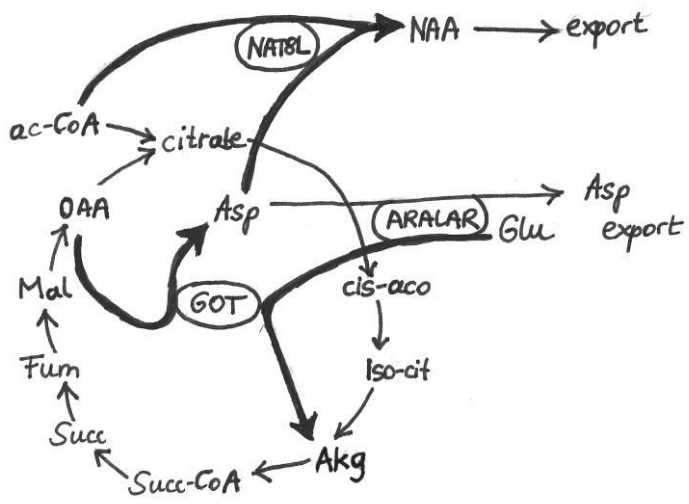

Figure 33: Proposed role of NAT8L in a so-called „mini TCA-cycle". Cis-aco, cis-aconitate; Fum, fumarate; Iso-cit, iso-citrate; Mal; malate; Succ, succinate; Succ-CoA, succinyl-CoA. All other abbreviations are listed in the text. Scheme adapted from ref. [81]

Another interesting aspect of NAT8L in mitochondrial substrate utilization is its role in facilitating respiration by participating in a so-called "mini TCA-cycle"[143]. Under normal conditions, the first step of the citric acid (TCA) cycle is the condensation of acetyl-CoA and OAA to form citrate. Alternatively, α-ketoglutarate that is produced by the action of GOT can directly enter the TCA cycle. Thus, additional energy could be derived from oxidation of glutamate. In neurons, it was shown that this is the fastest reaction to supply the TCA-cycle with substrates[143]. In our model, NAT8L would metabolize the produced aspartate from the GOT-mediated reaction, thereby creating a feed-forward loop (see fig. 33). Furthermore, this spares acetyl-CoA that can be used for NAA production. From our results a scenario like this is plausible, but the physiological stimuli that lead to this truncated TCA cycle in brown adipocytes remain to be elucidated.

In brain, NAA is shuttled from neurons to oligodendrocytes (a scheme is shown in fig. 6)[81]. The sodium-dependent solute carrier NaDC3 (Slc13A3) has been implicated in the transport out of neuronal cells[80]. Since NAA was detected in urine of patients[144], a secretion of NAA

from brown adipocytes is feasible. Therefore, we tested whether NaDC3 is expressed in brown adipocytes and influenced by *Nat8l* o/e. *NaDC3* mRNA expression was hardly detectable in iBACs and there was no change in mRNA expression level upon *Nat8l* o/e. From these results, we assume that if NAA transport out of brown adipocytes occurs, NaDC3 might not be the responsible transporter for NAA. On the other hand, the dicarboxylate-carrier DIC was proposed by Arun and associates[122] to be involved in mitochondrial NAA transport, although no functional studies have been included in this study. *Dic* mRNA levels are high in brown adipocytes, but instead of an anticipated increase of *Dic* upon *Nat8l* o/e, we see a decrease on day 7 of differentiation. In a different study, DIC was shown to mediate malate transport out of the mitochondria[145]. The downregulation of *Dic* would support the hypothesis that malate is retained in mitochondria to sustain OAA production. Since mRNA expression of *Dic* is very high in brown adipocytes, it is still possible that NAA is transported into the cytosol through this transporter. Together, NAA transport between cellular compartments and out of cells is poorly understood and a matter of further investigation.

BAT highly depends on the maintenance of intracellular lipid stores to sustain non-shivering thermogenesis[146,147]. Acetyl-CoA acts as a central substrate that is used for energy producing pathways as the TCA cycle, as well as building block for cellular lipid metabolism[148]. Those reactions require a constant acetyl-CoA supply, as does the synthesis of NAA. Therefore, NAA synthesis can only occur when acetyl-CoA is in excess of current metabolic requirements[81]. It has been shown by Jell and associates[72] that transgenic overexpression of an N-acetyltransferase (spermine/spermidine N1-acetyltransferase SSAT) in mice leads to altered acetyl-CoA metabolism and thereby inhibits lipid metabolism. These mice are characterized by a lean phenotype and increased glucose and palmitate oxidation[72]. Hence, we hypothesize that acetyl-CoA is similarly drained into mitochondria in *Nat8l* o/e iBACs to meet the acetyl-CoA need. Mitochondrial acetyl-CoA is mainly derived from two sources, carboxylation of glycolysis derived pyruvate and β-oxidation of FFA[148]. In brain, it has already been shown that glycolysis derived pyruvate is a primary source of mitochondrial acetyl-CoA for NAA production[149]. Concomitantly, insulin stimulated glucose uptake is slightly increased in *Nat8l* o/e iBACs. We assume that acetyl-CoA derived from pyruvate decarboxylation is an important substrate for the *Nat8l*-reaction, but not sufficient to maintain the energy pool in mitochondria of *Nat8l* o/e iBACs. Along with this hypothesis, we found increased release of FFAs from fully differentiated *Nat8l* o/e iBACs, indicating increased lipolytic activity in these cells. To maintain the energy supply in *Nat8l* o/e cells, lipolysis derived FFAs might be fueled into β-oxidation. Accordingly, there are indications for an increased FFA-oxidation in *Nat8l* o/e iBACs, since genes involved in delivering FFA to mitochondrial β-oxidation, such as *Fabp3*[131] and *Cpt1β*[19,150] are upregulated upon *Nat8l* o/e. Moreover, *Pdk4* mRNA expression shows a strong increase in *Nat8l* o/e iBACs. *Pdk4* inhibits the pyruvate-dehydrogenase complex, leading to a switch from glucose to fatty acid oxidation[151].

In addition to above mentioned pathways, we propose that mitochondrial Acss1 derived acetyl-CoA could be another source of acetyl-CoA important for NAA-synthesis. Acetate has been shown to be a primary substrate of mitochondrial *Acss1*, especially in conditions of increased energy need, such as fasting[121,152,153]. We found a massive upregulation of *Acss1* in *Nat8l* o/e iBACs which supports our hypothesis.

In contrast to the increased lipolysis intracellular TG pool is not affected in mature iBACs upon *Nat8l* o/e. We propose that the NAA pathway serves as an alternative pathway to provide acetyl-CoA for lipid synthesis in brown adipocytes and that overexpression of *Nat8l* produces increased amounts of cytosolic NAA that can be used for lipid synthesis (fig. 34).

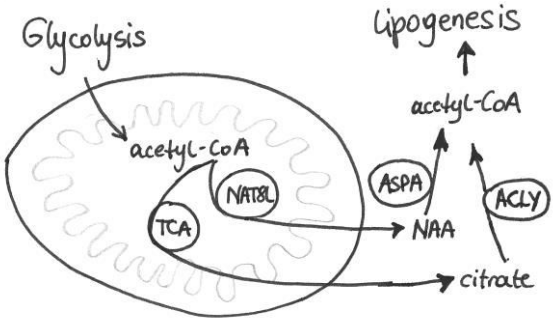

Figure 34: The NAA-pathway as an alternative pathway to produce cytosolic acetyl-CoA for lipogenesis. Adpated from ref. [104].

The classical pathway to generate cytosolic acetyl-CoA in peripheral tissues is the ATP-dependent cleavage of citrate into OAA and acetyl-CoA by ATP-citrate lyase (*Acly*)[153,154]. In neurons, NAA has been shown to serve as an alternative acetate source for the production of acetyl-CoA that is subsequently used for fatty acid synthesis[77]. In iBACs o/e *Nat8l* initial evidence that acetyl-CoA production from NAA is elevated comes from the increased expression of *Aspa* and acetyl-CoA synthetase *Acss2*. We propose that newly synthesized FFAs coming from NAA-derived acetyl-CoA are readily reesterified to prevent lipotoxicity. Accordingly, we show that neutral lipid production such as TG, DG, FFA, and CE from glucose is increased in *Nat8l* o/e iBACs.

As discussed above lipolysis is increased in *Nat8l* o/e iBACs. Lipolysis derived FFA are not only energy substrates, but also regulate the activation of transcription factor PPARα[133,155–157]. Sustained activation of PPARα in turn leads to increased β-oxidation[158]. We measured increased Pparα expression in *Nat8l* o/e iBACs already on day 3 of differentiation, which led us to the assumption that PPARα might be centrally involved in the regulation of the observed phenotype in *Nat8l* o/e iBACs. PPARα not only regulates fatty acid catabolism, together with PGC-1α it also increases the expression of *Ucp1*[159]. Therefore, the massive increase in *Ucp1* expression in *Nat8l* o/e iBACs could be explained by a sustained PPARα activation. Moreover, PPARα, PGC-1α and also PRDM16 have been shown to mediate mitochondrial biogenesis[47,51,128]. We see these genes elevated in *Nat8l* o/e iBACs which could contribute to the elevated mitochondrial number in these cells. Brown adipocytes are characterized by a high number of mitochondria that give them their high oxidative capacity. However, mainly responsible for a brown phenotype is UCP1[8]. Along with the massive

increase of UCP1 expression and the elevated mitochondrial number, we found higher basal, as well as norepinephrine stimulated oxygen consumption rate (OCR) in *Nat8l* o/e iBACs. The increase in basal OCR could result from a higher metabolic rate in *Nat8l* o/e iBACs resulting from increased oxidation of FFA and glucose. Norepinephrine stimulates β-adrenergic receptors which leads to a rise in intracellular cAMP and a subsequent activation of lipolysis[8]. The generated intracellular FFA are allosteric activators of UCP1[18]. Therefore, our obtained data suggests that UCP1 may be involved in the increased NE-stimulated OCR.

We assume that the phenotypes observed in *Nat8l* o/e iBACs are mediated through the production of NAA and its consequent catabolism. To test this hypothesis, we overexpressed an enzymatic inactive form of NAT8L and performed the same experiments as discussed above. Thereby, we changed aspartate on position 165 to alanine, as described by Tahay *et al.* for the human *NAT8L* gene[69]. Overexpressing this mutant, we could show that none of the observed phenotypes, such as elevated brown marker gene expression, decreased lipid accumulation on day 3 and increased FFA release, could be reproduced. This supports that NAT8L enzymatic activity is indeed required for the phenotypic alterations seen in *Nat8l* o/e iBACs.

In our study, we showed that *Nat8l* o/e increased *Pparα* expression. Therefore, we hypothesized that PPARα plays a central role in mediating *Nat8l*-initiated phenotypes. Currently, this hypothesis is addressed in our working group and results show that some of the effects (increased brown marker gene expression and oxygen consumption rate) can be reversed by addition of a PPARα antagonist (GW6471) to *Nat8l* o/e iBACs[104]. Additionally, when incubating iBACs with this PPARα inhibiting compound, we showed that *Nat8l* expression itself is decreased, arguing for a regulation of *Nat8l* gene transcription through PPARs. Additional evidence for a PPAR regulation, in this case PPARγ, is given by the observation that mice fed a rosiglitazone (Rosi) containing diet show higher *Nat8l* expression WAT. However, *Nat8l* expression is decreased in BAT of Rosi treated mice, indicating a differential expressional regulation in these tissues. Published data sets of ChIP experiments of WAT, BAT and differentiated 3T3-L1 cells[108,109] revealed a putative PPAR binding site in intron 2 (2610-3081 downstream from TSS) of the *Nat8l* gene. Functional luciferase reporter assays using the corresponding fragment in a luciferase reporter vector revealed a highly significant upregulation of luciferase activity after co-transfection with PPARγ and RXRα, which could further be elevated by Rosi addition. Additionally, *Nat8l* mRNA expression is hardly detectable in fibroblasts and strongly increased during differentiation of white and brown adipocytes. From these data we conclude that *Nat8l* expression is regulated by PPARγ during adipogenesis. Although we suppose that *Nat8l* is also regulated by PPARα, especially in BAT, we could not show a functional PPARα binding in luciferase reporter

assays. A possible reason for this may be the requirement of other co-factors than RXRα that were not included in the experiment.

In summary, this thesis provides strong data showing that the NAA producing pathway exists in brown adipocytes. By overexpression of *Nat8l*, the main enzyme in this pathway, we see a number of interesting phenotypes. These include the upregulation of brown marker genes (especially UCP1), increased lipid turnover, and elevated mitochondrial number accompanied by a higher oxygen consumption rate. Our data suggest that Pparα may play a central role in mediating those phenotypes. Many of these results could be explained by an increased acetyl-CoA flux into the NAA pathway, thereby producing a futile cycle that ultimately boosts the brown adipose phenotype.

Conclusively, we propose that the *Nat8l*-mediated NAA pathway could alternatively provide acetyl-CoA in tissues with high energy demand and lipid metabolism, such as brown adipocytes. Future approaches deal with the identification of physiological stimuli that lead to NAT8L activation. The elucidation of the NAT8L-mediated pathway will provide new insights into brown adipocyte energy metabolism. This could ultimately unravel new therapeutic approaches in the fight against obesity.

5.2 The role of Apmap in glucose homeostasis

In the second part of my thesis we elucidated the role of APMAP in adipogenesis and energy metabolism. Our published *in vitro* data showed that Apmap is required for adipogenesis. Furthermore, it was proven that *Apmap* is a direct and functional PPARγ target gene.[93] However, the biochemical function of APMAP in adipogenesis and adipocyte metabolism remained elusive. Therefore, we aimed to generate a mouse model deficient of *Apmap* gene expression, to elucidate its role *in vivo*. Because adipogenesis is impaired in *Apmap*-silenced 3T3-L1 cells, we expected those mice to be lean with less or no adipose tissue detectable.
Exon 1, together with parts of 5'UTR and intron 1, was chosen to be deleted, because this part of the gene harbors the transcription start site (marked with a green circle and an asterisk in fig. 35). Therefore, the production of a functional transcript should be prevented. Early on in the generation of the knockout mouse we had to face problems since we did not get male founders that transmitted the mutated gene region. Thus, we had to repeat the blastocyst injection and only used floxed ES cell clones. One of the high chimeric male founders produced litters that were recognized as heterozygous-floxed by their agouti coat color and by PCR analysis. We crossed these mice with CMV-Cre to gain the first heterozygous *Apmap*-ko stock. From the first heterozygous/heterozygous breedings, we learned that *Apmap* heterozygous mice are fertile and that their homozygous *Apmap*-ko offspring is viable. Furthermore, a normal Mendelian ratio was observed among the litters. From the first available *Apmap*-ko mice cohort we harvested several tissues and performed qRT-PCR with two primer sets. These results revealed that the knockout was successful, but in some tissues there was still a truncated version of the *Apmap* transcript detectable. Unfortunately, we also detected a protein band in liver and eWAT. Therefore, we went back to literature to examine the *Apmap* gene again in more detail. No splicing variants were described until then, but we could find an in-frame ATG that could possibly serve as a start-codon in exon 2 (marked with a green box and a cross in fig. 35). In December 2013 three more predicted transcript variants were published on the National Center for Biotechnology Information (NCBI) homepage (http://www.ncbi.nlm.nih.gov/nuccore/?term=apmap+mus+musculus, July 2014). The full-length version results in a 415 amino acids (aa) (~47 kDa) protein, as depicted in figure 35. Transcript variant X1 (XM_006500198.1) does not contain exon 1, but aligns starting with exon 2 with the described *Apmap* coding sequence. If the ATG in exon 2 in this variant takes over as a start-codon, a protein of 376 aa (42 kDa) would be translated. Transcript variant X2 (XM_006500199.1) does contain exon 1, but harbors an in-frame stop codon after exon 2 that prevents a full transcription of the *Apmap* gene. If the ATG in exon 1 would be the start-codon a protein of only around 10 kDa would be generated. A transcription from this ATG is

therefore unlikely. There is again alignment with the described *Apmap* gene from exon 3, which also contains an in-frame methionine (ATG). This would result in a protein of 38 kDa. Transcript variant X3 (XM_006500200.1), however, contains exon 3 and 4, but aligns with the described full-*Apmap* version from exon 5. A predicted coding sequence starts here in exon 6 and results in a 220 aa (25 kDa) big protein. The antibody, we used for APMAP detection would recognize all protein variant, because the peptide used for immunization is located in the C-terminal region of the protein (marked in yellow in figure 35). Although, the antigen used to produce the antibody originated from human APMAP (NPB1-59914, Novusbio) and the manufacturer did not give approval that it recognizes the murine protein, it detected the murine version. We sometimes observed a protein-band at ~25 kDa with the APMAP antibody. If this is indeed a truncated APMAP version has to be elucidated in the future using mass spectrometry analysis. The transmembrane region is coded within exon 2 of the *Apmap* gene. If transcript variant X2 and 3 exist, expression of these variants could result in a soluble form of *Apmap*. These proteins could have a totally different function than the membrane bound version. Although, these are all just bioinformatic predictions, we cannot exclude that there are alternative splicing variant in different tissues that are not affected by the knockout of exon 1. With this knowledge the transcription and protein expression of *Apmap* has to be newly assessed.

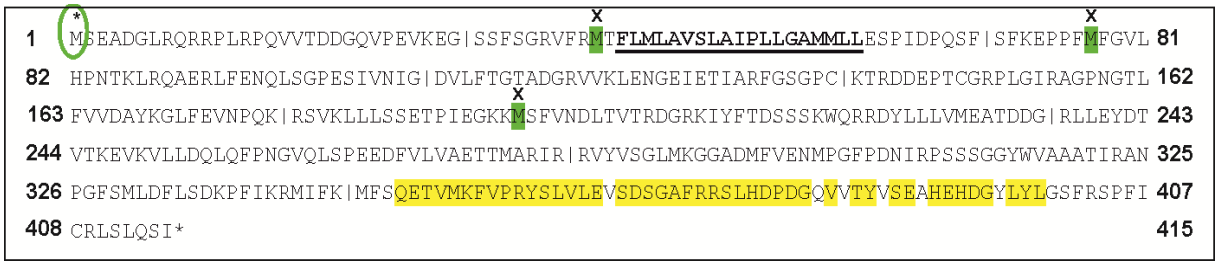

Figure 35: Full-length APMAP amino acid (aa) sequence. The start-codon in exon 1 is marked with a green circle and an asterisk. Alternative start-codons described in the text are marked with green boxes and crosses. The hydrophobic transmembrane region is highlighted with bold and underlined letters. Corresponding alternating exon borders are indicated with a straight line and the peptide sequence used for raising the APMAP antibody is highlighted in yellow.

We could not detect the full-length version of the APMAP protein in BAT, sWAT and lung, but there was an APMAP protein band at 47 kDa in eWAT and liver. Nevertheless, we wanted to elucidate whether a phenotype in *Apmap*-ko mice exists. During this thesis it was possible to initially characterize three different cohorts of *Apmap*-ko mice and according wt littermates. Cohorts 2 and 3 were litters of breedings that exceeded 5 generations of backcrossing. Therefore, the discussion concentrates on the results obtained from these cohorts. We observed decreased body weight in all cohorts of *Apmap*-ko mice on chow diet. They were also lighter throughout feeding with HFD, although they gained the same amount of weight when compared to controls. This could be due to decreased adipogenic ability *in vivo*, as we

saw impaired adipogenesis in 3T3-L1 cells *in vitro*[93]. Nevertheless, body composition was the same between *Apmap*-ko and wt littermates of cohort 2 (only measured in this cohort). Therefore, it will be interesting to elucidate adipocyte number and mass in *Apmap*-ko mice in future studies. Interestingly, short-term fasting glucose was elevated in male *Apmap*-ko mice in cohort 2 and 3. Furthermore, glucose tolerance was impaired in *Apmap*-ko mice in cohort 2 and insulin sensitivity was increased in both cohorts. Plasma insulin levels, which were measured in cohort 3 during GTT, did not differ between *Apmap*-ko mice and wt littermates. This indicates that insulin production from pancreatic β-cells is not influenced by *Apmap* knockdown. However, these data indicate that APMAP plays a role the regulation of glucose homeostasis in the acute response to diet restriction. In healthy individuals, plasma glucose remains in a narrow range. Nutritional glucose is absorbed in the intestine, transported through the blood stream and taken up from peripheral tissues. The primary regulator for these processes is insulin. In times of feeding, glucose production from the liver is inhibited by insulin, while it is activated by glucagon to provide glucose in fasting periods.[58] At a cellular level, insulin stimulates the translocation of GLUT4 from intracellular vesicles to the plasma membrane, where glucose uptake takes place[160]. Membrane bound APMAP may be involved in the translocation of GLUT4. It is possible that APMAP somehow tethers GLUT4 to the plasma membrane or facilitates its translocation. Our preliminary life-cell microscopy experiments indicated that this role is possible because it appeared that more GLUT4 could be found in the plasma membrane when APMAP is co-expressed in the cells. This result was obtained in unstimulated adipocytes. Since it is very difficult to perform co-transfections in differentiated adipocytes and results are hard to interpret, we will use a special 3T3-L1 cell model to address this hypothesis in the future. We received 3T3-L1 cells stably overexpressing GLUT4 tagged with a GFP-protein and a HA-tag from J. Bogan (Yale University, New Haven, USA). This cell line was previously used to study translocation processes of GLUT4 and allows to distinguish intracellular from membrane bound GLUT4[161]. By overexpressing *Apmap* in this cell line, we will be able to see whether more GLUT4 is shuttled to the plasma membrane. Additionally, it will be important to investigate how co-expressed APMAP and GLUT4 protein behave in response to insulin stimulation and fasting.
Another question that remains is the regulation of *Glut4* expression upon transient o/e of *Apmap*. *Glut4* expression has been shown to be controlled by PPARγ[162,163]. *Pparγ* is also downregulated in transient *Apmap* overexpressing 3T3-L1 cells. How *Apmap* influences *Pparγ* and *Glut4* expression, though, is a matter for further investigations.

In summary, there are indications for a possible role of *Apmap* in regulating glucose homeostasis. However, the biochemical function of APMAP remains still elusive. Apart from that, physiological stimuli that regulate *Apmap* expression are obscure. Some working groups propose a role for APMAP in detoxification or coagulation in plasma[100–102], but since we could not detect protein expression in plasma of normal fed mice, we did not deal with this aspect in this study. Moreover, it is unknown whether different splice-variants are expressed in murine tissues and whether these variants have different functions. Future investigations are needed to address these questions to elucidate the biochemical and physiological function of APMAP.

References

6 References

1. Wang, Y. C., McPherson, K., Marsh, T., Gortmaker, S. L. & Brown, M. Health and economic burden of the projected obesity trends in the USA and the UK. *Lancet* **378,** 815–825 (2011).
2. Smorlesi, A., Frontini, A., Giordano, A. & Cinti, S. The adipose organ: white-brown adipocyte plasticity and metabolic inflammation. *Obes. Rev. Off. J. Int. Assoc. Study Obes.* **13 Suppl 2,** 83–96 (2012).
3. Young, S. G. & Zechner, R. Biochemistry and pathophysiology of intravascular and intracellular lipolysis. *Genes Dev.* **27,** 459–484 (2013).
4. Waldén, T. B., Hansen, I. R., Timmons, J. A., Cannon, B. & Nedergaard, J. Recruited vs. nonrecruited molecular signatures of brown, 'brite,' and white adipose tissues. *Am. J. Physiol. Endocrinol. Metab.* **302,** E19–31 (2012).
5. Romacho, T., Elsen, M., Röhrborn, D. & Eckel, J. Adipose Tissue and its Role in Organ Crosstalk. *Acta Physiol. Oxf. Engl.* (2014). doi:10.1111/apha.12246
6. Rosen, E. D. & Spiegelman, B. M. What We Talk About When We Talk About Fat. *Cell* **156,** 20–44 (2014).
7. Bartelt, A. & Heeren, J. The holy grail of metabolic disease: brown adipose tissue. *Curr. Opin. Lipidol.* **23,** 190–195 (2012).
8. Cannon, B. & Nedergaard, J. Brown adipose tissue: function and physiological significance. *Physiol. Rev.* **84,** 277–359 (2004).
9. Cannon, B., Hedin, A. & Nedergaard, J. Exclusive occurrence of thermogenin antigen in brown adipose tissue. *FEBS Lett.* **150,** 129–132 (1982).
10. Arechaga, I., Ledesma, A. & Rial, E. The mitochondrial uncoupling protein UCP1: a gated pore. *IUBMB Life* **52,** 165–173 (2001).
11. Dawkins, M. J. & Scopes, J. W. Non-shivering thermogenesis and brown adipose tissue in the human new-born infant. *Nature* **206,** 201–202 (1965).
12. SMITH, R. E. & ROBERTS, J. C. THERMOGENESIS OF BROWN ADIPOSE TISSUE IN COLD-ACCLIMATED RATS. *Am. J. Physiol.* **206,** 143–148 (1964).
13. Nedergaard, J., Bengtsson, T. & Cannon, B. Unexpected evidence for active brown adipose tissue in adult humans. *Am. J. Physiol. Endocrinol. Metab.* **293,** E444–452 (2007).
14. Van Marken Lichtenbelt, W. D. *et al.* Cold-activated brown adipose tissue in healthy men. *N. Engl. J. Med.* **360,** 1500–1508 (2009).
15. Virtanen, K. A. *et al.* Functional brown adipose tissue in healthy adults. *N. Engl. J. Med.* **360,** 1518–1525 (2009).
16. Saito, M. *et al.* High incidence of metabolically active brown adipose tissue in healthy adult humans: effects of cold exposure and adiposity. *Diabetes* **58,** 1526–1531 (2009).
17. Cypess, A. M. *et al.* Identification and importance of brown adipose tissue in adult humans. *N. Engl. J. Med.* **360,** 1509–1517 (2009).
18. Fedorenko, A., Lishko, P. V. & Kirichok, Y. Mechanism of Fatty-Acid-Dependent UCP1 Uncoupling in Brown Fat Mitochondria. *Cell* **151,** 400–413 (2012).
19. Vergnes, L., Chin, R., Young, S. G. & Reue, K. Heart-type fatty acid-binding protein is essential for efficient brown adipose tissue fatty acid oxidation and cold tolerance. *J. Biol. Chem.* **286,** 380–390 (2011).
20. Festuccia, W. T., Blanchard, P.-G. & Deshaies, Y. Control of Brown Adipose Tissue Glucose and Lipid Metabolism by PPARγ. *Front. Endocrinol.* **2,** 84 (2011).
21. Kopecky, J., Clarke, G., Enerbäck, S., Spiegelman, B. & Kozak, L. P. Expression of the mitochondrial uncoupling protein gene from the aP2 gene promoter prevents genetic obesity. *J. Clin. Invest.* **96,** 2914–2923 (1995).
22. Kopecký, J. *et al.* Reduction of dietary obesity in aP2-Ucp transgenic mice: mechanism and adipose tissue morphology. *Am. J. Physiol.* **270,** E776–786 (1996).
23. Enerbäck, S. *et al.* Mice lacking mitochondrial uncoupling protein are cold-sensitive but not obese. *Nature* **387,** 90–94 (1997).

24. Feldmann, H. M., Golozoubova, V., Cannon, B. & Nedergaard, J. UCP1 Ablation Induces Obesity and Abolishes Diet-Induced Thermogenesis in Mice Exempt from Thermal Stress by Living at Thermoneutrality. *Cell Metab.* **9,** 203–209 (2009).
25. Lowell, B. B. *et al.* Development of obesity in transgenic mice after genetic ablation of brown adipose tissue. *Nature* **366,** 740–742 (1993).
26. Wu, J. *et al.* Beige adipocytes are a distinct type of thermogenic fat cell in mouse and human. *Cell* **150,** 366–376 (2012).
27. Seale, P. *et al.* PRDM16 controls a brown fat/skeletal muscle switch. *Nature* **454,** 961–967 (2008).
28. Sanchez-Gurmaches, J. & Guertin, D. A. Adipocyte lineages: tracing back the origins of fat. *Biochim. Biophys. Acta* **1842,** 340–351 (2014).
29. Peirce, V., Carobbio, S. & Vidal-Puig, A. The different shades of fat. *Nature* **510,** 76–83 (2014).
30. Vitali, A. *et al.* The adipose organ of obesity-prone C57BL/6J mice is composed of mixed white and brown adipocytes. *J. Lipid Res.* **53,** 619–629 (2012).
31. Rosenwald, M. & Wolfrum, C. The origin and definition of brite versus white and classical brown adipocytes. *Adipocyte* **3,** 4–9 (2014).
32. Sharp, L. Z. *et al.* Human BAT Possesses Molecular Signatures That Resemble Beige/Brite Cells. *PLoS ONE* **7,** e49452 (2012).
33. Boss, O. & Farmer, S. R. Recruitment of brown adipose tissue as a therapy for obesity-associated diseases. *Front. Endocrinol.* **3,** 14 (2012).
34. Rosen, E. D. *et al.* PPARγ Is Required for the Differentiation of Adipose Tissue In Vivo and In Vitro. *Mol. Cell* **4,** 611–617 (1999).
35. Issemann, I., Prince, R. A., Tugwood, J. D. & Green, S. The peroxisome proliferator-activated receptor:retinoid X receptor heterodimer is activated by fatty acids and fibrate hypolipidaemic drugs. *J. Mol. Endocrinol.* **11,** 37–47 (1993).
36. Tontonoz, P., Hu, E., Graves, R. A., Budavari, A. I. & Spiegelman, B. M. mPPAR gamma 2: tissue-specific regulator of an adipocyte enhancer. *Genes Dev.* **8,** 1224–1234 (1994).
37. Martin, G., Schoonjans, K., Lefebvre, A. M., Staels, B. & Auwerx, J. Coordinate regulation of the expression of the fatty acid transport protein and acyl-CoA synthetase genes by PPARalpha and PPARgamma activators. *J. Biol. Chem.* **272,** 28210–28217 (1997).
38. Berg, A. H., Combs, T. P., Du, X., Brownlee, M. & Scherer, P. E. The adipocyte-secreted protein Acrp30 enhances hepatic insulin action. *Nat. Med.* **7,** 947–953 (2001).
39. Lefterova, M. I. *et al.* PPARgamma and C/EBP factors orchestrate adipocyte biology via adjacent binding on a genome-wide scale. *Genes Dev.* **22,** 2941–2952 (2008).
40. MacDougald, O. A. & Lane, M. D. Transcriptional regulation of gene expression during adipocyte differentiation. *Annu. Rev. Biochem.* **64,** 345–373 (1995).
41. Lefterova, M. I. & Lazar, M. A. New developments in adipogenesis. *Trends Endocrinol. Metab. TEM* **20,** 107–114 (2009).
42. Wu, Z. *et al.* Cross-regulation of C/EBPα and PPARγ controls the transcriptional pathway of adipogenesis and insulin sensitivity. *Mol. Cell* **3,** 151–158 (1999).
43. Darlington, G. J., Ross, S. E. & MacDougald, O. A. The Role of C/EBP Genes in Adipocyte Differentiation. *J. Biol. Chem.* **273,** 30057–30060 (1998).
44. Reginato, M. J., Krakow, S. L., Bailey, S. T. & Lazar, M. A. Prostaglandins promote and block adipogenesis through opposing effects on peroxisome proliferator-activated receptor gamma. *J. Biol. Chem.* **273,** 1855–1858 (1998).
45. Lehmann, J. M. *et al.* An antidiabetic thiazolidinedione is a high affinity ligand for peroxisome proliferator-activated receptor gamma (PPAR gamma). *J. Biol. Chem.* **270,** 12953–12956 (1995).
46. Ohno, H., Shinoda, K., Spiegelman, B. M. & Kajimura, S. PPARγ agonists induce a white-to-brown fat conversion through stabilization of PRDM16 protein. *Cell Metab.* **15,** 395–404 (2012).
47. Murholm, M. *et al.* Dynamic regulation of genes involved in mitochondrial DNA replication and transcription during mouse brown fat cell differentiation and recruitment. *PloS One* **4,** e8458 (2009).

48. Koppen, A. & Kalkhoven, E. Brown vs white adipocytes: the PPARgamma coregulator story. *FEBS Lett.* **584,** 3250–3259 (2010).
49. Hansen, J. B. & Kristiansen, K. Regulatory circuits controlling white versus brown adipocyte differentiation. *Biochem. J.* **398,** 153–168 (2006).
50. Seale, P. *et al.* Transcriptional control of brown fat determination by PRDM16. *Cell Metab.* **6,** 38–54 (2007).
51. Puigserver, P. *et al.* A cold-inducible coactivator of nuclear receptors linked to adaptive thermogenesis. *Cell* **92,** 829–839 (1998).
52. Hondares, E. *et al.* Peroxisome proliferator-activated receptor α (PPARα) induces PPARγ coactivator 1α (PGC-1α) gene expression and contributes to thermogenic activation of brown fat: involvement of PRDM16. *J. Biol. Chem.* **286,** 43112–43122 (2011).
53. Kajimura, S. *et al.* Initiation of myoblast to brown fat switch by a PRDM16-C/EBP-beta transcriptional complex. *Nature* **460,** 1154–1158 (2009).
54. Seale, P. *et al.* Prdm16 determines the thermogenic program of subcutaneous white adipose tissue in mice. *J. Clin. Invest.* **121,** 96–105 (2011).
55. Cohen, P. *et al.* Ablation of PRDM16 and beige adipose causes metabolic dysfunction and a subcutaneous to visceral fat switch. *Cell* **156,** 304–316 (2014).
56. Geerling, J. J. *et al.* Sympathetic nervous system control of triglyceride metabolism: novel concepts derived from recent studies. *J. Lipid Res.* **55,** 180–189 (2014).
57. Zimmet, P., Alberti, K. G. & Shaw, J. Global and societal implications of the diabetes epidemic. *Nature* **414,** 782–787 (2001).
58. Saltiel, A. R. & Kahn, C. R. Insulin signalling and the regulation of glucose and lipid metabolism. *Nature* **414,** 799–806 (2001).
59. Abel, E. D. *et al.* Adipose-selective targeting of the GLUT4 gene impairs insulin action in muscle and liver. *Nature* **409,** 729–733 (2001).
60. Yamauchi, T. & Kadowaki, T. Physiological and pathophysiological roles of adiponectin and adiponectin receptors in the integrated regulation of metabolic and cardiovascular diseases. *Int. J. Obes. 2005* **32 Suppl 7,** S13–18 (2008).
61. Osborn, O. & Olefsky, J. M. The cellular and signaling networks linking the immune system and metabolism in disease. *Nat. Med.* **18,** 363–374 (2012).
62. Hotamisligil, G. S., Shargill, N. S. & Spiegelman, B. M. Adipose expression of tumor necrosis factor-alpha: direct role in obesity-linked insulin resistance. *Science* **259,** 87–91 (1993).
63. Bartelt, A. *et al.* Brown adipose tissue activity controls triglyceride clearance. *Nat. Med.* **17,** 200–205 (2011).
64. Stanford, K. I. *et al.* Brown adipose tissue regulates glucose homeostasis and insulin sensitivity. *J. Clin. Invest.* **123,** 215–223 (2013).
65. Pinent, M. *et al.* Differential transcriptional modulation of biological processes in adipocyte triglyceride lipase and hormone-sensitive lipase-deficient mice. *Genomics* **92,** 26–32 (2008).
66. Wiame, E. *et al.* Molecular identification of aspartate N-acetyltransferase and its mutation in hypoacetylaspartia. *Biochem. J.* **425,** 127–136 (2010).
67. Ariyannur, P. S. *et al.* Methamphetamine-induced neuronal protein NAT8L is the NAA biosynthetic enzyme: implications for specialized acetyl coenzyme A metabolism in the CNS. *Brain Res.* **1335,** 1–13 (2010).
68. Madhavarao, C. N., Chinopoulos, C., Chandrasekaran, K. & Namboodiri, M. A. A. Characterization of the N-acetylaspartate biosynthetic enzyme from rat brain. *J. Neurochem.* **86,** 824–835 (2003).
69. Tahay, G., Wiame, E., Tyteca, D., Courtoy, P. J. & Van Schaftingen, E. Determinants of the enzymatic activity and the subcellular localization of aspartate N-acetyltransferase. *Biochem. J.* **441,** 105–112 (2012).
70. Pegg, A. E. Spermidine/spermine-N(1)-acetyltransferase: a key metabolic regulator. *Am. J. Physiol. Endocrinol. Metab.* **294,** E995–1010 (2008).
71. Ishii, I. *et al.* Polyamine metabolism is involved in adipogenesis of 3T3-L1 cells. *Amino Acids* **42,** 619–626 (2012).

72. Jell, J. *et al.* Genetically altered expression of spermidine/spermine N1-acetyltransferase affects fat metabolism in mice via acetyl-CoA. *J. Biol. Chem.* **282,** 8404–8413 (2007).
73. TALLAN, H. H. Studies on the distribution of N-acetyl-L-aspartic acid in brain. *J. Biol. Chem.* **224,** 41–45 (1957).
74. TALLAN, H. H., MOORE, S. & STEIN, W. H. N-Acetyl-L-aspartic acid in brain. *J. Biol. Chem.* **219,** 257–264 (1956).
75. Moffett, J. R., Ross, B., Arun, P., Madhavarao, C. N. & Namboodiri, A. M. A. N-Acetylaspartate in the CNS: from neurodiagnostics to neurobiology. *Prog. Neurobiol.* **81,** 89–131 (2007).
76. Patel, T. B. & Clark, J. B. Synthesis of N-acetyl-L-aspartate by rat brain mitochondria and its involvement in mitochondrial/cytosolic carbon transport. *Biochem. J.* **184,** 539–546 (1979).
77. Mehta, V. & Namboodiri, M. A. N-acetylaspartate as an acetyl source in the nervous system. *Brain Res. Mol. Brain Res.* **31,** 151–157 (1995).
78. Chakraborty, G., Mekala, P., Yahya, D., Wu, G. & Ledeen, R. W. Intraneuronal N-acetylaspartate supplies acetyl groups for myelin lipid synthesis: evidence for myelin-associated aspartoacylase. *J. Neurochem.* **78,** 736–745 (2001).
79. Niwa, M. *et al.* A novel molecule 'shati' is involved in methamphetamine-induced hyperlocomotion, sensitization, and conditioned place preference. *J. Neurosci. Off. J. Soc. Neurosci.* **27,** 7604–7615 (2007).
80. George, R. L., Huang, W., Naggar, H. A., Smith, S. B. & Ganapathy, V. Transport of N-acetylaspartate via murine sodium/dicarboxylate cotransporter NaDC3 and expression of this transporter and aspartoacylase II in ocular tissues in mouse. *Biochim. Biophys. Acta* **1690,** 63–69 (2004).
81. Moffett, J. R., Arun, P., Ariyannur, P. S. & Namboodiri, A. M. N-Acetylaspartate reductions in brain injury: impact on post-injury neuroenergetics, lipid synthesis, and protein acetylation. *Front. Neuroenergetics* **5,** 11 (2013).
82. Madhavarao, C. N. *et al.* Defective N-acetylaspartate catabolism reduces brain acetate levels and myelin lipid synthesis in Canavan's disease. *Proc. Natl. Acad. Sci. U. S. A.* **102,** 5221–5226 (2005).
83. Matalon, R., Michals-Matalon, K., Surendran, S. & Tyring, S. K. Canavan disease: studies on the knockout mouse. *Adv. Exp. Med. Biol.* **576,** 77–93; discussion 361–363 (2006).
84. Boltshauser, E. *et al.* Follow-up of a child with hypoacetylaspartia. *Neuropediatrics* **35,** 255–258 (2004).
85. Burlina, A. P. *et al.* Hypoacetylaspartia: clinical and biochemical follow-up of a patient. *Adv. Exp. Med. Biol.* **576,** 283–287; discussion 361–363 (2006).
86. Clark, J. B. N-acetyl aspartate: a marker for neuronal loss or mitochondrial dysfunction. *Dev. Neurosci.* **20,** 271–276 (1998).
87. Clark, J. F. *et al.* N-acetylaspartate as a reservoir for glutamate. *Med. Hypotheses* **67,** 506–512 (2006).
88. Bates, T. E. *et al.* Inhibition of N-acetylaspartate production: implications for 1H MRS studies in vivo. *Neuroreport* **7,** 1397–1400 (1996).
89. Signoretti, S. *et al.* N-Acetylaspartate reduction as a measure of injury severity and mitochondrial dysfunction following diffuse traumatic brain injury. *J. Neurotrauma* **18,** 977–991 (2001).
90. Pelzmann, H. J. Expression levels of N-acetyltransferase 8-like (NAT8L) influence adipogenesis in brown and white adipocytes. (2012). Unpublished diploma thesis. Graz University of Technology.
91. Albrektsen, T., Richter, H. E., Clausen, J. T. & Fleckner, J. Identification of a novel integral plasma membrane protein induced during adipocyte differentiation. *Biochem. J.* **359,** 393–402 (2001).
92. Von Heijne, G. & Manoil, C. Membrane proteins: from sequence to structure. *Protein Eng.* **4,** 109–112 (1990).

93. Bogner-Strauss, J. G. *et al.* Reconstruction of gene association network reveals a transmembrane protein required for adipogenesis and targeted by PPARγ. *Cell. Mol. Life Sci. CMLS* **67,** 4049–4064 (2010).
94. Safran, M. *et al.* GeneCards Version 3: the human gene integrator. *Database J. Biol. Databases Curation* **2010,** (2010).
95. Stöckigt, J., Barleben, L., Panjikar, S. & Loris, E. A. 3D-Structure and function of strictosidine synthase--the key enzyme of monoterpenoid indole alkaloid biosynthesis. *Plant Physiol. Biochem. PPB Société Fr. Physiol. Végétale* **46,** 340–355 (2008).
96. Harel, M. *et al.* Structure and evolution of the serum paraoxonase family of detoxifying and anti-atherosclerotic enzymes. *Nat. Struct. Mol. Biol.* **11,** 412–419 (2004).
97. Scharff, E. I., Koepke, J., Fritzsch, G., Lücke, C. & Rüterjans, H. Crystal structure of diisopropylfluorophosphatase from Loligo vulgaris. *Struct. Lond. Engl. 1993* **9,** 493–502 (2001).
98. Yamaguchi, M. & Murata, T. Involvement of regucalcin in lipid metabolism and diabetes. *Metabolism.* **62,** 1045–1051 (2013).
99. Monroy-Noyola, A. *et al.* Dichlorophenyl phosphoramidates as substrates for avian and mammalian liver phosphotriesterases: Activity levels, calcium dependence and stereospecificity. *Chem. Biol. Interact.* **119-120,** 257–262 (1999).
100. Ilhan, A. *et al.* Localization and characterization of the novel protein encoded by C20orf3. *Biochem. J.* **414,** 485–495 (2008).
101. Theopold, U., Krautz, R. & Dushay, M. S. The Drosophila clotting system and its messages for mammals. *Dev. Comp. Immunol.* **42,** 42–46 (2014).
102. Niessen, S., Hoover, H. & Gale, A. J. Proteomic analysis of the coagulation reaction in plasma and whole blood using PROTOMAP. *Proteomics* **11,** 2377–2388 (2011).
103. Hackl, H. *et al.* Molecular processes during fat cell development revealed by gene expression profiling and functional annotation. *Genome Biol.* **6,** R108 (2005).
104. Pessentheiner, A. R. *et al.* NAT8L (N-acetyltransferase 8-like) accelerates lipid turnover and increases energy expenditure in brown adipocytes. *J. Biol. Chem.* **288,** 36040–36051 (2013).
105. Pabinger, S. *et al.* QPCR: Application for real-time PCR data management and analysis. *BMC Bioinformatics* **10,** 268 (2009).
106. Frezza, C., Cipolat, S. & Scorrano, L. Organelle isolation: functional mitochondria from mouse liver, muscle and cultured fibroblasts. *Nat. Protoc.* **2,** 287–295 (2007).
107. Aflaki, E. *et al.* Triacylglycerol Accumulation Activates the Mitochondrial Apoptosis Pathway in Macrophages. *J. Biol. Chem.* **286,** 7418–7428 (2011).
108. Nielsen, R. *et al.* Genome-wide profiling of PPARgamma:RXR and RNA polymerase II occupancy reveals temporal activation of distinct metabolic pathways and changes in RXR dimer composition during adipogenesis. *Genes Dev.* **22,** 2953–2967 (2008).
109. Siersbæk, M. S. *et al.* Genome-wide profiling of peroxisome proliferator-activated receptor γ in primary epididymal, inguinal, and brown adipocytes reveals depot-selective binding correlated with gene expression. *Mol. Cell. Biol.* **32,** 3452–3463 (2012).
110. Kim, J. B., Wright, H. M., Wright, M. & Spiegelman, B. M. ADD1/SREBP1 activates PPARgamma through the production of endogenous ligand. *Proc. Natl. Acad. Sci. U. S. A.* **95,** 4333–4337 (1998).
111. INGALLS, A. M., DICKIE, M. M. & SNELL, G. D. Obese, a new mutation in the house mouse. *J. Hered.* **41,** 317–318 (1950).
112. MAYER, J., BATES, M. W. & DICKIE, M. M. Hereditary diabetes in genetically obese mice. *Science* **113,** 746–747 (1951).
113. Abbrescia, D. I., La Piana, G. & Lofrumento, N. E. Malate-aspartate shuttle and exogenous NADH/cytochrome c electron transport pathway as two independent cytosolic reducing equivalent transfer systems. *Arch. Biochem. Biophys.* **518,** 157–163 (2012).
114. Satrústegui, J. *et al.* Role of aralar, the mitochondrial transporter of aspartate-glutamate, in brain N-acetylaspartate formation and Ca(2+) signaling in neuronal mitochondria. *J. Neurosci. Res.* **85,** 3359–3366 (2007).

115. Musrati, R. A., Kollárová, M., Mernik, N. & Mikulásová, D. Malate dehydrogenase: distribution, function and properties. *Gen. Physiol. Biophys.* **17,** 193–210 (1998).
116. Obaru, K., Nomiyama, H., Shimada, K., Nagashima, F. & Morino, Y. Cloning and sequence analysis of mRNA for mouse aspartate aminotransferase isoenzymes. *J. Biol. Chem.* **261,** 16976–16983 (1986).
117. Tordjman, J. *et al.* Cytosolic aspartate aminotransferase, a new partner in adipocyte glyceroneogenesis and an atypical target of thiazolidinedione. *J. Biol. Chem.* **282,** 23591–23602 (2007).
118. Jalil, M. A. *et al.* Reduced N-acetylaspartate levels in mice lacking aralar, a brain- and muscle-type mitochondrial aspartate-glutamate carrier. *J. Biol. Chem.* **280,** 31333–31339 (2005).
119. Wise, E. M. & Ball, E. G. MALIC ENZYME AND LIPOGENESIS*. *Proc. Natl. Acad. Sci. U. S. A.* **52,** 1255–1263 (1964).
120. Luong, A., Hannah, V. C., Brown, M. S. & Goldstein, J. L. Molecular Characterization of Human Acetyl-CoA Synthetase, an Enzyme Regulated by Sterol Regulatory Element-binding Proteins. *J. Biol. Chem.* **275,** 26458–26466 (2000).
121. Fujino, T., Kondo, J., Ishikawa, M., Morikawa, K. & Yamamoto, T. T. Acetyl-CoA synthetase 2, a mitochondrial matrix enzyme involved in the oxidation of acetate. *J. Biol. Chem.* **276,** 11420–11426 (2001).
122. Arun, P., Moffett, J. R. & Namboodiri, A. M. A. Evidence for mitochondrial and cytoplasmic N-acetylaspartate synthesis in SH-SY5Y neuroblastoma cells. *Neurochem. Int.* **55,** 219–225 (2009).
123. Kelley, R. I. & Stamas, J. N. Quantification of N-acetyl-L-aspartic acid in urine by isotope dilution gas chromatography-mass spectrometry. *J. Inherit. Metab. Dis.* **15,** 97–104 (1992).
124. Michal, G. *Biochemical Pathways - An Atlas of Biochemistry and Molecular Biology*. (John Wiley & Sons, Inc., 1999). ISBN 0-471-33130-9
125. Beigneux, A. P. *et al.* ATP-citrate lyase deficiency in the mouse. *J. Biol. Chem.* **279,** 9557–9564 (2004).
126. Buckley, M. G. & Rath, E. A. Regulation of fatty acid synthesis and malonyl-CoA content in mouse brown adipose tissue in response to cold-exposure, starvation or re-feeding. *Biochem. J.* **243,** 437–442 (1987).
127. Abu-Elheiga, L., Matzuk, M. M., Abo-Hashema, K. A. & Wakil, S. J. Continuous fatty acid oxidation and reduced fat storage in mice lacking acetyl-CoA carboxylase 2. *Science* **291,** 2613–2616 (2001).
128. Wu, Z. *et al.* Mechanisms controlling mitochondrial biogenesis and respiration through the thermogenic coactivator PGC-1. *Cell* **98,** 115–124 (1999).
129. Pendergrass, W., Wolf, N. & Poot, M. Efficacy of MitoTracker Green and CMXrosamine to measure changes in mitochondrial membrane potentials in living cells and tissues. *Cytom. Part J. Int. Soc. Anal. Cytol.* **61,** 162–169 (2004).
130. Keij, J. F., Bell-Prince, C. & Steinkamp, J. A. Staining of mitochondrial membranes with 10-nonyl acridine orange MitoFluor Green, and MitoTracker Green is affected by mitochondrial membrane potential altering drugs. *Cytometry* **39,** 203–210 (2000).
131. Buckman, J. F. *et al.* MitoTracker labeling in primary neuronal and astrocytic cultures: influence of mitochondrial membrane potential and oxidants. *J. Neurosci. Methods* **104,** 165–176 (2001).
132. Walenta, E. *et al.* α/β-hydrolase domain containing protein 15 (ABHD15)--an adipogenic protein protecting from apoptosis. *PloS One* **8,** e79134 (2013).
133. Mottillo, E. P., Bloch, A. E., Leff, T. & Granneman, J. G. Lipolytic products activate peroxisome proliferator-activated receptor (PPAR) α and δ in brown adipocytes to match fatty acid oxidation with supply. *J. Biol. Chem.* **287,** 25038–25048 (2012).
134. Sauer, B. & Henderson, N. The cyclization of linear DNA in Escherichia coli by site-specific recombination. *Gene* **70,** 331–341 (1988).
135. Yagi, T. *et al.* Homologous recombination at c-fyn locus of mouse embryonic stem cells with use of diphtheria toxin A-fragment gene in negative selection. *Proc. Natl. Acad. Sci. U. S. A.* **87,** 9918–9922 (1990).

136. Magin, T. M., McWhir, J. & Melton, D. W. A new mouse embryonic stem cell line with good germ line contribution and gene targeting frequency. *Nucleic Acids Res.* **20,** 3795–3796 (1992).
137. Su, H., Mills, A. A., Wang, X. & Bradley, A. A targeted X-linked CMV-Cre line. *Genes. N. Y. N 2000* **32,** 187–188 (2002).
138. Yu, C., Cresswell, J., Löffler, M. G. & Bogan, J. S. The glucose transporter 4-regulating protein TUG is essential for highly insulin-responsive glucose uptake in 3T3-L1 adipocytes. *J. Biol. Chem.* **282,** 7710–7722 (2007).
139. Haemmerle, G. *et al.* Defective lipolysis and altered energy metabolism in mice lacking adipose triglyceride lipase. *Science* **312,** 734–737 (2006).
140. De Jesus, L. A. *et al.* The type 2 iodothyronine deiodinase is essential for adaptive thermogenesis in brown adipose tissue. *J. Clin. Invest.* **108,** 1379–1385 (2001).
141. Carmona, M. C. *et al.* Defective thermoregulation, impaired lipid metabolism, but preserved adrenergic induction of gene expression in brown fat of mice lacking C/EBPbeta. *Biochem. J.* **389,** 47–56 (2005).
142. Li, P. Cidea, brown fat and obesity. *Mech. Ageing Dev.* **125,** 337–338 (2004).
143. Yudkoff, M., Nelson, D., Daikhin, Y. & Erecińska, M. Tricarboxylic acid cycle in rat brain synaptosomes. Fluxes and interactions with aspartate aminotransferase and malate/aspartate shuttle. *J. Biol. Chem.* **269,** 27414–27420 (1994).
144. Al-Dirbashi, O. Y. *et al.* Quantification of N-acetylaspartic acid in urine by LC-MS/MS for the diagnosis of Canavan disease. *J. Inherit. Metab. Dis.* **30,** 612 (2007).
145. Huypens, P. *et al.* The dicarboxylate carrier plays a role in mitochondrial malate transport and in the regulation of glucose-stimulated insulin secretion from rat pancreatic beta cells. *Diabetologia* **54,** 135–145 (2011).
146. Moura, M. A. F. *et al.* Brown adipose tissue glyceroneogenesis is activated in rats exposed to cold. *Pflüg. Arch. Eur. J. Physiol.* **449,** 463–469 (2005).
147. Moura, M. A. *et al.* Effect of cold acclimation on brown adipose tissue fatty acid synthesis in rats adapted to a high-protein, carbohydrate-free diet. *Metabolism.* **50,** 1493–1498 (2001).
148. Nikolau, B. J., Oliver, D. J., Schnable, P. S. & Wurtele, E. S. Molecular biology of acetyl-CoA metabolism. *Biochem. Soc. Trans.* **28,** 591–593 (2000).
149. Bauer, D. E., Hatzivassiliou, G., Zhao, F., Andreadis, C. & Thompson, C. B. ATP citrate lyase is an important component of cell growth and transformation. *Oncogene* **24,** 6314–6322 (2005).
150. Ji, S. *et al.* Homozygous carnitine palmitoyltransferase 1b (muscle isoform) deficiency is lethal in the mouse. *Mol. Genet. Metab.* **93,** 314–322 (2008).
151. Zhao, G. *et al.* Overexpression of pyruvate dehydrogenase kinase 4 in heart perturbs metabolism and exacerbates calcineurin-induced cardiomyopathy. *Am. J. Physiol. Heart Circ. Physiol.* **294,** H936–943 (2008).
152. Knowles, S. E., Jarrett, I. G., Filsell, O. H. & Ballard, F. J. Production and utilization of acetate in mammals. *Biochem. J.* **142,** 401–411 (1974).
153. Goldberg, R. P. & Brunengraber, H. Contributions of cytosolic and mitochondrial acetyl-CoA syntheses to the activation of lipogenic acetate in rat liver. *Adv. Exp. Med. Biol.* **132,** 413–418 (1980).
154. Jones, C. T. & Ashton, I. K. Lipid biosynthesis in liver slices of the foetal guinea pig. *Biochem. J.* **154,** 149–158 (1976).
155. Ahmadian, M. *et al.* Desnutrin/ATGL is regulated by AMPK and is required for a brown adipose phenotype. *Cell Metab.* **13,** 739–748 (2011).
156. Haemmerle, G. *et al.* ATGL-mediated fat catabolism regulates cardiac mitochondrial function via PPAR-α and PGC-1. *Nat. Med.* **17,** 1076–1085 (2011).
157. Chakravarthy, M. V. *et al.* Identification of a physiologically relevant endogenous ligand for PPARalpha in liver. *Cell* **138,** 476–488 (2009).
158. Huang, J. *et al.* Sustained activation of PPARα by endogenous ligands increases hepatic fatty acid oxidation and prevents obesity in ob/ob mice. *FASEB J. Off. Publ. Fed. Am. Soc. Exp. Biol.* **26,** 628–638 (2012).

159. Barbera, M. J. *et al.* Peroxisome proliferator-activated receptor alpha activates transcription of the brown fat uncoupling protein-1 gene. A link between regulation of the thermogenic and lipid oxidation pathways in the brown fat cell. *J. Biol. Chem.* **276,** 1486–1493 (2001).
160. Pessin, J. E., Thurmond, D. C., Elmendorf, J. S., Coker, K. J. & Okada, S. Molecular Basis of Insulin-stimulated GLUT4 Vesicle Trafficking LOCATION! LOCATION! LOCATION! *J. Biol. Chem.* **274,** 2593–2596 (1999).
161. Bogan, J. S., McKee, A. E. & Lodish, H. F. Insulin-responsive compartments containing GLUT4 in 3T3-L1 and CHO cells: regulation by amino acid concentrations. *Mol. Cell. Biol.* **21,** 4785–4806 (2001).
162. Olefsky, J. M. & Saltiel, A. R. PPAR gamma and the treatment of insulin resistance. *Trends Endocrinol. Metab. TEM* **11,** 362–368 (2000).
163. Armoni, M., Harel, C. & Karnieli, E. Transcriptional regulation of the GLUT4 gene: from PPAR-gamma and FOXO1 to FFA and inflammation. *Trends Endocrinol. Metab. TEM* **18,** 100–107 (2007).

Figure and Table legends

7 Figure and table legends

7.1 Figure legends

Figure 1: Distribution of white, brown and beige adipose depots in the mouse.. 4
Figure 2: Different types of adipocytes derive from different progenitor cells 5
Figure 3: The glucose and lipid metabolism of brown adipocytes in response to β-adrenergic stimuli. 8
Figure 4: Molecular structure of NAA. 9
Figure 5: Structural model of NAT8L based on *in silico* homology mappings with other N-acetyltransferases. 9
Figure 6: Scheme of NAT8L pathway and shutteling of metabolites between different cell types of the brain 11
Figure 7: Protein architecture of APMAP. 12
Figure 8: Three dimensional structure of APMAP 13
Figure 9: Tissue expression of *Nat8l* in mice with an obese phenotype 31
Figure 10: Localization of NAT8L in fractionates of iBACs and BAT 32
Figure 11: mRNA expression of genes directly and indirectly connected to the NAT8L pathway in *Nat8l* overexpressing iBACs 35
Figure 12: The expression of white and brown adipogenic genes in *Nat8l* o/e iBACs 37
Figure 13: The impact of *Nat8l* o/e on glucose uptake and lipogenesis in iBACs 39
Figure 14: The impact of *Nat8l* o/e on TG synthesis and breakdown 41
Figure 15: *Nat8l* influences expression of genes directly or indirectly involved in β-oxidation and FFA utilization and increases oxygen consumption rate (OCR). 43
Figure 16: *Nat8l* o/e increases the number of mitochondria in iBACs. 45
Figure 17: Overexpression of enzymatic defective *Nat8l* mutant D165A in iBACs has no influence on marker gene expression, TG accumulation and FFA release 46
Figure 18: *Nat8l* is a PPAR target 48
Figure 19: Scheme for generation of the *Apmap*-ko mouse 50
Figure 20: PCR of ES cell clones after homologous recombination. 50
Figure 21: Southern blot of ES cell clones after homologous and Cre-mediated recombination. 51
Figure 22: qRT-PCR from *Apmap*-wt and -ko tissues from a male and a female mouse 52
Figure 23: Western blot of mouse tissues of *Apmap*-ko mice and wt littermates 53
Figure 24: Body weight changes of male *Apmap*-ko and wt littermates on HFD. 54
Figure 25: Glucose levels, glucose, insulin, and fasting tolerance tests of male *Apmap*-ko mice compared to wt littermates after 12-14 weeks on HFD 57
Figure 26: Body composition of male *Apmap*-ko and wt littermates after 24 weeks of HFD. 58

Figure 27: Body weight gain of female and male *Apmap*-ko mice and wt littermates on HFD. ... 59
Figure 28: Glucose levels, glucose and insulin tolerance tests of male *Apmap*-ko mice compared to wt littermates after 6-7 weeks of HFD ... 60
Figure 29: Effects of transient overexpression or silencing on lipid and glucose metabolism of 3T3-L1 cells ... 63
Figure 30: Life-cell imaging of electroporated 3T3-L1 expressing CFP-tagged APMAP and/or YFP-tagged GLUT4. ... 64
Figure 31: Working model of the proposed NAT8L action in brown adipocytes. ... 67
Figure 32: The malate-aspartate shuttle (MAS). ... 69
Figure 33: Proposed role of NAT8L in a so-called „mini TCA-cycle". ... 70
Figure 34: The NAA-pathway as an alternative pathway to produce cytosolic acetyl-CoA for lipogenesis ... 72
Figure 35: Full-length APMAP amino acid (aa) sequence. ... 76

Figure A 1: Individual NAT8L luciferase assays ... 113

7.2 Table Legends

Table 1: Primer pairs used for qRT-PCR. ... 19
Table 2: Primary antibodies used for western blot analysis, including used concentration, origin and company. ... 21
Table 3: Secondary antibodies used for detection of primary antibodies. ... 21
Table 4: Body weight and blood parameters of the first cohort of male wt and *Apmap*-ko mice on normal chow diet at the age of 16 weeks. ... 54
Table 5: Body weight and blood parameters of the first cohort of male wt and *Apmap*-ko mice on HFD. ... 54
Table 6: Body weight and blood parameters of the first cohort of female wt, *Apmap*-heterozygous and *Apmap*-ko mice on chow diet at the age of 16 weeks. ... 55
Table 7: Body weight and blood parameters of the second cohort of male wt and *Apmap*-ko mice at the age of 8 weeks fed a chow diet. ... 55
Table 8: Body weight and blood parameters of the second cohort of male wt and *Apmap*-ko mice after 16 weeks of HFD. ... 56
Table 9: Body weight and blood parameters of the third cohort of female wt and *Apmap*-ko mice on chow diet at the age of 12 weeks. ... 59
Table 10: Body weight and blood parameters of the third cohort of male wt and *Apmap*-ko mice on chow diet at the age of 8 weeks. ... 59

Abbreviations

8 Abbreviations

Apmap	adipocyte plasma membrane associated protein
Aspa	aspartoacylase
AT	adipose tissue
ATG	adenine, thymine, guanine – refers to a startcodon
ATP	adenosine triphosphate
BAT	brown adipose tissue
BSA	bovine serum albumin
cAMP	cyclic adenosine monophosphate
cDNA	complementary DNA
CE	cholesterol esters
C/EBP (α, β, δ)	CCAAT/enhancer binding protein (α, β, δ)
CFP	cyan fluorescent protein
CMV	cytomegalovirus
Cre	Cre-recombinase
DG	diglyceride(s)
DMEM	Dulbecco's modified eagle medium
DMSO	dimethylsulfoxide
ER	endoplasmic reticulum
ES cells	embryonic stem cells
eWAT	epididymal white adipose tissue
FA	fatty acid
FABP	fatty acid binding protein
FACS	fluorescence activated cell sorting
FAS	Fatty acid synthase
FBS	foetal bovine serum
FFA	free fatty acid
Fig.	figure
gDNA	genomic DNA
GLUT4	glucose transporter type 4 protein
GOT	glutamate-oxaloacetate transaminase
GTT	glucose tolerance test
h	hour(s)
HFD	high fat diet
HH3	Histone H3 protein
HK1	Hexokinase 1 protein
HRP	Horseradish peroxidase
iBACs	immortalized brown adipogenic cells
IBMX	3-Isobutyl-1-methylxanthine
i.p.	intra peritoneal
ITT	insulin tolerance test
kbp	kilo base pairs
kDa	kilo Dalton
KRB	Krebs-Ringer-buffer
ko	knockout
MG	monoglyceride(s)
MM	maintenance medium for iBACs

mRNA	messenger ribonucleic acid
NAA	N-acetyl aspartate
Nat8l	N-acetyltransferase 8-like
NE	norepinephrine
ntc	non-targeting control
ob	obese gene
o/e	overexpression, overexpressed
PBS	phosphate buffered saline
PDI	protein disulfide isomerase
PGC-1α	PPARγ coactivator-1α protein
PIC	protease inhibitor cocktail
pMSCV	murine stem cell virus plasmid
PPAR (α/γ2)	peroxisome proliferator-activated receptor (α/γ2)
PPRE	peroxisome proliferator-activated receptor response element
P/S	penicillin/streptomycin
qRT-PCR	quantitative real-time polymerase chain reaction
Rosi	rosiglitazone maleate
RT	room temperature
RXRα	retinoid X receptor alpha
shRNA	small hairpin RNA
siRNA	small interfering RNA
SDS	sodium dodecyl sulfate
SNS	sympathetic nervous system
sWAT	subcutaneous white adipose tissue
T3	3,5,3'-triiodothyronine
TEM	Transmission electron microscopy
TCA	Trichloroacetic acid
TG	triglyceride(s)
TLC	thin layer chromatography
TZD	thiazolidinedione
UCP1	uncoupling protein 1
5'(3')UTR	5'(3') untranslated region
vol	volume
WAT	white adipose tissue
wt	wild type
wt/vol	weight per volume
YFP	yellow fluorescent protein

8.1 Nomenclature

Murine genes are written in lowercase italics, human genes in uppercase italics. All proteins are expressed as uppercase letters.

Appendix

9 Appendix

9.1 Published manuscript – N-acetyltransferase 8-like accelerates lipid turnover and increases energy expenditure in brown adipocytes

Published in Journal of Biological Chemistry, 2013 Dec 13;288(50):36040-51.

Lipids:

NAT8L (*N*-Acetyltransferase 8-Like) Accelerates Lipid Turnover and Increases Energy Expenditure in Brown Adipocytes

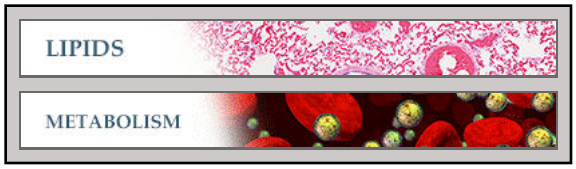

Ariane R. Pessentheiner, Helmut J. Pelzmann, Evelyn Walenta, Martina Schweiger, Lukas N. Groschner, Wolfgang F. Graier, Dagmar Kolb, Kyosuke Uno, Toh Miyazaki, Atsumi Nitta, Dietmar Rieder, Andreas Prokesch and Juliane G. Bogner-Strauss

J. Biol. Chem. 2013, 288:36040-36051.
doi: 10.1074/jbc.M113.491324 originally published online October 23, 2013

THE JOURNAL OF BIOLOGICAL CHEMISTRY VOL. 288, NO. 50, pp. 36040–36051, December 13, 2013

NAT8L (*N*-Acetyltransferase 8-Like) Accelerates Lipid Turnover and Increases Energy Expenditure in Brown Adipocytes*

Received for publication, June 4, 2013, and in revised form, October 15, 2013 Published, JBC Papers in Press, October 23, 2013, DOI 10.1074/jbc.M113.491324

Ariane R. Pessentheiner[‡§1], Helmut J. Pelzmann[‡§1], Evelyn Walenta[‡], Martina Schweiger[¶], Lukas N. Groschner[‖], Wolfgang F. Graier[‖], Dagmar Kolb[‡‡], Kyosuke Uno[§§], Toh Miyazaki[§§], Atsumi Nitta[§§], Dietmar Rieder[¶¶], Andreas Prokesch[‡§], and Juliane G. Bogner-Strauss[‡§2]**

From the [‡]Institute for Genomics and Bioinformatics, Graz University of Technology, Petergasse 14, 8010 Graz, Austria, the [§]Institute of Biochemistry, Graz University of Technology, Petergasse 12, 8010 Graz, Austria, the [¶]Institute for Molecular Biosciences, University of Graz, Heinrichstrasse 31, 8010 Graz, Austria, the [‖]Institute of Molecular Biology and Biochemistry and [**]Institute of Cell Biology, Histology, and Embryology, Medical University of Graz, Harrachgasse 21, 8010 Graz, Austria, the [‡‡]Core Facility Ultrastructure Analysis, Center for Medical Research, Medical University of Graz, Stiftingtalstrasse 24, 8010 Graz, Austria, the [§§]Department of Pharmaceutical Therapy and Neuropharmacology, Faculty of Pharmaceutical Sciences, Graduate School of Medicine and Pharmaceutical Sciences, University of Toyama, 2630 Sugitani, Toyama 930-0194, Japan, and the [¶¶]Division of Bioinformatics, Biocenter, Innsbruck Medical University, Innrain 80, 6020 Innsbruck, Austria

Background: NAT8L (*N*-acetyltransferase 8-like) synthesizes *N*-acetylaspartate and is required for myelination in the brain. Its function in other tissues was undefined.
Results: *Nat8l* is highly expressed in adipose tissues and impacts adipogenic marker gene expression, lipid turnover, and energy metabolism in brown adipocytes.
Conclusion: *Nat8l* expression influences cellular bioenergetics in adipocytes.
Significance: These findings establish a novel pathway in brown adipocyte metabolism.

NAT8L (*N*-acetyltransferase 8-like) catalyzes the formation of *N*-acetylaspartate (NAA) from acetyl-CoA and aspartate. In the brain, NAA delivers the acetate moiety for synthesis of acetyl-CoA that is further used for fatty acid generation. However, its function in other tissues remained elusive. Here, we show for the first time that *Nat8l* is highly expressed in adipose tissues and murine and human adipogenic cell lines and is localized in the mitochondria of brown adipocytes. Stable overexpression of *Nat8l* in immortalized brown adipogenic cells strongly increases glucose incorporation into neutral lipids, accompanied by increased lipolysis, indicating an accelerated lipid turnover. Additionally, mitochondrial mass and number as well as oxygen consumption are elevated upon *Nat8l* overexpression. Concordantly, expression levels of brown marker genes, such as *Prdm16*, *Cidea*, *Pgc1α*, *Pparα*, and particularly UCP1, are markedly elevated in these cells. Treatment with a PPARα antagonist indicates that the increase in UCP1 expression and oxygen consumption is PPARα-dependent. *Nat8l* knockdown in brown adipocytes has no impact on cellular triglyceride content, lipogenesis, or oxygen consumption, but lipolysis and brown marker gene expression are increased; the latter is also observed in BAT of *Nat8l*-KO mice. Interestingly, the expression of ATP-citrate lyase is increased in *Nat8l*-silenced adipocytes and BAT of *Nat8l*-KO mice, indicating a compensatory mechanism to sustain the acetyl-CoA pool once *Nat8l* levels are reduced. Taken together, our data show that *Nat8l* impacts on the brown adipogenic phenotype and suggests the existence of the NAT8L-driven NAA metabolism as a novel pathway to provide cytosolic acetyl-CoA for lipid synthesis in adipocytes.

Adipose tissue depots are critical organs for the control of energy homeostasis. White adipose tissue (WAT) is the major fat-storing organ in the body, and its adipocytes are characterized by large, unilocular lipid droplets and only few mitochondria. During energy demand, triglycerides (TG)[3] are broken down to supply peripheral tissues with fatty acids (1, 2). Brown adipocytes are characterized by multiple, smaller lipid droplets and numerous mitochondria, which contain UCP1, a protein that uncouples oxidative phosphorylation from ATP production to dissipate energy into heat (3). With the discovery of active brown adipose tissue (BAT) in adult humans (4–7) and its association with leanness (5), much attention has been paid to the investigation of BAT development and homeostasis due to its possible role in fighting obesity and its associated disorders (8). Recently, it has been shown that adipose triglyceride lipase-mediated breakdown of TG is required for a distinct brown adipose phenotype in mice (9). Thus, it seems that a

* This work was supported by Austrian Science Fund FWF Grants DK-MCD W01226 and P24143, by Program for Next Generation World-leading Researchers Grant LS047, and by a Smoking Research Foundation Grant for Biomedical Research.
[1] Both authors contributed equally to this work.
[2] To whom correspondence should be addressed: Petersgasse 14/5, 8010 Graz, Austria. Tel.: 43-316-873-5337; E-mail: juliane.bogner-strauss@tugraz.at.

[3] The abbreviations used are: TG, triglyceride(s); WAT, white adipose tissue; BAT, brown adipose tissue; FFA, free fatty acids; PPAR, peroxisome proliferator-activated receptor; NAA, *N*-acetylaspartate; iBACs, immortalized brown adipogenic cells; ER, endoplasmic reticulum; BisTris, 2-[bis(2-hydroxyethyl)amino]-2-(hydroxymethyl)propane-1,3-diol; OCR, oxygen consumption rate.

large proportion of fatty acid has first to be stored as TG and thereafter hydrolyzed before they can be used for UCP1 activation (and mitochondrial β-oxidation). Additionally, activated BAT shows high rates of glucose uptake (10), but glucose is suggested to play only a minor role as a direct oxidative substrate (11). Therefore, enzymes involved in *de novo* lipid synthesis are highly expressed in BAT and further increased upon thermogenic activation (12).

Many of the identified molecular network components controlling white and brown metabolism have been disclosed by the use of novel high throughput technologies. Among others, we performed microarray studies in white and brown adipose tissue of *Atg*- and *Hsl*-KO mice (13) and focused on candidate genes that might be of interest in the development and metabolism of adipose tissues. Among these was a gene encoding for the enzyme NAT8L (*N*-acetyltransferase 8-like).

In the brain, NAT8L was shown to catalyze the formation of *N*-acetylaspartate (NAA) from acetyl-CoA and L-aspartate (14, 15). NAA then acts as a carrier of acetyl groups between neurons and oligodendrocytes where NAA is catabolized by aspartoacylase into acetate and L-aspartate (16). The acetate moiety is reutilized for acetyl-CoA synthesis and can subsequently be incorporated into lipids (16, 17). The metabolic importance of NAA has been shown in two inborn human neurodegenerative disorders, where defects in NAA biosynthesis (14, 18) as well as catabolism (19) lead to reduced myelin synthesis.

Here, we describe for the first time that *Nat8l* is highly expressed in adipocytes and that its expression is induced during the differentiation of various mouse and human adipogenic cells. Furthermore, overexpression of *Nat8l* in an immortalized brown adipogenic cell line influenced lipid turnover, increased mitochondrial mass, and accelerated energy expenditure, most likely by increasing the expression of UCP1 in a PPARα-dependent manner. Our results from *Nat8l* silencing in brown adipocytes and from examining BAT in *Nat8l*-KO mice support the hypothesis that the NAT8L/NAA pathway acts as an alternative source to provide acetyl-CoA as a building block for lipid biosynthesis in adipocytes. These data suggest that the NAA pathway exists and is functional in adipose tissue and that modulating this pathway could be a valuable new approach to increase energy dissipation in (brown) adipocytes.

EXPERIMENTAL PROCEDURES

Cell Culture, Differentiation, Lipid Staining, and Quantification—Immortalized brown adipogenic cells (iBACs) were grown in DMEM containing 10% FBS, 50 μg/ml streptomycin, 50 units/ml penicillin, and 20 mM Hepes. C3H-10T1/2 cells were grown and maintained in DMEM containing 10% FBS and penicillin/streptomycin. C3H-10T1/2 cells were induced to differentiate 2 days after confluence with 0.5 mM 3-isobutyl-1-methylxanthine, 1 μM dexamethasone, 2 μg/ml insulin, and 1 μM rosiglitazone (Cayman Chemical). After 3 days, medium was changed to maintenance medium with 2 μg/ml insulin and 1 μM rosiglitazone, and 48 h thereafter, normal growth medium was used until harvest. Simpson-Golabi-Behmel syndrome cells were cultured and differentiated as described by us elsewhere (20). iBACs were induced to differentiate at the day of confluence with 0.5 mM 3-isobutyl-1-methylxanthine, 0.5 μM dexamethasone, 20 nM insulin, 1 nM triiodthyronine, and 125 μM indomethacin. Two days after induction, medium was changed to maintenance medium containing 20 nM insulin and 1 nM triiodthyronine, and cells were kept in this medium until harvest. Cells were fixed (10% formalin in PBS for 30 min), rinsed in PBS, and stained with oil red O (0.25% in 60% isopropyl alcohol stock solution diluted 3:2 with distilled H_2O for 30 min). To stimulate thermogenesis, cells were incubated with 1 μM isoproterenol for 4 h. iBACs were treated with 10 μM PPARα antagonist GW6471 (Tocris Bioscience) from day 4 until harvest. Cellular triglyceride content was determined in differentiated iBACs using Infinity Triglyceride Reagent (Thermo). Free fatty acid content was measured using the NEFA C test kit (WAKO). Values were corrected by protein content measurement using BCA reagent (Pierce).

Animal Studies—Male C57BL/6 and ob/ob mice at the age of 24–26 weeks were used for this study. Before harvesting tissue pads, mice were fasted for 12 h, following refeeding for 1 h. *Nat8l*-knock-out mice (21) and their controls were used at the age of 3–4 months and fed *ad libitum* before harvesting tissues. Animals were kept on a 12-h light/dark cycle on a normal chow diet. All animal procedures followed the National Institutes of Health Guidelines for the Care and Use of Laboratory Animals and were approved by the Austrian Ministry for Science and Research and the Committee for Animal Experiments of the University of Toyama.

Retroviral Expression of Nat8l in Monoclonal Cell Lines—Full-length coding sequence of murine *Nat8l* was amplified by PCR from murine adipose tissue cDNA using *Phusion* polymerase (Fermentas) and cloned into a murine stem cell virus vector (pMSCV puro, BD Biosciences Clontech) using the restriction sites XhoI/EcoRI. To produce infectious but replication-incompetent recombinant retroviruses expressing *Nat8l*, PhoenixEco packaging cells (cultured in DMEM with 10% FBS in 5% CO_2) were transfected with pMSCV-*Nat8l* using Metafectene (Biontex Laboratories GmbH). The supernatant containing the viral particles was collected 48 h after transfection. Viral supernatants were supplemented with 8 μg/ml Polybrene and added to iBACs (30–40% confluence) for infections for 18–24 h. Because cells could not be selected with puromycin, single cells were picked under the microscope and expanded as monoclonal populations, and overexpression was controlled by quantitative RT-PCR. Differentiation was induced as described above. As a control for the above described stable cell lines, the empty pMSCVpuro was used and underwent the same procedure.

Silencing of Nat8l Using Short Hairpin RNA (shRNA)-containing Lentiviral Particles—One control non-targeting shRNA lentivirus and two shRNA lentiviruses directed against *Nat8l* were purchased from Sigma (MISSION™ shRNA lentiviral particles NM_001001985). iBACs were seeded into 6-well plates 12 h before transduction using 3×10^4 cells/well (around 30% confluence). Cells were infected for 16 h with a multiplicity of infection of 10 in complete medium containing 8 μg/ml Polybrene (Sigma). After transduction, the infection medium was replaced with fresh medium, and the cells underwent the same selection process as *Nat8l*-overexpressing iBACs.

TABLE 1
Primer pairs used for quantitative RT-PCR
All primers were used with murine cDNA except for the indicated human primers.

Target gene	Forward primer (5′ → 3′)	Reverse primer (5′ → 3′)
Human *NAT8L*	TGTGCATCCGCGAGTTCCGT	CGGAAGGCCGTGTTAGGGAT
Human *β-ACTIN*	CGCCGCATCCTCCTCTTC	GACACCGGAACCGCTCATT
Murine *Nat8l*	TGTGCATCCGCGAGTTCCGC	GCGGAAAGCCGTGTTGGGGA
Tfiiβ	GTCACATGTCCGAATCATCCA	TCAATAACTCGGTCCCCTACAA
Pparγ2	TGCCTATGAGCACTTCACAAGAAAT	CGAAGTTGGTGGGCCAGAA
Fabp4/aP2	CGACAGGAAGGTGAAGAGCATC	ACCACCAGCTTGTCACCATCTC
Adipoq	TGTTCCTCTTAATCCTGCCCA	CCAACCTGCACAAGTTCCCTT
Fads3	GTGATCCACACGAACCAGTG	TCCCGCTTTTTCTTGTCCTAC
Retn	AAGAAGGAGCTGTGGGACAGG	CAGCAGTTCAGGGACAAGGAA
Psat1	AGTGGAGCGCCAGAATAGAA	TACCGCCTTGTCAAGAAACC
Pgc1α	TCTCTGGAACTGCAGGCCTAAC	TCAGCTTTGGCGAAGCCTT
Pparα	CCTGAACATCGAGTGTCGAATATG	GCGAATTGCATTGTGTGACATC
Prdm16	TCCACAGCACGGTGAAGCCA	ATCTGCGTCCTGCAGTCGGC
C/ebpβ	GGACTTGATGCAATCCGGA	AACCCCGCAGGAACATCTTTA
Cox8b	GCGAAGTTCACAGTGGTTCC	AACCATGAAGCCAACGACTATG
Cidea	TGACATTCATGGGATTGCAGAC	GGCCAGTTGTGATGACTAAGAC
Ucp1	ACACCTGCCTCTCTCGGAAA	TAGGCTGCCCAATGAACACT
Dio2	AACAGCTTCCTCCTAGATGCC	CATCAGCGGTCTTCTCCGAG
Cox1	TGAGCCCACCACATATTCACAG	AGGGTTGCAAGTCAGCTAAATAC
Cpt1b	TGTATCGCCGCAAACTGGACCG	TCTGGTAGGAGCACATGGGCAC
Pdk4	TTTCTCGTCTCTACGCCAAG	GATACACCAGTCATCAGCTTCG
Fabp3	CCTTTGTCGGTACCTGGAAGCT	AAAGCCCACACCGAGTGACTT
Acly	AGGAAGTGCCACCTCCAACAGT	CGCTCATCACAGATGCTGGTCA

Site-directed Mutagenesis of Nat8l and Subsequent Stable Transfection of iBACs—For better selectivity, *Nat8l* coding sequence was transferred into a pMSCV-hygro vector (kind gift from E. D. Rosen). Site-directed mutagenesis was performed by PCR amplification with *Phusion* polymerase using pMSCV-*Nat8l* as template with the following primers (base substitution is marked as a lowercase letter): *Nat8l*_D165A_fw, 5′-TGCACACGGCcATGGCTGACATTGAGCAGTACTACATGAAGC-3′; *Nat8l*_D165A_rv, 5′-AGCCATgGCCGTGTGCAGCGCACACTCCAGGTAGGC-3′. This led to a subsequent change from aspartic acid to alanine. The purified PCR product was digested for 1 h at 37 °C with 20 units of DpnI in order to eliminate the template, and the mutated vector was transformed into *Escherichia coli*. The complete *Nat8l* coding region was sequenced to verify the presence of the introduced mutation and the absence of random mutations. iBACs overexpressing *Nat8l*_D165A were generated as described above with pMSCV-hygro as a control. Selection of positive clones was performed with 500 μg/ml hygromycin for at least 7 days.

Mitochondria Isolation and Western Blot Analysis—Mitochondria were isolated from cell pellets of differentiated iBACs with a commercially available kit (Thermo Scientific) using the Dounce homogenizer and 3000 × *g* to pellet the mitochondria. BAT mitochondria were isolated as described previously (22). Modifications to the protocol were as follows. The tissues were excised from male mice fed *ad libitium*, washed in ice-cold PBS, and cut into small pieces with a razorblade. Subsequently, they were homogenized using a Dounce homogenizer with about 60 strokes. The centrifugation steps to pellet the mitochondria were carried out at 3000 × *g* to reduce peroxisomal contamination. Nuclear fraction, mitochondrial fraction, and post-mitochondrial supernatant containing cytosol and ER remnants were lysed in SDS-lysis buffer (50 mM Tris-HCl, pH 6.8, 10% glycerol, 2.5% SDS, 1× protease inhibitor mixture, 1 mM PMSF) and used for further analysis. Cytosolic/ER proteins have been precipitated using the trichloroacetic acid (TCA) method. Briefly, cytolytic protein lysate was mixed with 50% ice-cold TCA to obtain a concentration of 10% TCA and incubated for 1.5 h on ice. Then it was centrifuged for 10 min at 13,000 rpm and 4 °C. The pellet was washed twice with ice-cold acetone, air-dried, and dissolved in SDS-lysis buffer. Control and *Nat8l*-overexpressing iBACs (at several differentiation time points) were harvested for protein analysis by scraping with SDS-lysis buffer. After benzonase digestion, protein concentrations were determined with the BCA protein assay kit (Pierce). 50 μg of sample were subjected to a 12% BisTris gel (NuPAGE, Invitrogen), and gels were blotted to nitrocellulose membranes. The following antibodies were used: anti-NAT8L (1:1000) (Novus Biologicals, catalog no. NBP1-06599); anti-UCP1 (1:1000) (Calbiochem); anti-hexokinase (1:1000), anti-histone H3 (1:2000), and anti-protein-disulfide isomerase (1:1000) (all from Cell Signaling Technology); and anti-β-Actin (1:25,000) (Sigma). For chemiluminescent detection, a horseradish peroxidase-conjugated secondary antibody was used (anti-rabbit; 1:5000) (DAKO), and ECL (Pierce) served as substrate.

RNA Isolation, Reverse Transcription, and Gene Expression Analysis—Total RNA from cells was isolated using the Total RNA isolation kit (Sigma). Tissue RNA was isolated with TRIzol reagent (Invitrogen). cDNA was generated using Superscript II reverse transcriptase (Invitrogen). mRNA expression was assessed using real-time PCR as described (20). Gene expression was normalized to *Tfiiβ* in murine tissues and cells and to *β-ACTIN* in human cells. For a primer list, see Table 1.

Measurement of Cellular Oxygen Consumption Rate (OCR)—Six days after inducing differentiation, iBACs were plated in XF96 polystyrene cell culture microplates (Seahorse Bioscience) at a density of 40,000 cells/well. After an overnight incubation, cells were washed and preincubated for 30 min in unbuffered XF assay medium (Seahorse Bioscience) supplemented with 5.5 mM D-glucose and 1 mM sodium pyruvate at 37 °C in a non-CO_2 environment. OCR was subsequently measured every 7 min using an XF96 extracellular flux analyzer (Seahorse Bioscience). Optimal concentrations of specific inhibitors/accelerators of the electron transport chain were

determined in prior titration experiments, and working concentrations used were 1 μM oligomycin, 2 μM carbonyl cyanide *p*-trifluoromethoxyphenylhydrazone, 2.5 μM antimycin A, and 10 μM norepinephrine.

[^{14}C]Glucose Uptake and Lipid Extraction—iBACs were incubated overnight with DMEM supplemented with 1 nM triiodthyronine, 20 nM insulin, 0.5 g/liter glucose, and 0.1 μCi of D-[^{14}C(U)]glucose/ml (ARC). After that, cells were washed four times with ice-cold PBS, and neutral lipids were extracted with hexane/isopropyl alcohol (3:2, v/v). Thin layer chromatography was performed with hexane/diethylether/acetic acid (70/29/1, v/v/v) as solvent, and lipids were visualized with iodine vapor and cut out. The incorporated radioactivity was measured by liquid scintillation counting. Total glucose incorporation in each lipid class was calculated, and values were corrected by protein content.

Detection of Mitochondrial Mass by Flow Cytometry—iBACs were grown until day 7 of differentiation, trypsinized, incubated for 20 min in DMEM supplemented with 200 nM MitoTracker™ Green (Invitrogen), washed with PBS, and subjected directly to flow cytometry (BD FACSCalibur, BD Biosciences). 90% of all cells were found in sectors II and IV. Sector II was chosen to compare fluorescence intensities between control and *Nat8l*-overexpressing cells.

Transmission Electron Microscopy—Transmission electron microscopy was performed as described (23). In brief, iBACs grown on an Aclar film (Gröpl, Tulln, Austria) were fixed on day 7 in 2.5% (w/v) glutaraldehyde and 2% (w/v) paraformaldehyde in 0.1 M phosphate buffer, pH 7.4, for 1 h, postfixed in 2% (w/v) osmium tetroxide for 1 h at room temperature, dehydrated in a graded series of ethanol, and embedded in a TAAB epoxy resin (Gröpl). Ultrathin sections (75 nm) were cut with a Leica UC 6 Ultramicrotome and stained with lead citrate for 5 min and with uranyl acetate for 15 min. Images were taken using a FEI Tecnai G2 20 transmission electron microscope (FEI Eindhoven) with a Gatan ultrascan 1000 CCD camera. The acceleration voltage was 120 kV.

Measurement of Mitochondrial Membrane Potential—iBACs were plated on 30-mm glass coverslips on day 7. Following overnight incubation, cells were loaded with a 500 nM concentration of the ratiometric indicator JC-1 (Invitrogen) in full medium at 37 °C for 30 min. Cells were then washed, and fluorescence intensities were detected over mitochondrial regions using an array confocal laser-scanning microscope built on an inverse, automatic microscope (Axio Observer.Z1, Zeiss, Germany) equipped with a ×100, 1.45 numerical aperture oil immersion objective (Plan-Fluor, Zeiss), an acousto-optic tunable filter-based laser merge system (Visitron Systems), and a CCD camera (CoolSNAP-HQ, Photometrics). Excitation/emission wavelengths were 488/529 and 535/590 nm for green fluorescent monomers and red fluorescent J-aggregates, respectively. During experiments, cells were perfused with a buffer containing 145 mM NaCl, 5 mM KCl, 2 mM $CaCl_2$, 1 mM $MgCl_2$, 10 mM D-glucose, and 10 mM HEPES, pH 7.4. Basal fluorescence intensity ratios were normalized to corresponding ratios after dissipation of mitochondrial membrane potential using 2 μM carbonyl cyanide *p*-trifluoromethoxyphenylhydrazone.

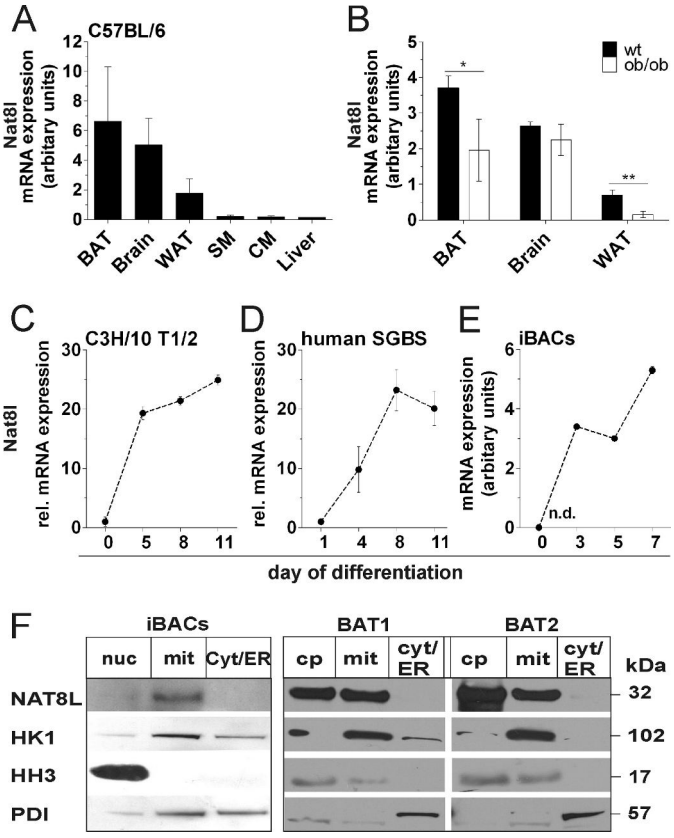

FIGURE 1. ***Nat8l* is expressed in adipocytes, is strongly decreased in WAT and BAT of genetically obese mice, and localizes in mitochondria *in vitro* and *in vivo*.** *A* and *B*, quantitative real-time PCR analysis of *Nat8l* mRNA expression in various tissues of male, refed C57BL/6 mice (*A*), and ob/ob mice (*B*) ($n = 4$). *BAT*, brown adipose tissue; *WAT*, white adipose tissue; *SM*, skeletal muscle; *CM*, cardiac muscle. *C–E*, *Nat8l* mRNA in various adipogenic cell lines during differentiation ($n \geq 3$). *C* and *D*, expression at the start of differentiation is set to 1. *C*, murine, mesenchymal white adipogenic cells C3H/10 T1/2. *D*, human, white adipogenic Simpson-Golabi-Behmel syndrome (*SGBS*) cells. *E*, murine iBACs. All data are presented as means ± S.D. (*error bars*). *F*, protein expression of NAT8L in iBACs and C57BL/6 BAT fractionates (*cp*, crude pellet; *mit*, mitochondria; *nuc*, nucleus; *cyt/ER*, cytosol/endoplasmic reticulum). Shown is one representative blot of $n = 3$ (*left*) and $n = 2$ (*right*). *, $p < 0.05$; **, $p < 0.01$.

Statistical Analysis—If not otherwise stated, results are mean values ± S.D. of at least three independent experiments, or results show one representative experiment of three. Statistical analysis was done on all available data. Statistical significance was determined using the two-tailed Student's *t* test. *, $p < 0.05$; **, $p < 0.01$; ***, $p < 0.001$.

RESULTS

Nat8l Is Expressed in Adipocytes and Located in Mitochondria—NAT8L is often referred to as a brain-specific enzyme, and it is still under debate whether it is located in the mitochondria or ER/cytoplasm of neurons (24–26). Fig. 1*A* shows that *Nat8l* is expressed to a similar extent in brain and BAT, to a lower extent in WAT, and hardly detectable in skeletal muscle (*SM*), cardiac muscle (*CM*), and liver of C57BL/6 mice. In genetically obese mice (ob/ob), the *Nat8l* mRNA level was unchanged in the brain, whereas it was 50% decreased in BAT and nearly blunted in WAT when compared with WT mice (Fig. 1*B*). We next determined the expression profile of *Nat8l* during the differentiation of several adipogenic cell lines.

Nat8l mRNA expression increases about 20-fold during white adipogenic differentiation of C3H10 T1/2 cells (Fig. 1*C*). A similar increase was observed in human Simpson-Golabi-Behmel syndrome adipogenic cells (Fig. 1*D*). Most relevant for this work, *Nat8l* mRNA levels highly increased during differentiation of iBACs (Fig. 1*E*). Next, we investigated the localization of endogenous NAT8L in differentiating iBACs and BAT by subjecting subcellular fractionations to Western blot analysis. NAT8L protein could be clearly detected in the mitochondrial fraction, both *in vitro* (Fig. 1*F*, *left panel*) and *in vivo* (Fig. 1*F*, *right panels*), and there was no detectable NAT8L protein in the ER/cytosolic fraction. To control proper fractionation, we included hexokinase 1 (mitochondrial), histone H3 (nuclear), and protein disulfide isomerase (cytosolic) detection. Due to its high expression in BAT, we focused on iBACs as a model system to study the role of *Nat8l* in adipocyte biology.

Overexpression of Nat8l in Differentiating iBACs Increases Lipid Turnover—In brain, NAT8L has been shown to be required for lipid synthesis, especially for myelination (14, 16). To analyze the influence of *Nat8l* on lipid metabolism in brown fat cells, we generated iBACs stably overexpressing *Nat8l*. After clonal expansion, cells were induced to differentiate into brown adipocytes. Two monoclonal populations exhibited substantial overexpression of *Nat8l* (-fold expression relative to control on day 3 of differentiation: 28.9 ± 8.4 and 12.3 ± 0.5, respectively). To measure neutral lipid synthesis from glucose, iBACs were incubated with ^{14}C-labeled glucose. *Nat8l*-overexpressing iBACs showed an up to 4-fold increased incorporation of glucose into neutral lipids, such as diglycerides, TG, FFA, and cholesteryl ester, on day 3 (Fig. 2*A*) and day 7 of differentiation (Fig. 2*B*). However, oil red O staining and TG measurements of *Nat8l*-overexpressing and control iBACs showed decreased TG levels on day 3 (Fig. 2*C*; quantified in Fig. 2*D*), whereas even a slight increase in lipid accumulation could be observed on day 7 of differentiation (Fig. 2*C*; quantified in Fig. 2*E*). The fact that, despite higher glucose incorporation into neutral lipids, TG accumulation was delayed in differentiating *Nat8l*-overexpressing iBACs prompted us to investigate lipolysis. Therefore, we measured glycerol and FFA content in cell lysates and supernatants of *Nat8l*-overexpressing and control iBACs on day 7. Whereas glycerol release (Fig. 2*E*) showed a tendency to decrease, FFA release was increased 4-fold in differentiated *Nat8l*-overexpressing iBACs compared with control cells (Fig. 2*F*). Additionally, we observed a 3-fold increase in FFA release upon isoproterenol stimulation in *Nat8l*-overexpressing cells (Fig. 2*F*). However, FFA content in cell lysates was not changed in any condition (Fig. 2*F*). Collectively, our data suggest an increased lipid turnover upon *Nat8l* overexpression in brown adipocytes.

Nat8l Overexpression Increases Mitochondrial Mass, Number, and Cellular Respiration Rate—Because lipolysis is a requirement for a distinct brown adipose phenotype *in vivo* (9), we asked whether mitochondrial mass, number, and cellular respiration rates are changed in *Nat8l*-overexpressing iBACs. Transmission electron microscopy clearly demonstrates an increased number of mitochondria in *Nat8l*-overexpressing cells (Fig. 3*A*). Counting 14 individual cells from two biological replicates from either control or *Nat8l*-overexpressing iBACs

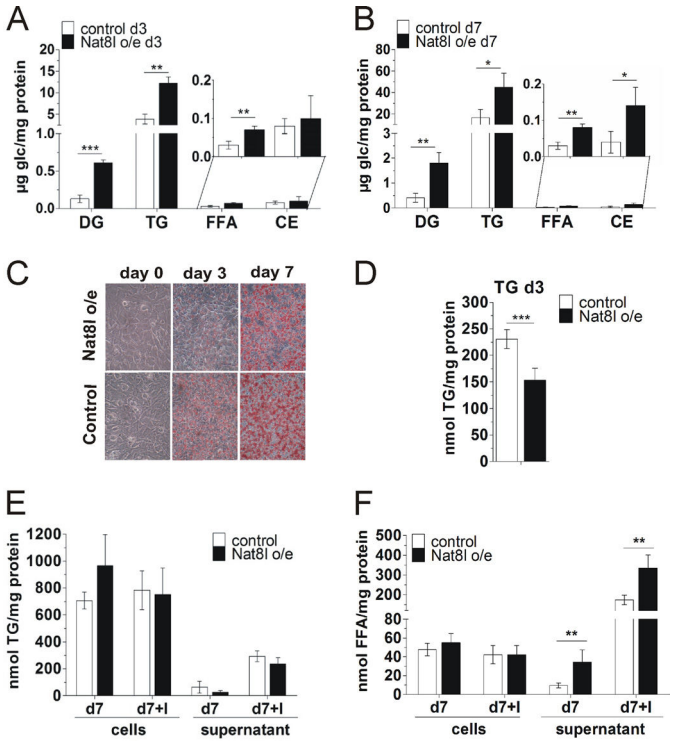

FIGURE 2. **Overexpression of *Nat8l* increases lipid turnover in iBACs.** iBACs were infected with retroviral particles harboring either *Nat8l* coding sequence or empty vector as control. *A*, incorporation of [^{14}C]glucose into neutral lipids of day 3 iBACs. iBACs were incubated with D-[^{14}C(U)]glucose overnight, neutral lipids were extracted and separated by TLC, and incorporated radioactivity was counted and calculated as glucose uptake ($n = 3$). *B*, incorporation of [^{14}C]glucose into neutral lipids of day 7 iBACs. *C*, oil red O stainings of *Nat8l*-overexpressing (*o/e*) and control iBACs during differentiation. Representative micrographs of $n = 3$ are shown. *D*, triglyceride quantification of cell lysates of *Nat8l*-overexpressing and control iBACs on day 3 of differentiation ($n = 3$). *E*, TG content in control and *Nat8l*-overexpressing cell lysates and supernatants in basal conditions and after isoproterenol stimulation (10 µM for 4 h; *+I*) ($n = 3$). *F*, fatty acid content in cell lysates and supernatants of *Nat8l*-overexpressing and control cells with and without isoproterenol treatment (10 µM for 4 h; *+I*) ($n = 3$). All data are presented as means ± S.D. (*error bars*), two-tailed Student's *t* test. *, $p < 0.05$; **, $p < 0.01$; ***, $p < 0.001$.

revealed a doubling of mitochondria/cell upon *Nat8l* overexpression (Fig. 3*B*). Furthermore, we incubated cells with MitoTracker Green, which stains mitochondria in a membrane potential-independent manner (27) and subjected them to flow cytometry. As depicted in Fig. 3, *C* (*sector II*) and *D*, *Nat8l*-overexpressing cells showed increased fluorescence intensity, indicating an increased mitochondrial mass. Nevertheless, others reported that MitoTracker Green changes its abilities with regard to the membrane potential (28). To ascertain that the increase in fluorescence intensity was not due to a membrane potential change, we measured membrane potential via incubation with the mitochondrial stain JC-1. As shown in Fig. 3*E*, there was no significant change in membrane potential in *Nat8l*-overexpressing cells when compared with controls. The increased mitochondrial mass led us to hypothesize that *Nat8l*-overexpressing cells may have an elevated OCR. Therefore, we studied the cells with a Seahorse extracellular flux analyzer. This experiment revealed that *Nat8l*-overexpressing cells have an increased OCR (Fig. 3*F*). Specifically, basal respiration and maximal respiration were elevated by at least 40%. Even in an activated state, after preincubation with 10 µM norepinephrine for

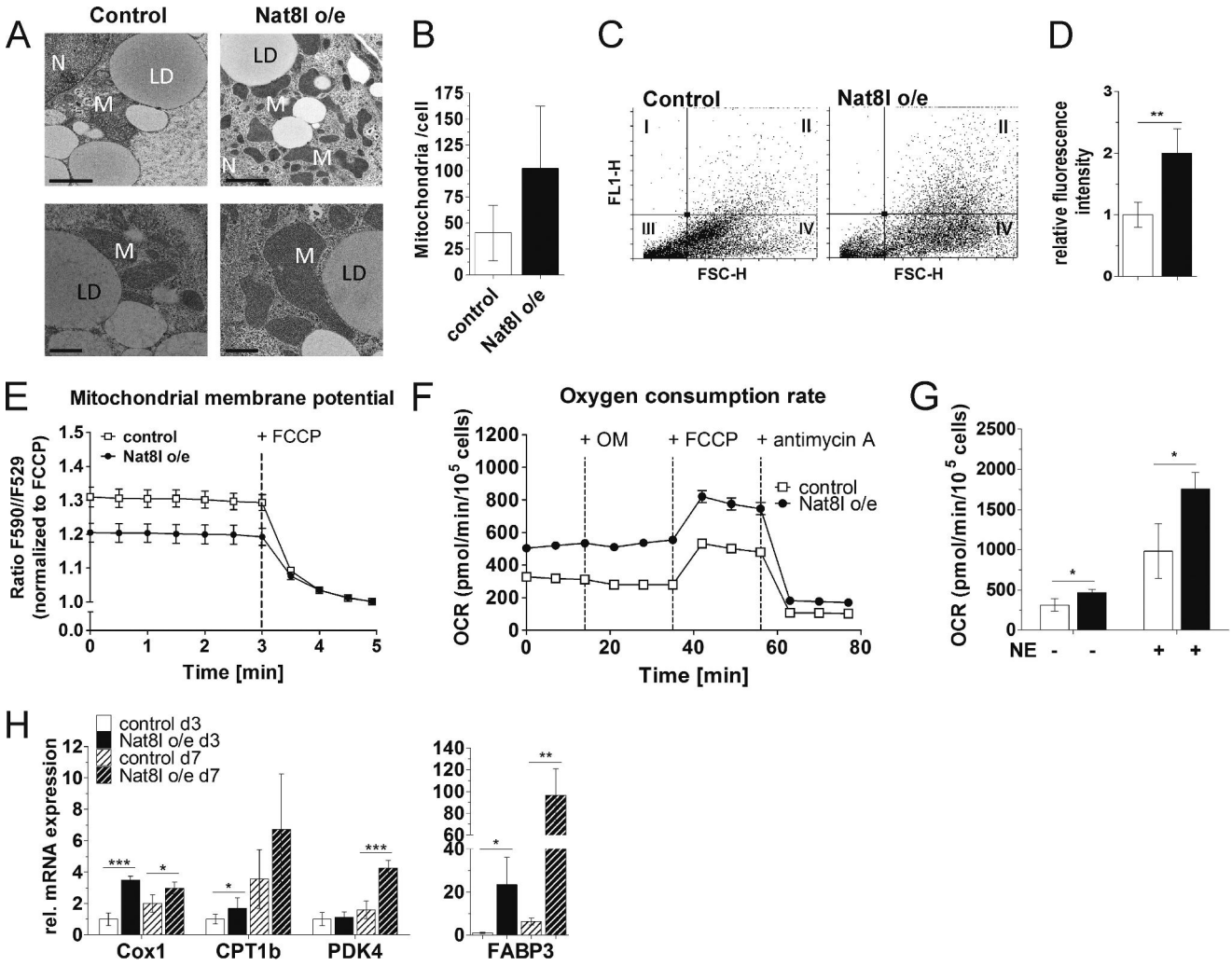

FIGURE 3. ***Nat8l* overexpression increases mitochondrial mass and energy expenditure in iBACs.** *A*, transmission electron micrograph of *Nat8l*-overexpressing and control iBACs on day 7. *Scale bars*, 2 μm (*top panels*) and 1 μm (*bottom panels*); *LD*, lipid droplet; *M*, mitochondria; *N*, nucleus. *B*, mitochondria count of 14 individual cells from control and *Nat8l*-overexpressing cells. *C*, iBACs were incubated with 200 nM MitoTracker Green and subjected to flow cytometry. Fluorescence intensity was measured in FL-1. FSC-H is a measure for cell size ($n = 3$). *D*, quantification of fluorescence intensity in sector II shows the relative increase in mitochondrial mass ($n = 3$). *E*, mitochondrial membrane potential was measured using JC1 as a mitochondrial stain. JC1 fluorescence shifts from 529 nm (*green*) to 590 nm (*red*) upon a drop in membrane potential. The ratio from 590/529 nm was measured to estimate the relative membrane potential before and after carbonyl cyanide *p*-trifluoromethoxyphenylhydrazone (*FCCP*) treatment. Data are shown as means ± S.E. (*error bars*), $n = 2$. *F*, OCR of iBACs on day 7 measured with the Seahorse extracellular flux analyzer. Cells were treated at the indicated time points with 1 μM oligomycin (*OM*), 2 μM carbonyl cyanide *p*-trifluoromethoxyphenylhydrazone, and 2.5 μM antimycin A. Data shown as means ± S.E. (*error bars*) ($n = 3$). *G*, OCR of iBACs after a 1-h preincubation with 10 μM norepinephrine (*NE*) ($n = 3$). *H*, mRNA expression of genes involved in mitochondrial oxidative phosphorylation (*Cox1*) and β-oxidation (*Cpt1b*, *Pdk4*, and *Fabp3*) was measured in day 3 and day 7 iBACs ($n = 3$). If not otherwise stated, data are presented as means ± S.D. (*error bars*), two-tailed Student's *t* test. *, $p < 0.05$; **, $p < 0.01$; ***, $p < 0.001$.

1 h, increased respiration was evident in *Nat8l*-overexpressing cells compared with control cells (Fig. 3*G*). In addition, genes that are directly involved in mitochondrial oxidative phosphorylation (*Cox1*, mitochondrial coded subunit of *Cytc*) and indirectly in β-oxidation (*Cpt1b* (carnitine palmitoyltransferase 1b), *Pdk4* (pyruvate dehydrogenase kinase 4), and *Fabp3* (fatty acid-binding protein 3)) were significantly up-regulated on day 3 and/or day 7 of differentiation of *Nat8l*-overexpressing cells, respectively (Fig. 3*H*). In summary, these data indicate increased energy expenditure in iBACs upon *Nat8l* overexpression.

Nat8l Overexpression Augments the Brown Adipose Phenotype—Although TG accumulation is significantly decreased in *Nat8l*-overexpressing iBACs on day 3, no significant changes in expression profiles of general adipogenic markers, such as aP2 and adiponectin (*AdipoQ*), could be observed (Fig. 4*A*). As an exception, *Pparγ2* levels were 3-fold increased on day 3 but reached the level of control cells by day 7. Additionally, three white selective markers (29) were investigated. Whereas the expression of fatty acid desaturase 3 (*Fads3*) did not change, phosphoserine aminotransferase 1 (*Psat1*) and resistin (*Retn*) were significantly decreased in *Nat8l*-overexpressing cells (Fig. 4*A*). Notably, the expression of genes that are crucial in the development of brown adipocytes, such as *Pparα*, *Pgc1α* (*Pparγ* coactivator 1 α), *Prdm16*, *C/ebpβ*, *Cox8b*, *Dio2*, and *Cidea*, were all increased in *Nat8l*-overexpressing iBACs on day 7 (Fig. 4*B*). Strikingly, *Ucp1* mRNA expression was increased up to 17-fold in *Nat8l*-overexpressing iBACs on day 7 (Fig. 4*C*), and its expression could be further elevated upon the addition of 10 μM isoproterenol (Fig. 4*C*), showing that *Nat8l*-overexpressing cells still have the potential to be activated by β-adrenergic stim-

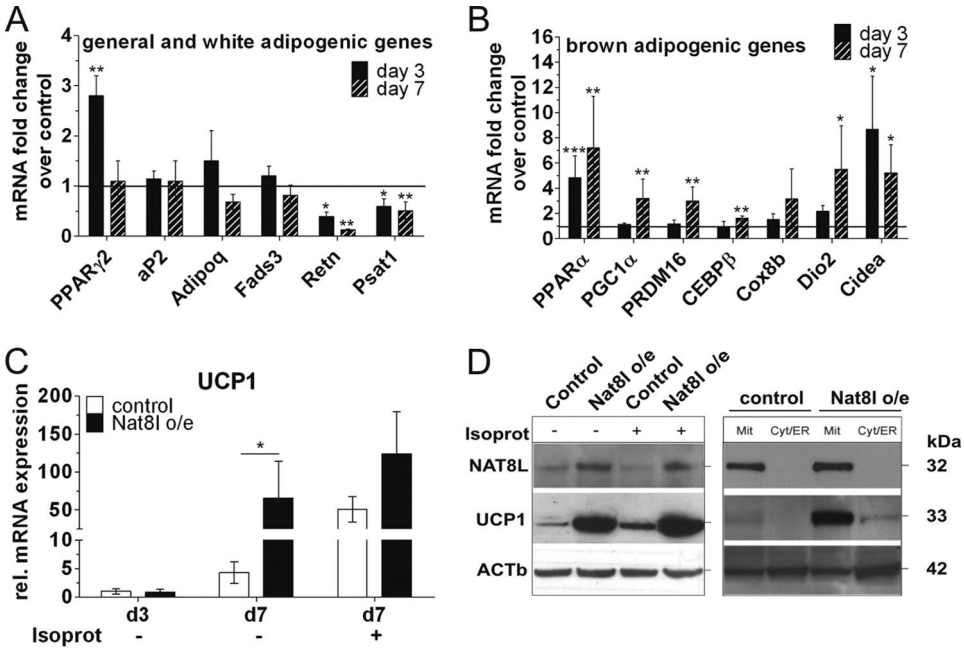

FIGURE 4. ***Nat8l* overexpression augments the brown adipose phenotype.** *A*, mRNA expression of general (*Pparγ2*, *aP2*, and *Adipoq*) and white adipogenic genes (*Fads3*, *Psat1*, and *Retn*) in day 3 and day 7 iBACs ($n \geq 3$). *B*, mRNA expression of brown marker genes in day 3 and day 7 iBACs ($n \geq 3$). Data in *A* and *B* are expressed as -fold change of Nat8l-overexpressing *versus* control iBACs. Shown is *Ucp1* mRNA (*C*) and UCP1 and NAT8L protein expression (*D*, *left*) with and without 10 μM isoproterenol stimulation for 4 h on day 7 in control and *Nat8l*-overexpressing iBACs. *D* (*right*), protein expression of NAT8L in fractionated iBACs. UCP1 served as a mitochondrial marker. *Mit*, mitochondria; *Cyt/ER*, cytosol/ER. β-ACTIN (*ACTb*) served as a loading control. One representative blot of $n = 3$ is shown. All data are presented as means ± S.D. (*error bars*), two-tailed Student's *t* test. *, $p < 0.05$; **, $p < 0.01$; ***, $p < 0.001$.

ulation. This enormous induction of UCP1 upon *Nat8l* overexpression could also be confirmed at the protein level (Fig. 4*D*, *left*). To test whether overexpressed NAT8L protein is located in mitochondria like the endogenous one (Fig. 1*E*), a fractionation of *Nat8l*-overexpressing iBACs was performed on day 7. NAT8L localized exclusively in the mitochondria, as did UCP1, a described mitochondrial protein (Fig. 4*D*, *right*). Hence, we observe an increased brown phenotype upon *Nat8l* overexpression.

Nat8l Overexpression Increases UCP1 Levels and OCR in a PPARα-dependent Manner—PPARα was shown to increase expression of *Ucp1*, the protein mainly responsible for a brown phenotype. Furthermore, the activation potential of PPARα is enhanced by lipolytic products (30). We observed both increased lipolysis (Fig. 2*F*) and enhanced expression of *Ucp1* in *Nat8l*-overexpressing iBACs (Fig. 4*C*). Hence, we reasoned that these changes are mediated by PPARα. Therefore, we treated *Nat8l*-overexpressing iBACs with a PPARα antagonist (10 μM GW6471) from day 4 of differentiation until day 7. This treatment did not change differentiation capacity as judged by microscopy and cellular TG content (Fig. 5*E*). Measuring mRNA levels of marker genes upon PPARα antagonist treatment, we found that *Pgc1α* and *aP2* were unchanged, and *Cox1* and *Pdk4* were slightly decreased, whereas the direct PPARα target genes *Cpt1b* (31) and *Ucp1* (32) were significantly blunted (Fig. 5*A*). Importantly, the massive *Nat8l*-mediated up-regulation in UCP1 protein was nearly reduced to control level (Fig. 5*B*). In accordance, OCR was reduced close to the level of control cells after GW6471 treatment of Nat8l-overexpressing cells (Fig. 5*C*). On the other hand, neither the increased lipogenesis (Fig. 5*D*) nor the elevated basal and isoproterenol-stimulated FFA release evoked by *Nat8l* overexpression was affected by GW6471 treatment (Fig. 5*F*). These results underline our hypothesis that *Nat8l per se* influences lipid turnover, but other effects, such as UCP1 and *Cpt1b* expression and respiration, require PPARα activation.

Enzymatic Activity Is Required for the Function of NAT8L in Adipocytes—Recently, Tahay *et al.* (24) investigated which regions of the human NAT8L protein are important for its catalytic activity by introducing several point mutations into the *Nat8l* gene and subsequent measurement of their enzymatic activities. We generated a mutant of NAT8L, exchanging aspartate 165 to alanine, which is described as having no residual enzymatic activity (24), and used this mutated construct to study the effects upon its overexpression. Although we reached a 7-fold increased expression of the mutated enzyme in iBACs (Fig. 6*A*), we observed no changes in the expression of adipogenic marker genes (Fig. 6*A*) and no impact on cellular lipid content or glycerol/FFA release (Fig. 6, *B* and *C*, unstimulated and isoproterenol-stimulated). Thus, we conclude that the enzymatic activity of NAT8L is required for its function in brown adipocytes.

Nat8l Silencing in iBACs and Knock-out of Nat8l in Mice Lead to Compensatory Up-regulation of ATP-Citrate Lyase—To analyze the influence of *Nat8l* knockdown on lipid and energy metabolism in brown fat cells, we generated iBACs stably silenced for *Nat8l*. Although various clonal populations were tested, *Nat8l* silencing efficiency did not exceed 50% (Fig. 7, *A* and *F*). Although *Nat8l* silencing in iBACs did not affect differentiation, as shown by cellular TG content (Fig. 7*D*) and neutral lipid synthesis (Fig. 7*B*), lipolysis was significantly increased in basal and isoproterenol-stimulated conditions, as reflected by increased FFA and glycerol release at day 7 when compared with control cells (Fig. 7, *D* and *E*). Additionally, the

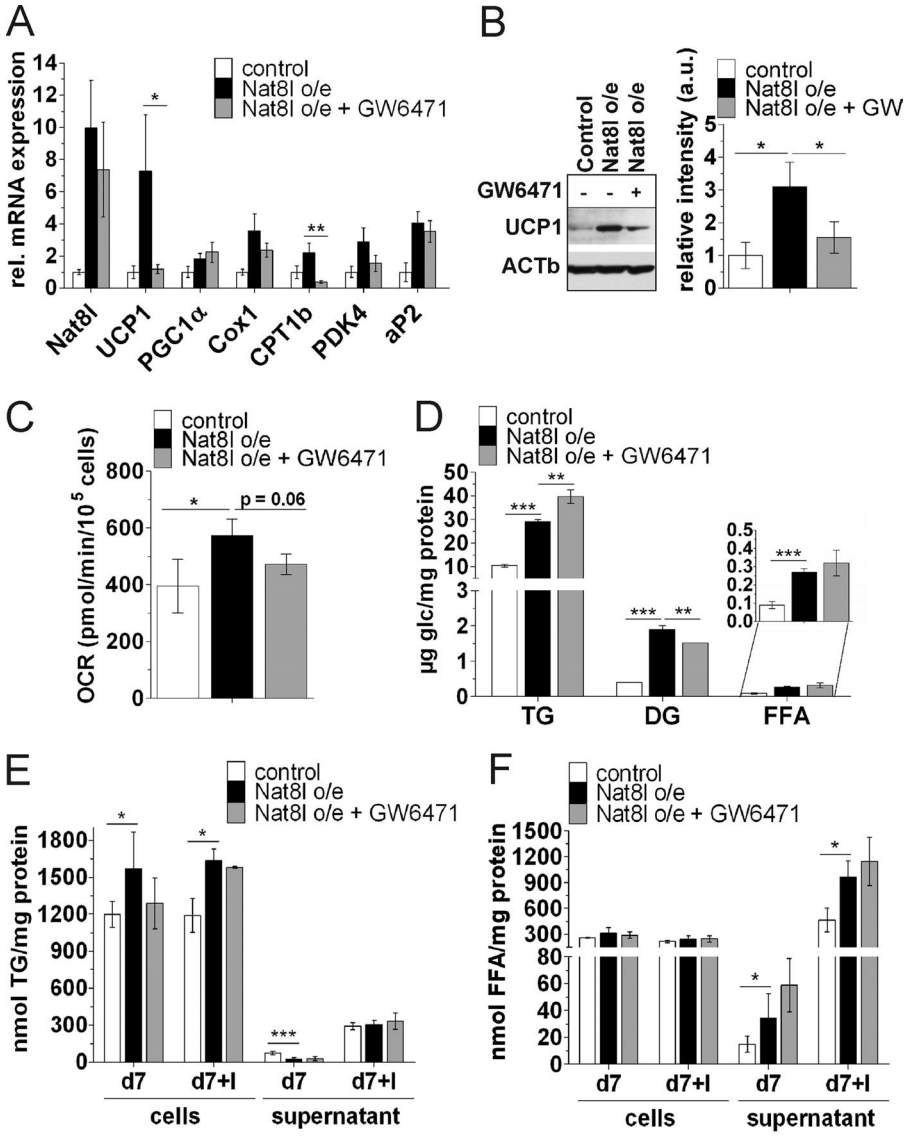

FIGURE 5. ***Nat8l*-mediated induction of *Ucp1* mRNA and oxygen consumption is PPARα-dependent, whereas lipid turnover is not.** iBACs were incubated with a 10 μM concentration of the PPARα antagonist GW6471 from day 4 until day 7 of differentiation. All experiments were performed with day 7 cells. *A*, mRNA expression of adipogenic marker genes (*aP2*, *Ucp1*, and *Pgc1α*) and genes involved in mitochondrial oxidative phosphorylation (*Cox1*) and β-oxidation (*Cpt1b* and *Pdk4*) ($n = 3$). *B*, UCP1 protein expression. One representative blot of $n = 3$ is shown. Relative band intensity is calculated from $n = 3$ and normalized to β-ACTIN. *C*, OCR measured with the Seahorse extracellular flux analyzer ($n = 3$). *D*, incorporation of [^{14}C]glucose into neutral lipids ($n = 3$). Shown are TG content (*E*) and fatty acid content (*F*) in cell lysates and supernatants of cells with and without isoproterenol treatment (10 μM for 4 h; +*l*) ($n \geq 3$). All data are presented as means ± S.D. (*error bars*), two-tailed Student's *t* test. *, $p < 0.05$; **, $p < 0.01$; ***, $p < 0.001$.

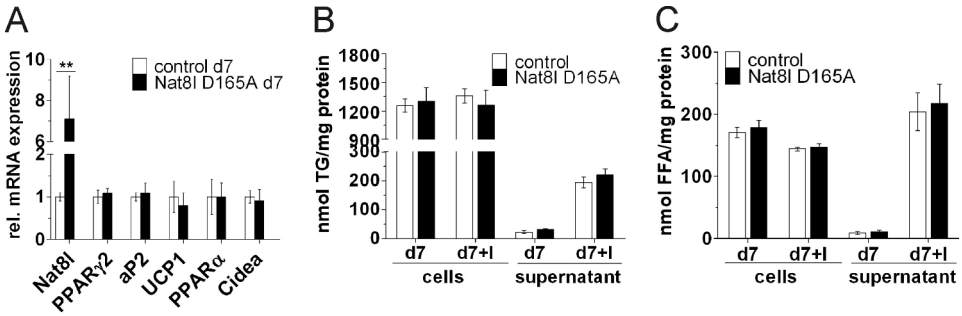

FIGURE 6. **Enzymatic activity is required for the function of *Nat8l* in brown adipocytes.** iBACs were infected with retroviral particles harboring a *Nat8l* coding sequence for producing the enzymatically inactive D165A mutant of the NAT8L protein or an empty vector as control. Cells were differentiated, and all experiments were performed with day 7 cells. *A*, mRNA expression of general (*Pparγ2* and *aP2*) and brown adipogenic genes (*Ucp1*, *Ppara*, and *Cidea*) ($n = 3$). Shown are TG content (*B*) and fatty acid content (*C*) in cell lysates and supernatants of cells with and without isoproterenol treatment (10 μM for 4 h; +*l*) ($n = 3$). All data are presented as means ± S.D. (*error bars*), two-tailed Student's *t* test. **, $p < 0.01$.

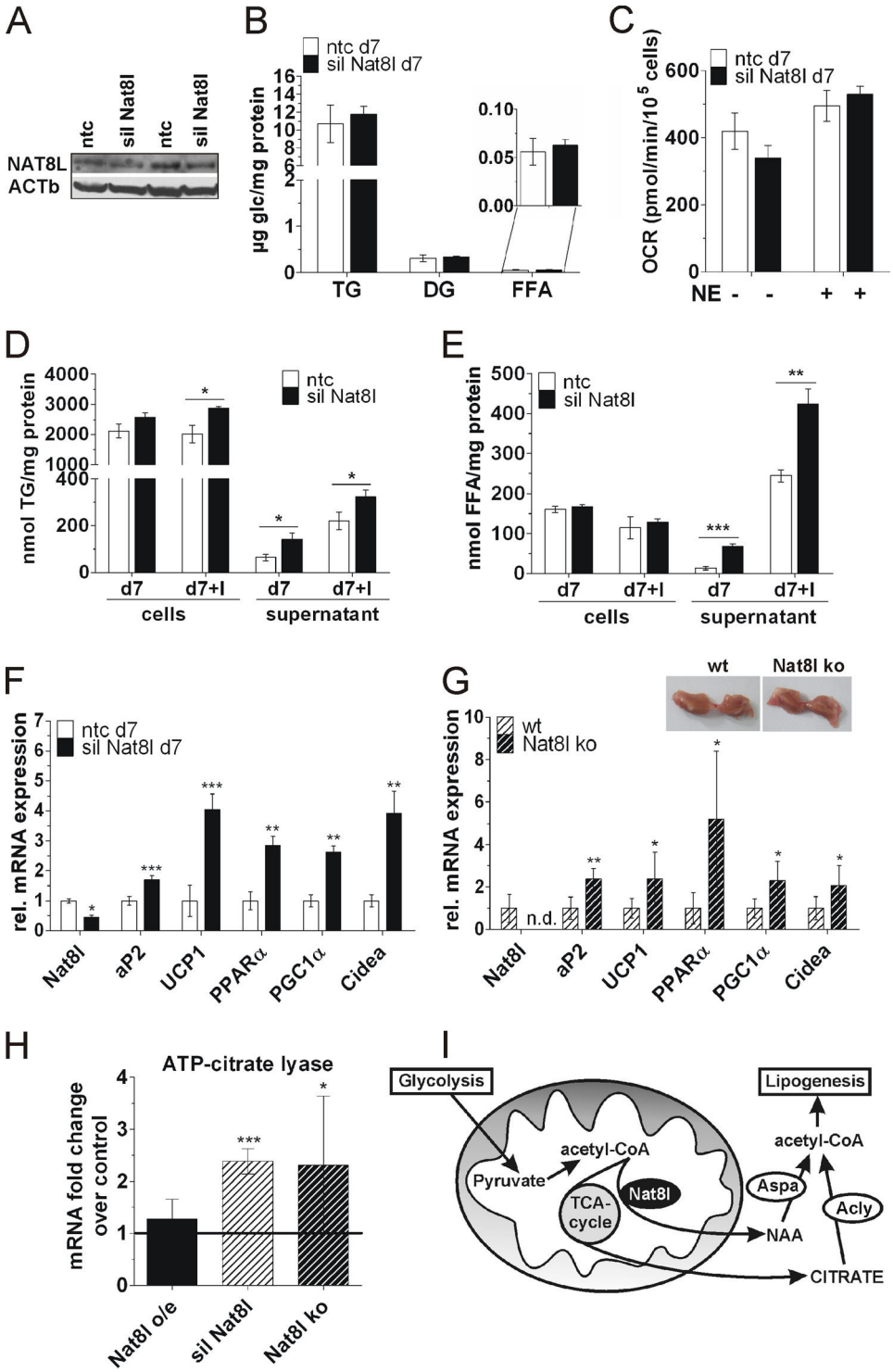

FIGURE 7. ***Nat8l* silencing in iBACs and knock-out of *Nat8l* in mice.** iBACs were infected with lentiviral particles coding for *Nat8l* shRNA (*sil Nat8l*) or using a non-target shRNA as control (*ntc*). If not otherwise stated, cells were differentiated, and all experiments were performed on day 7 (*d7*). *Nat8*-knock-out (*Nat8l KO*) and control mice (*WT*) were fed *ad libitum*, and tissues were harvested at the age of 3–4 months. *A*, protein expression of *Nat8l* in day 3 iBACs. β-actin (*ACTb*) served as a loading control. ($n = 2$). *B*, incorporation of [^{14}C]glucose into neutral lipids. ($n = 3$). *C*, OCR measured with the Seahorse extracellular flux analyzer ($n = 3$). Shown are TG content (*D*) and fatty acid content (*E*) in cell lysates and supernatants of cells with and without isoproterenol treatment (10 μM for 4 h; +*I*) ($n = 3$). Shown are expression of adipogenic genes in *Nat8l*-silenced iBACs ($n = 3$) (*F*) and in *Nat8l*-KO and WT mice ($n \geq 5$) (*G*). *Inset*, pictures of BAT of *Nat8l*-KO and WT mice. *H*, ATP citrate lyase (*Acly*) mRNA expression in *Nat8l*-overexpressing iBACs ($n = 3$), *Nat8l*-silenced iBACs ($n = 3$) and BAT of *Nat8l*-KO mice ($n \geq 5$). *I*, model proposing the NAA pathway as an alternative acetate source for cytosolic acetyl-CoA production. Data are presented as means ± S.D. (*error bars*; two-tailed Student's *t* test). *, $p < 0.05$; **, $p < 0.01$; ***, $p < 0.001$.

expression of adipogenic marker genes, such as *aP2*, *Ucp1*, *Pparα*, *Pgc1α*, and *Cidea*, was significantly increased in *Nat8l*-silenced iBACs in comparison with control cells (Fig. 7*F*). However, *Nat8l*-silenced cells did not show a difference in OCR, neither under basal nor under norepinephrine-stimulated conditions (Fig. 7*C*). Because we could not reach a very strong

Nat8l silencing in iBACs, we examined BAT from *Nat8l*-knock-out mice to evaluate some of our *in vitro* data. BAT from *Nat8l*-KO and WT mice were similar in weight (0.13 ± 0.04 g for *Nat8l*-KO *versus* 0.12 ± 0.06 g for WT mice, respectively; $n = 3$) and gross anatomy (Fig. 7*G*, *inset*), in agreement with our *in vitro* data showing that *Nat8l* silencing does not influence differentiation capacity. Moreover, we used *Nat8l*-KO mice to investigate the expression of several adipogenic marker genes. As seen for *Nat8l*-silenced iBACs (Fig. 7*F*), *aP2*, *Ucp1*, *Pparα*, *Pgc1α*, and *Cidea* mRNA expression was also significantly increased in our *in vivo* model (Fig. 7*G*).

Our data from *Nat8l*-overexpressing iBACs strongly suggest that NAA, the product of the enzymatic activity of NAT8L, can be used as an alternative source for lipid synthesis in adipocytes. Due to the fact that *Nat8l* silencing does not contrarily influence lipogenesis, we wondered whether another acetyl-CoA-producing pathway might be up-regulated to compensate for the decreased NAA-derived acetyl-CoA. Indeed, we found ATP-citrate lyase, the cytosolic enzyme converting citrate to acetyl-CoA and thereby linking cellular glucose catabolism and lipogenesis (33), significantly increased in both *Nat8l*-silenced iBACs and BAT of *Nat8l*-KO mice, whereas it was unchanged in *Nat8l*-overexpressing iBACs when compared with the respective controls (Fig. 7*H*). These data further strengthen our hypothesis that the NAT8L/NAA pathway acts as an alternative source to provide acetyl-CoA as a building block for lipid biosynthesis in adipocytes (Fig. 7*I*).

DISCUSSION

NAT8L is the enzyme responsible for the formation of NAA. In the brain, it has been shown that NAA acts as a transport molecule to provide acetate, which is used as a precursor for lipid synthesis (17). Here, we report that *Nat8l* is expressed not only in the brain but also to a high extent in adipose tissues, and its expression is induced during the differentiation of several murine and human white and brown adipogenic cell lines. Stable overexpression of *Nat8l* in iBACs leads to an increased brown marker gene expression, especially that of *Ucp1*, concomitant with an increased mitochondrial mass, number, and oxygen consumption. Supported by direct and indirect evidence from our data, we propose a model (see Fig. 8) that is based on a mitochondrial localization of NAT8L, as evidenced by our fractionation analyses of brown adipocytes *in vitro* and *in vivo*. However, in neurons, it is still under debate whether NAT8L is localized in mitochondria or ER (24–26). Neuronal NAT8L is described as using acetyl-CoA as a substrate to produce NAA, which is then transported to oligodendrocytes (16). There it is hydrolyzed by the activity of aspartoacylase (Aspa) to yield acetate, which can in turn be used for lipid synthesis (19). The expression portal BioGPS (34) and our unpublished data[4] reveal that Aspa is also highly expressed in BAT, arguing for the existence of the NAA pathway in this tissue. In the brain, it has been shown that NAA-derived acetate has a 3-fold higher potential to be incorporated into lipids than free acetate (35). Because we see elevated ^{14}C incorporation into lipids when providing labeled

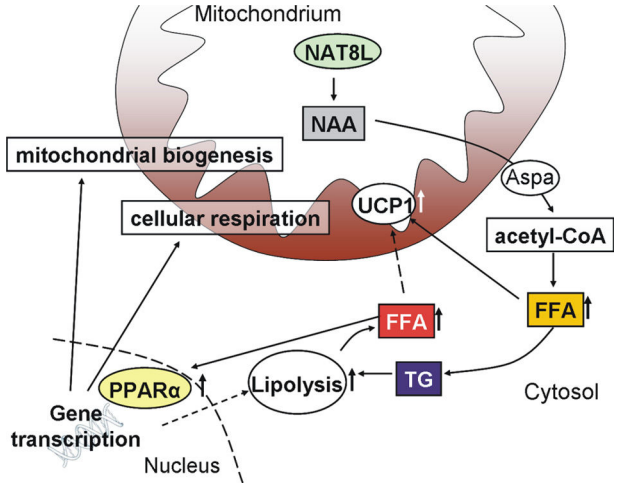

FIGURE 8. **Working model for the proposed Nat8l action in brown adipocytes as described under "Discussion."**

glucose, we speculate that, in brown adipocytes, glycolytic products are used by NAT8L to produce NAA. NAA delivers the acetate moiety for synthesis of cytosolic acetyl-CoA that is further used for FFA synthesis. These FFA are readily esterified to prevent lipotoxicity. Thus, an increase in *Nat8l* expression could drain acetyl-CoA from mitochondria. To maintain the mitochondrial acetyl-CoA pool, acetyl-CoA is mainly provided by decarboxylation of pyruvate via the pyruvate dehydrogenase complex or via β-oxidation of fatty acids. We suppose that glycolysis-derived pyruvate is not sufficient to compensate for acetyl-CoA drained into the NAA pathway because we see *Pdk4* up-regulated upon *Nat8l* overexpression. *Pdk4* inactivates the pyruvate dehydrogenase complex, resulting in a switch from glucose to fatty acid oxidation (36). Additionally, upon *Nat8l* overexpression, we see increased lipolysis providing FFA as substrate for β-oxidation. Concomitantly, the expression of *Fabp3* and *Cpt1b* is elevated. Both proteins have been shown to deliver FFA to mitochondrial β-oxidation in BAT (37, 38).

It is known that fatty acids and their derivatives are crucial for the activation of PPARα and UCP1 (9, 30, 39–41) and that sustained activation of PPARα increases β-oxidation (42). Recently, Ahmadian *et al.* (9) showed that lipolysis via adipose triglyceride lipase plays an essential role in maintaining adaptive thermogenesis in BAT. Together with the results of Haemmerle *et al.* (40) in cardiac muscle, this substantiates that lipolytic action is required for PPARα activation. PPARα, together with PGC1α, induces *Ucp1* expression (32). Therefore, the massive increase in *Ucp1* expression in *Nat8l*-overexpressing cells could be explained by a prominent PPARα activation by elevated lipolysis-derived FFA. Using the PPARα antagonist GW6471, we found that the *Nat8l*-induced UCP1 expression and the concomitant OCR increase were diminished to control cell levels, indicating that it is indeed a PPARα-mediated mechanism. However, increased lipogenesis and FFA release are retained during GW6471 treatment. The fact that *Nat8l* levels are still high in this condition (Fig. 5*A*) argues for a dissociation of PPARα-mediated effects and NAA-mediated lipid turnover in adipocytes. Hence, delivery of acetyl-CoA via NAT8L-mediated NAA seems to be upstream of PPARα-related effects. Moreover, our studies using the enzymatically inactive protein

[4] A. R. Pessentheiner, H. J. Pelzmann, A. Prokesch, and J. G. Bogner-Strauss, unpublished data.

support this concept because the D165A mutant does not increase lipogenesis. PPARα, its coactivator PGC1α (43, 44), and PRDM16 (45) have been shown to be important for mitochondrial biogenesis. Elevated expression of all of these genes upon *Nat8l* overexpression could explain the increase in mitochondria in these cells. Also, other brown phenotypic marker genes, such as *Dio2* (46), *C/ebpβ* (47), and *Cidea* (48), are upregulated in *Nat8l*-overexpressing cells, rendering NAT8L as a factor to enhance "browning." This is further supported by the fact that white-specific genes, like *Retn* and *Psat1* (29), are repressed. All of the observations mentioned above are consistent with our measurement of increased basal and norepinephrine-stimulated OCR and explain why these cells have a higher metabolic rate *per se*.

Knockdown of *Nat8l* in brown adipocytes had no impact on TG content, lipogenesis, and OCR, whereas lipolysis and the expression of several adipogenic marker genes were still increased. The increased lipolysis observed upon *Nat8l* knockdown might be a mechanism to generate acetyl-CoA for energy production. Lipolysis provides fatty acids that eventually can become acetylated and are further used for β-oxidation, thereby contributing to the acetyl-CoA pool. In parallel, the FFA produced by lipolysis might also activate PPARα (9) and thus increase the expression of PPARα target genes, such as *Ucp1* and *Cidea* (49), as seen in *Nat8l*-silenced iBACs and *Nat8l*-KO mice. Most interestingly, ATP-citrate lyase was significantly increased upon *Nat8l*-silencing *in vitro* and in BAT of *Nat8l*-KO mice. ATP-citrate lyase is well described to link glucose catabolism to lipogenesis by catalyzing the production of acetyl-CoA from citrate. Thus, the increase of ATP-citrate lyase mRNA expression might present a compensatory mechanism (as outlined in Fig. 7*I*) to sustain the acetyl-CoA pool upon *Nat8l* knockdown.

Although NAT8L has been implicated in many functions in the brain (mainly in the generation of substrates for myelination), its main function in adipose tissue was unknown. We imagine that, under certain circumstances, the NAA pathway could similarly serve as an additional acetyl-CoA-metabolizing mechanism in adipocytes. Our data propose (Fig. 8) that elevating *Nat8l* expression in brown adipocytes results in increased acetyl-CoA flux via the NAA pathway and concomitant higher cytoplasmic FFA anabolism, resulting in elevated TG synthesis. A parallel increase in lipolysis followed by an activation of β-oxidation can then restore acetyl-CoA back to the mitochondria. This "futile" cycle may result in increased lipid turnover and raise the oxidative potential of the brown fat cell and thereby boost the brown adipogenic phenotype. However, it remains to be seen which physiological stimuli are contributing to the regulation of the NAA pathway.

Acknowledgments—iBACs were kindly provided by Patrick Seale. We acknowledge the technical assistance provided by Corina Madreiter, Florian Stoeger, Thomas Schreiner, and Claudia Gaug. We thank Rudolf Zechner for critically reviewing the manuscript and for fruitful discussions.

REFERENCES

1. Zimmermann, R., Strauss, J. G., Haemmerle, G., Schoiswohl, G., Birner-Gruenberger, R., Riederer, M., Lass, A., Neuberger, G., Eisenhaber, F., Hermetter, A., and Zechner, R. (2004) Fat mobilization in adipose tissue is promoted by adipose triglyceride lipase. *Science* **306,** 1383–1386
2. Haemmerle, G., Zimmermann, R., Strauss, J. G., Kratky, D., Riederer, M., Knipping, G., and Zechner, R. (2002) Hormone-sensitive lipase deficiency in mice changes the plasma lipid profile by affecting the tissue-specific expression pattern of lipoprotein lipase in adipose tissue and muscle. *J. Biol. Chem.* **277,** 12946–12952
3. Cannon, B., and Nedergaard, J. (2004) Brown adipose tissue. Function and physiological significance. *Physiol. Rev.* **84,** 277–359
4. Nedergaard, J., Bengtsson, T., and Cannon, B. (2007) Unexpected evidence for active brown adipose tissue in adult humans. *Am. J. Physiol. Endocrinol. Metab.* **293,** E444–E452
5. Cypess, A. M., Lehman, S., Williams, G., Tal, I., Rodman, D., Goldfine, A. B., Kuo, F. C., Palmer, E. L., Tseng, Y.-H., Doria, A., Kolodny, G. M., and Kahn, C. R. (2009) Identification and importance of brown adipose tissue in adult humans. *N. Engl. J. Med.* **360,** 1509–1517
6. Virtanen, K. A., Lidell, M. E., Orava, J., Heglind, M., Westergren, R., Niemi, T., Taittonen, M., Laine, J., Savisto, N.-J., Enerbäck, S., and Nuutila, P. (2009) Functional brown adipose tissue in healthy adults. *N. Engl. J. Med.* **360,** 1518–1525
7. van Marken Lichtenbelt, W. D., Vanhommerig, J. W., Smulders, N. M., Drossaerts, J. M., Kemerink, G. J., Bouvy, N. D., Schrauwen, P., and Teule, G. J. (2009) Cold-activated brown adipose tissue in healthy men. *N. Engl. J. Med.* **360,** 1500–1508
8. Boss, O., and Farmer, S. R. (2012) Recruitment of brown adipose tissue as a therapy for obesity-associated diseases. *Front. Endocrinol.* (*Lausanne*) **3,** 14
9. Ahmadian, M., Abbott, M. J., Tang, T., Hudak, C. S., Kim, Y., Bruss, M., Hellerstein, M. K., Lee, H.-Y., Samuel, V. T., Shulman, G. I., Wang, Y., Duncan, R. E., Kang, C., and Sul, H. S. (2011) Desnutrin/ATGL is regulated by AMPK and is required for a brown adipose phenotype. *Cell Metab.* **13,** 739–748
10. Bartelt, A., Bruns, O. T., Reimer, R., Hohenberg, H., Ittrich, H., Peldschus, K., Kaul, M. G., Tromsdorf, U. I., Weller, H., Waurisch, C., Eychmüller, A., Gordts, P. L., Rinninger, F., Bruegelmann, K., Freund, B., Nielsen, P., Merkel, M., and Heeren, J. (2011) Brown adipose tissue activity controls triglyceride clearance. *Nat. Med.* **17,** 200–205
11. Ma, S. W., and Foster, D. O. (1986) Uptake of glucose and release of fatty acids and glycerol by rat brown adipose tissue *in vivo*. *Can. J. Physiol. Pharmacol.* **64,** 609–614
12. Darnley, A. C., Carpenter, C. A., and Saggerson, E. D. (1988) Changes in activities of some enzymes of glycerolipid synthesis in brown adipose tissue of cold-acclimated rats. *Biochem. J.* **253,** 351–355
13. Pinent, M., Hackl, H., Burkard, T. R., Prokesch, A., Papak, C., Scheideler, M., Hämmerle, G., Zechner, R., Trajanoski, Z., and Strauss, J. G. (2008) Differential transcriptional modulation of biological processes in adipocyte triglyceride lipase and hormone-sensitive lipase-deficient mice. *Genomics* **92,** 26–32
14. Wiame, E., Tyteca, D., Pierrot, N., Collard, F., Amyere, M., Noel, G., Desmedt, J., Nassogne, M.-C., Vikkula, M., Octave, J.-N., Vincent, M.-F., Courtoy, P. J., Boltshauser, E., and van Schaftingen, E. (2010) Molecular identification of aspartate *N*-acetyltransferase and its mutation in hypoacetylaspartia. *Biochem. J.* **425,** 127–136
15. Ariyannur, P. S., Moffett, J. R., Manickam, P., Pattabiraman, N., Arun, P., Nitta, A., Nabeshima, T., Madhavarao, C. N., and Namboodiri, A. M. (2010) Methamphetamine-induced neuronal protein NAT8L is the NAA biosynthetic enzyme. Implications for specialized acetyl coenzyme A metabolism in the CNS. *Brain Res.* **1335,** 1–13
16. Chakraborty, G., Mekala, P., Yahya, D., Wu, G., and Ledeen, R. W. (2001) Intraneuronal *N*-acetylaspartate supplies acetyl groups for myelin lipid synthesis. Evidence for myelin-associated aspartoacylase. *J. Neurochem.* **78,** 736–745
17. Mehta, V., and Namboodiri, M. A. (1995) *N*-Acetylaspartate as an acetyl source in the nervous system. *Brain Res. Mol. Brain Res.* **31,** 151–157
18. Burlina, A. P., Schmitt, B., Engelke, U., Wevers, R. A., Burlina, A. B., and Boltshauser, E. (2006) Hypoacetylaspartia. Clinical and biochemical follow-up of a patient. *Adv. Exp. Med. Biol.* **576,** 283–287; discussion 361–363

19. Madhavarao, C. N., Arun, P., Moffett, J. R., Szucs, S., Surendran, S., Matalon, R., Garbern, J., Hristova, D., Johnson, A., Jiang, W., and Namboodiri, M. A. (2005) Defective *N*-acetylaspartate catabolism reduces brain acetate levels and myelin lipid synthesis in Canavan's disease. *Proc. Natl. Acad. Sci. U.S.A.* **102,** 5221–5226
20. Bogner-Strauss, J. G., Prokesch, A., Sanchez-Cabo, F., Rieder, D., Hackl, H., Duszka, K., Krogsdam, A., Di Camillo, B., Walenta, E., Klatzer, A., Lass, A., Pinent, M., Wong, W.-C., Eisenhaber, F., and Trajanoski, Z. (2010) Reconstruction of gene association network reveals a transmembrane protein required for adipogenesis and targeted by PPARγ. *Cell. Mol. Life Sci.* **67,** 4049–4064
21. Furukawa-Hibi, Y., Nitta, A., Fukumitsu, H., Somiya, H., Toriumi, K., Furukawa, S., Nabeshima, T., and Yamada, K. (2012) Absence of SHATI/Nat8l reduces social interaction in mice. *Neurosci. Lett.* **526,** 79–84
22. Frezza, C., Cipolat, S., and Scorrano, L. (2007) Organelle isolation: functional mitochondria from mouse liver, muscle and cultured fibroblasts. *Nat. Protoc.* **2,** 287–295
23. Aflaki, E., Radovic, B., Chandak, P. G., Kolb, D., Eisenberg, T., Ring, J., Fertschai, I., Uellen, A., Wolinski, H., Kohlwein, S.-D., Zechner, R., Levak-Frank, S., Sattler, W., Graier, W. F., Malli, R., Madeo, F., and Kratky, D. (2011) Triacylglycerol accumulation activates the mitochondrial apoptosis pathway in macrophages. *J. Biol. Chem.* **286,** 7418–7428
24. Tahay, G., Wiame, E., Tyteca, D., Courtoy, P. J., and Van Schaftingen, E. (2012) Determinants of the enzymatic activity and the subcellular localization of aspartate *N*-acetyltransferase. *Biochem. J.* **441,** 105–112
25. Ariyannur, P. S., Madhavarao, C. N., and Namboodiri, A. M. (2008) *N*-Acetylaspartate synthesis in the brain. Mitochondria *vs*. microsomes. *Brain Res.* **1227,** 34–41
26. Lu, Z.-H., Chakraborty, G., Ledeen, R. W., Yahya, D., and Wu, G. (2004) N-Acetylaspartate synthase is bimodally expressed in microsomes and mitochondria of brain. *Brain Res. Mol. Brain Res.* **122,** 71–78
27. Pendergrass, W., Wolf, N., and Poot, M. (2004) Efficacy of MitoTracker Green and CMXrosamine to measure changes in mitochondrial membrane potentials in living cells and tissues. *Cytometry A* **61,** 162–169
28. Keij, J. F., Bell-Prince, C., and Steinkamp, J. A. (2000) Staining of mitochondrial membranes with 10-nonyl acridine orange, MitoFluor Green, and MitoTracker Green is affected by mitochondrial membrane potential altering drugs. *Cytometry* **39,** 203–210
29. Seale, P., Kajimura, S., Yang, W., Chin, S., Rohas, L. M., Uldry, M., Tavernier, G., Langin, D., and Spiegelman, B. M. (2007) Transcriptional control of brown fat determination by PRDM16. *Cell Metab.* **6,** 38–54
30. Mottillo, E. P., Bloch, A. E., Leff, T., and Granneman, J. G. (2012) Lipolytic products activate peroxisome proliferator-activated receptor (PPAR) α and δ in brown adipocytes to match fatty acid oxidation with supply. *J. Biol. Chem.* **287,** 25038–25048
31. Brandt, J. M., Djouadi, F., and Kelly, D. P. (1998) Fatty acids activate transcription of the muscle carnitine palmitoyltransferase I gene in cardiac myocytes via the peroxisome proliferator-activated receptor α. *J. Biol. Chem.* **273,** 23786–23792
32. Barbera, M. J., Schluter, A., Pedraza, N., Iglesias, R., Villarroya, F., and Giralt, M. (2001) Peroxisome proliferator-activated receptor α activates transcription of the brown fat uncoupling protein-1 gene. A link between regulation of the thermogenic and lipid oxidation pathways in the brown fat cell. *J. Biol. Chem.* **276,** 1486–1493
33. Sugden, M. C., Watts, D. I., Marshall, C. E., and McCormack, J. G. (1982) Brown-adipose-tissue lipogenesis in starvation. Effects of insulin and (−)-hydroxycitrate. *Biosci. Rep.* **2,** 289–297
34. Wu, C., Macleod, I., and Su, A. I. (2013) BioGPS and MyGene.info. Organizing online, gene-centric information. *Nucleic Acids Res.* **41,** D561–565
35. D'Adamo, A. F., Jr., and Yatsu, F. M. (1966) Acetate metabolism in the nervous system. *N*-Acetyl-L-aspartic acid and the biosynthesis of brain lipids. *J. Neurochem.* **13,** 961–965
36. Zhao, G., Jeoung, N. H., Burgess, S. C., Rosaaen-Stowe, K. A., Inagaki, T., Latif, S., Shelton, J. M., McAnally, J., Bassel-Duby, R., Harris, R. A., Richardson, J. A., and Kliewer, S. A. (2008) Overexpression of pyruvate dehydrogenase kinase 4 in heart perturbs metabolism and exacerbates calcineurin-induced cardiomyopathy. *Am. J. Physiol. Heart Circ. Physiol.* **294,** H936–H943
37. Vergnes, L., Chin, R., Young, S. G., and Reue, K. (2011) Heart-type fatty acid-binding protein is essential for efficient brown adipose tissue fatty acid oxidation and cold tolerance. *J. Biol. Chem.* **286,** 380–390
38. Ji, S., You, Y., Kerner, J., Hoppel, C. L., Schoeb, T. R., Chick, W. S., Hamm, D. A., Sharer, J. D., and Wood, P. A. (2008) Homozygous carnitine palmitoyltransferase 1b (muscle isoform) deficiency is lethal in the mouse. *Mol. Genet. Metab.* **93,** 314–322
39. Fedorenko, A., Lishko, P. V., and Kirichok, Y. (2012) Mechanism of fatty-acid-dependent UCP1 uncoupling in brown fat mitochondria. *Cell* **151,** 400–413
40. Haemmerle, G., Moustafa, T., Woelkart, G., Büttner, S., Schmidt, A., van de Weijer, T., Hesselink, M., Jaeger, D., Kienesberger, P. C., Zierler, K., Schreiber, R., Eichmann, T., Kolb, D., Kotzbeck, P., Schweiger, M., Kumari, M., Eder, S., Schoiswohl, G., Wongsiriroj, N., Pollak, N. M., Radner, F. P., Preiss-Landl, K., Kolbe, T., Rülicke, T., Pieske, B., Trauner, M., Lass, A., Zimmermann, R., Hoefler, G., Cinti, S., Kershaw, E. E., Schrauwen, P., Madeo, F., Mayer, B., and Zechner, R. (2011) ATGL-mediated fat catabolism regulates cardiac mitochondrial function via PPAR-α and PGC-1. *Nat. Med.* **17,** 1076–1085
41. Chakravarthy, M. V., Lodhi, I. J., Yin, L., Malapaka, R. R., Xu, H. E., Turk, J., and Semenkovich, C. F. (2009) Identification of a physiologically relevant endogenous ligand for PPARα in liver. *Cell* **138,** 476–488
42. Huang, J., Jia, Y., Fu, T., Viswakarma, N., Bai, L., Rao, M. S., Zhu, Y., Borensztajn, J., and Reddy, J. K. (2012) Sustained activation of PPARα by endogenous ligands increases hepatic fatty acid oxidation and prevents obesity in ob/ob mice. *FASEB J.* **26,** 628–638
43. Puigserver, P., Wu, Z., Park, C. W., Graves, R., Wright, M., and Spiegelman, B. M. (1998) A cold-inducible coactivator of nuclear receptors linked to adaptive thermogenesis. *Cell* **92,** 829–839
44. Wu, Z., Puigserver, P., Andersson, U., Zhang, C., Adelmant, G., Mootha, V., Troy, A., Cinti, S., Lowell, B., Scarpulla, R. C., and Spiegelman, B. M. (1999) Mechanisms controlling mitochondrial biogenesis and respiration through the thermogenic coactivator PGC-1. *Cell* **98,** 115–124
45. Murholm, M., Dixen, K., Qvortrup, K., Hansen, L. H., Amri, E.-Z., Madsen, L., Barbatelli, G., Quistorff, B., and Hansen, J. B. (2009) Dynamic regulation of genes involved in mitochondrial DNA replication and transcription during mouse brown fat cell differentiation and recruitment. *PLoS One* **4,** e8458
46. de Jesus, L. A., Carvalho, S. D., Ribeiro, M. O., Schneider, M., Kim, S. W., Harney, J. W., Larsen, P. R., and Bianco, A. C. (2001) The type 2 iodothyronine deiodinase is essential for adaptive thermogenesis in brown adipose tissue. *J. Clin. Invest.* **108,** 1379–1385
47. Carmona, M. C., Hondares, E., Rodríguez de la Concepción, M. L., Rodríguez-Sureda, V., Peinado-Onsurbe, J., Poli, V., Iglesias, R., Villarroya, F., and Giralt, M. (2005) Defective thermoregulation, impaired lipid metabolism, but preserved adrenergic induction of gene expression in brown fat of mice lacking C/EBPβ. *Biochem. J.* **389,** 47–56
48. Li, P. (2004) Cidea, brown fat and obesity. *Mech. Ageing Dev.* **125,** 337–338
49. Viswakarma, N., Yu, S., Naik, S., Kashireddy, P., Matsumoto, K., Sarkar, J., Surapureddi, S., Jia, Y., Rao, M. S., and Reddy, J. K. (2007) Transcriptional regulation of Cidea, mitochondrial cell death-inducing DNA fragmentation factor α-like effector A, in mouse liver by peroxisome proliferator-activated receptor α and γ. *J. Biol. Chem.* **282,** 18613–18624

9.2 Additional data-files – Luciferase Assays

Figure A1 resembles individual luciferase experiments, whereof one representative dataset is described in chapter 3.5.

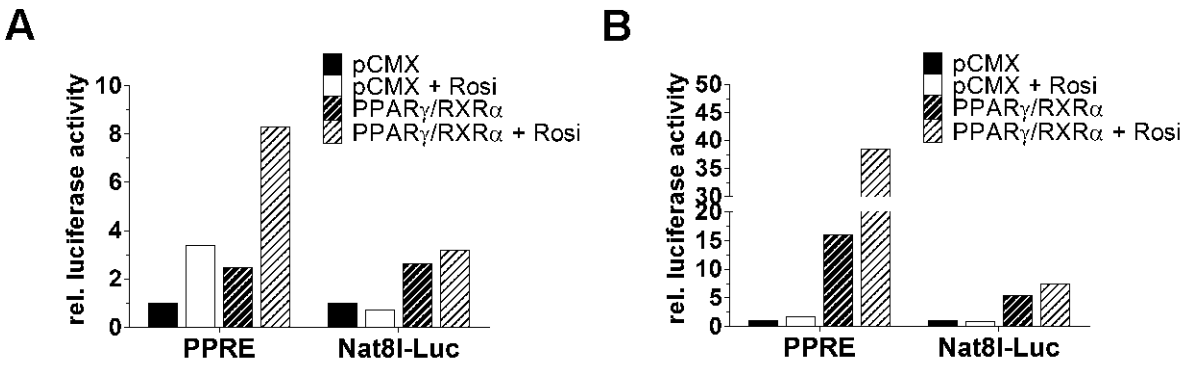

Figure A 1: Individual NAT8L luciferase assays. (A) and (B) Transfected Cos7 cells have been used for the luciferase reporter assays. Cells were stimulated with 10 µM rosiglitazone (Rosi) for 24 hours. Bars include two technical replicates.